AD-A246 793

PL-TR-91-2211

DESIGN AND DEVELOPMENT OF THE INTELLIGENT EVENT IDENTIFICATION SYSTEM: DESIGN CONSIDERATIONS AND PROCESSING FOR REGIONAL EVENT IDENTIFICATION

Douglas R. Baumgardt
Gregory B. Young
Kathleen A. Ziegler

ENSCO, Inc.
5400 Port Royal Road
Springfield, Virginia 22151-2301

29 August 1991

DTIC
SELECTE
JAN 15 1992
B
D

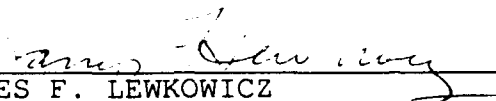Scientific Report No. 1

92-01238

DISCLAIMER NOTICE
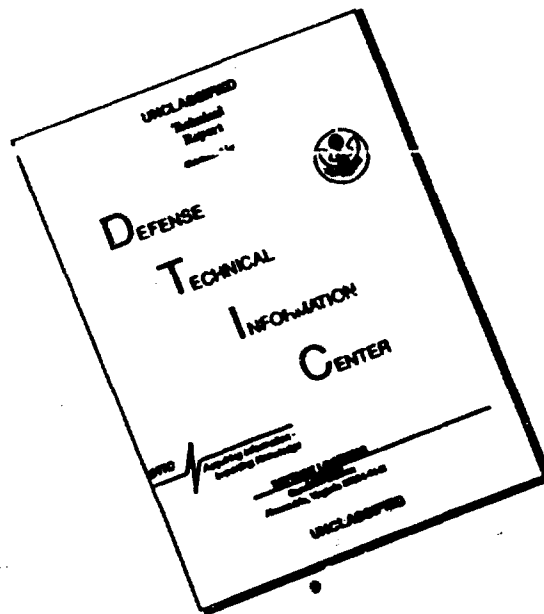
THIS DOCUMENT IS BEST
QUALITY AVAILABLE. THE COPY
FURNISHED TO DTIC CONTAINED
A SIGNIFICANT NUMBER OF
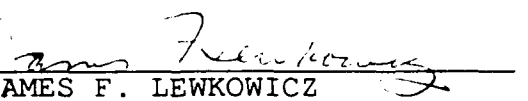PAGES WHICH DO NOT
REPRODUCE LEGIBLY.

SPONSORED BY
Defense Advanced Research Projects Agency
Nuclear Monitoring Research Office
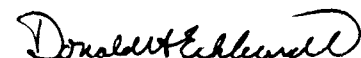ARPA ORDER NO. 5307

MONITORED BY
Phillips Laboratory
Contract F19628-90-C-0049

The views and conclusions contained in this document are those of
the authors and should not be interpreted as representing the
official policies, either expressed or implied, of the Defense
Advanced Research Projects Agency or the U.S. Government.

This technical report has been reviewed and is approved for
publication.

This report has been reviewed by the ESD Public Affairs Office
(PA) and is releasable to the National Technical Information
Service (NTIS).

Qualified requestors may obtain additional copies from the Defense
Technical Information Center. All others should apply to the
National Technical Information Service.

If your address has changed, or if you wish to be removed from the
mailing list, or if the addressee is no longer employed by your
organization, please notify PL/IMA, Hanscom AFB, MA 01731-5000.
This will assist us in maintaining a current mailing list.

Do not return copies of this report unless contractual obligations
or notices on a specific document requires that it be returned.

REPORT DOCUMENTATION PAGE

13 ABSTRACT (Maximum 200 words)

This report describes the design of the Intelligent Event Identification System (ISEIS) and the key processing algorithms of the system. ISEIS will characterize seismic events utilizing discriminants to classify source types, explosion or earthquake, and by comparing waveform features with reference events to estimate how similar the events are to previously observed events. Various graphics interfaces will provide explanations to the analyst about the event characterization results as well as various graphics displays of the data processing results. ISEIS will initially be developed to identify small events at regional distances, recorded at the regional arrays. A discrimination study of regional discriminants at NORESS for mine explosions and earthquakes in Norway is presented. This study has revealed that ratios of regional-phase amplitudes at frequencies above 6 Hz provide the best discrimination capability. Spectral discriminants, such as Lg spectral ratio, appear to be less useful. However, the identification of time-independent spectral modulations effectively identifies most mine explosions which are ripple fired. A process called Multiple Event Recognition System (MERSY) is described which automatically identifies ripple-fired explosions using cepstral methods. Finally, the Dynamic Time Warp (DTW) algorithm is described which will be used in ISEIS to do waveform matching of regional seismic codas.

TABLE OF CONTENTS

SECTION   **PAGE**

iii

LIST OF FIGURES

Figure 15: Example of the fit of a second-order polynomial to the spectrum recorded at NORESS. The dashed line indicates the pre-Pn noise spectrum. The top plot is the spectrum after the quadriatic trend has been removed.

Figure 16: Example of a MERSY display for a presumed Estonia mine blast using the X window graphics, Version 10.4. The upper left plot shows three beam waveforms (vertical, horizontal, incoherent). The left three panels show the spectra, FFT cepstra, and MEM cepstra for the four phases detected and associated with the event and the pre-Pn noise. The vertical lines on the cepstra indicate the peaks picked by the MERSY algorithm. The lower right window is a textual display of the processing results.

Figure 17: An example of two-array processing of a Leningrad mine blast (V12). The left and center three windows are the processing results for the detections at NORESS and FINESS the Plots on the right were obtained by averaging the spectra and cepstra of the phases detected at each array.

Figure 18: Example of NORESS/FINESS multi-array processing, MERSY display for a presumed mine explosion. Notice the spurious FFT cepstral peaks, particularly at FINESS, caused by the truncation of the spectrum at Nyquist in the middle of a spectral modulation.

Figure 19: Example of NORESS/ARCESS processing of a presumed earthquake. The spectra are essentially flat with no strong, consistent modulations apparent with quefrencies less than 1.0 second.

Figure 20: Map showing the locations of events which we presume are underwater blasts.

Figure 21: NORESS spectra and cepstra for the presumed underwater blasts shown on the map in Figure 20. Each event has a strong consistent modulation in the 0.4 to 0.6 second quefrency range.

Figure 22: Schematic illustration of DTW match as a path minimization problem.

Figure 23: Allowed paths for movement through the DTW grid shown in Figure 22.

Figure 24: Slope constraints for the paths allowed for movement through the DTW grid shown in Figure 22.

Figure 25: Map showing the locations of the events used in this study.

Figure 26: Flow diagram for the DTW algorithm.

Figure 27: Example of a DTW solution for the match of unknown event, eqa (top) against a known earthquake eq^9 (bottom).

Figure 28: DTW solution for the best match to event eqa.

Figure 29: DTW solution for the match of a known explosion, ex1, to the unknown event, eqa.

Figure 30: The best matching templates in the 2 to 4 Hz band to the unknown event, eqa, shown at the bottom.

Figure 31: The best matching templates in the 8 to 16 Hz band to the unknown event, eqa, shown at the bottom.

LIST OF TABLES

SUMMARY

The objective of this project is to design and develop an Intelligent Event Identification System, or ISEIS, which will be a prototype for routine event identification and to serve as a research tool for discrimination research. In stating this goal, it is important to define what is meant by "intelligent." We have tried to design ISEIS such that, when presented a specific seismic event, the system will approach the characterization of the event in a systematic fashion in the same way that a seismologist would. For example, a seismologist would be aware of the latest results of discrimination research and would try to apply the same discriminants. However, the seismologist would be careful not to blindly apply the discriminants, since they may be affected by regional path effects. Thus, it is important that event identifications be "qualified" based on what the limitations are about our understanding of the discriminants in terms of how they may be affected by non-source effects. The analyst should also be flexible enough to learn new discrimination methods based on the results of the analysis of additional data. Finally, any seismologist would want to compare the event with other nearby events and/or waveform features extracted from reference-event waveforms. Such comparisons would be important in any informed characterization of the event, particularly since regional seismic discrimination is not well understood.

ISEIS will be capable of doing this kind of detailed, systematic analysis of every event which is detected and located by the NMRD system, in both an automated and interactive mode. In the automated mode, the system will apply a set of standard discriminants in routine fashion on any new events which appear in the database. In the interactive mode, the user can review the results of the automated processing. Additional analysis can be done, if necessary, to improve or enhance the processing results. Discriminants can then be run again, either individually or all together.

This project has been a combined system design and development project and a research project. The initial ISEIS system will be an "experimental prototype," meaning that it may be modified and improved in the future after it has been evaluated. As of this writing, the first prototype of the ISEIS system has been designed and development is nearing completion.

However, the system itself will not be described in this report. User documentation and the final report will describe the actual ISEIS system in more detail. The purpose of this report is to describe the design considerations which went into the ISEIS development and to present the theoretical and seismological basis for the processing procedures which are part of ISEIS.

Section 1.0 gives the design considerations and an overall top-level design of the system. Section 2.0, taken from the paper by Baumgardt and Young (1990), presents the results of a discrimination study of western Norway mine explosions and earthquakes. The results of this study were used in the development of the initial event-identification rules of ISEIS. Section 3.0 describes the Multiple Event Recognition System, or MERSY, which we have developed specifically for the identification of ripple-fired explosions using the observation of time-independent spectral modulations or spectral "scalloping." Section 4.0 discusses a speech processing algorithm, called dynamic time warping (DTW), which we have adapted for seismic event characterization by pattern matching of regional event codas. Finally, Section 5.0 presents our overall conclusions related to our experience in the design of ISEIS, and its application to the characterization and identification of regional seismic events.

SECTION 1.0

DESIGN CONSIDERATION FOR THE INTELLIGENT EVENT
IDENTIFICATION SYSTEM

1.1 OBJECTIVES

The Intelligent Seismic Event Identification System (ISEIS) is a prototype system for the systematic identification of seismic events using both regional and teleseismic seismic data. Regional data from regional arrays and in-country regional networks will be required for the identification of small seismic events. However, teleseismic data may have to be processed for the identification of larger events in countries for which in-country seismic network data is unavailable. ISEIS will incorporate the latest seismological knowledge of seismic discriminants, both regional and teleseismic, to provide as complete as possible, characterization of seismic events for identification. In addition to serving as the primary subsystem for event identification in the Nuclear Monitoring Research and Development (NMRD) system, ISEIS is also being designed as an analysis tool to support research efforts in seismic discrimination. A major goal is to develop a system which is flexible enough to easily incorporate new seismic knowledge and event identification techniques, as a result of event processing and event identification research.

1.2 DESIGN CONSIDERATION

ISEIS is being designed as a post-processor to analyze seismic events after they have been detected and located, using some combination of data from regional arrays and seismic networks of single stations. We assume that the basic event parameters (phase identifications, hypocenter, magnitudes) have been determined by the front-end processors of the NMRD system and are available in the ORACLE relational database. The task of ISEIS is to take as input the event parameters, to make additional waveform or spectral measurements as required for a particular event-identification method, and to apply knowledge to characterize and identify the event.

1

The basis for our design of ISEIS has come from the latest results in seismic discrimination research as well as knowledge derived from other system development projects. Most of the focus of current seismic event identification has been in regional event identification, since small-event identification will require data from regional stations near the source. Seismic discrimination using the NORESS regional array has been discussed by Pulli and Dysart (1987), Baumgardt and Ziegler (1989), and Baumgardt and Young (1990). Bennett et al (1989) has presented the most recent results on regional event identification methods using regional data recorded at single stations for events inside the Soviet Union. Regional seismic event identification is uncertain and regional seismic discriminants are highly experimental, which means that event identifications using regional data must be qualified. Baumgardt (1990) has suggested the use of *case-based* event characterization, where events are characterized on the basis of how similar they are to previous events in a region. This differs from *model-based* event identification, where event characterization in terms of source type (i.e., explosion or earthquake) is made based on a source-type model, derived either from first principles or from training data. Because of the uncertainties of regional seismic-event identification, both case-based and model-based event identification will be utilized.

Teleseismic discriminants must be implemented to identify events which could occur in third countries (i.e., outside the Soviet Union). Although many research studies have tried to apply waveform discriminants (e.g., spectral ratios, complexity) to classify seismic events as explosion or earthquake, we have chosen to concentrate primarily on physically based discriminants which are reasonably well understood, principally location, depth and the *Ms-mb*.

Finally, our design is based on results of ENSCO efforts as part of the Intelligent Event Identification (IAS) project (Bache, 1990). This includes the first implementation of a case-based reasoning system, called seismic script-matching (Baumgardt, 1987; Kandt et al, 1987), and the application of spectral methods for identifying ripple-firing in economic explosions to distinguish

2

them from earthquakes (Baumgardt and Ziegler, 1989). Also, many of the software system development concepts of the IAS development project have been applied to the development of ISEIS, including the exploitation of distributed systems using message passing, X11 graphics, database techniques using SQL, artificial intelligence methods, and rapid prototyping.

1.3 OVERALL DESIGN CONCEPT

Figure 1 shows the overall design concept currently being developed in ISEIS. ISEIS will provide a set of seismic-event identification techniques or discriminants which will each be applied to the seismic data input to the system. As shown on the left of Figure 1, a standard set of "primary" or "active" discriminants can be applied to seismic events input from a database or selected from a base map by the user. Active discriminants are those which are judged to be reliable and relatively well understood. Other "secondary" or "inactive" discriminants will also be available which may be more experimental or possibly redundant with other "active" discriminants. "Inactive" discriminants can be "activated" and applied to an event by the user in an interactive mode for research purposes or to provide a more complete characterization of the events. The discriminants we now believe to be the most robust are those shown under *Primary Discriminants* in Figure 1. (However, research by Bennett et al (1989) and Baumgardt and Young (1990) indicate that the Lg spectral ratio may not be a particularly effective discriminant in Scandinavia and the Soviet Union, although it has proven effective in other regions.)

In addition to the single discriminants, the ISEIS user will also have access to a number of signal-analysis and display functions, as shown on the right of Figure 1. Some of these functions will be used to compute features needed by the discriminants, but can also be applied by the user for special event analysis and discrimination research. Results of these processes can also be made available to the event-identification modules.

The center column shows how an event to be identified will flow through the system. The *Event Assessment* receives as inputs event-parameter and waveform data information from the

DARPA INTELLIGENT DISCRIMINATION PROGRAM

FUNCTIONAL OVERVIEW

Event Characterization and Research

- Single FK
- Continous FK
- Single Spectrum
- Sonograms
- Deconvolution
- Incoherent Beamforming
- Source Mechanism

PROCESS FLOW

Event Assessmen → Single Discriminan Analysis → Multi-Discriminan Analysis → Integrated Discrimination → Final Even Report

Primary Discriminants

Teleseismic Discriminants
- Hypocenter Depth
- Ms - mb

Regional Discriminants
- Ripple Fire)
- Dynamic Time Warp
- S/P Ratio
- Lg Spectral Ratio

Secondary Discriminants
- Third Moment
- Complexity
- First Motion
- Spectral Ratio

Intelligent Event Identification

Event Identification Rules

Case-Based Templates

FIGURE 1: Intelligent Seismic Event Identification

4

Oracle database. The system will access this information from Version 3.0 of the seismic database of the Center for Seismic Studies (CSS), described by Anderson et al (1990). Event parameters will include information about the location and magnitudes, stored for the *origin* and *origerr* relations, phase identification information from the *assoc*. and *arrival* relations, and information about the availability of waveform data, contained in the *wftag*, *affiliation*, and *wfdisc* relations. It is assumed that this information will be placed in the database by the front-end detection, association, and location processors of the NMRD system. *Event Assessment* will then determine the data "status" of the seismic data vis-a-vis the data requirements of the different discriminants. The status will be determined by rules in an expert system which will be associated with each discriminant. Status rules might reason on such things as the minimum number of stations required for a discriminant, whether or not a certain type of phase has been identified, and whether or not the signal-to-noise ratio exceeds a certain required minimum, etc. The status assessment will be either *complete*, meaning that the minimum requirements to run the discriminant are available, *incomplete* meaning that additional data is required to run the discriminant, and *no-data* which means the event has no waveform data or the required phase identifications have not been made. An explanation of the status will then be presented to the user and what should be done to upgrade the status, if necessary.

In *Single Discriminant Analysis*, each discriminant is applied one by one and the event is characterized using either case-based reasoning (CBR) or model-based reasoning (MBR), or both. In MBR, the event is determined to be either earthquake or explosion with some confidence or classed as unknown. In CBR, the discriminant feature is compared to those for reference events and the event is classed as either "typical" or "atypical" of the reference events, with an associated confidence. MBR will be accomplished using rules. CBR will consist of matching of the features of the new event to templates of reference-events and the confidence of match will be computed, using the same method as was done in the IAS script matcher. In *Multidiscriminant Analysis*, each discriminant will "vote" on the identity of the event, using both MBR and CBR, and an overall

assessment of the events characterization will be made. This overall characterization, along with the specific discrimination results, will then be placed in the database as feature and event-characterization relations.

An expert system approach will be used to reason on data availability for status assessment and for MBR and CBR of the discriminant processing. The expert system will be coded in the C Language Integrated Production System (CLIPS), an expert system shell developed by NASA at the Lyndon B. Johnson Space Center. The version we will use initially will be Version 4.3, described in NASA (1989). An evaluation of CLIPS and other expert-system shells has been done by Mettrey (1991). CLIPS has been developed in the C language and is designed to be easily integrated with other C and Fortran languages. In ISEIS, information about data status and the results of the discriminant signal processes will be extracted from the Oracle database using C-language SQL queries. This data will then be passed to CLIPS in the form of logical "assertions" which are processed by the CLIPS rules through C language calls to routines in the CLIPS libraries. When all the input assertions have been processed, the rules will make conclusions which will be output in the form of textual information in disk files that will later be displayed to the analyst. In addition, the CLIPS rules themselves will call other C language routines that will write the results to special relations in the database. The text files and the database relations will then be accessed by the ISEIS explanation functions.

1.4 AUTOMATED AND INTERACTIVE PROCESSING

ISEIS is being designed to be run in either an automated or interactive mode. The functional flow for the automated processing is shown in Figure 2. In the automated mode, a standard set of active discriminants will be selected which will be run on all the events placed in the database by the front-end NMRD processors. The *Database Monitor* will constantly query the database for new events which have been added and must be identified, subject to some location and size constraints (e.g., those events in the area of interest with m_b or M_l greater then 2.5). The

OTHER NMRD SYSTEMS

Event Bulletins

NMRD DATABASE

Other Event Data

Technique Data Table

Event Bulletins

ISEIS Database Monitor

Selected Events

Technique Data Analysis

Identification Bulletins

Hypo Depth

Depth Phase Depth

●●●

Other Methods

Intelligent Event Identification
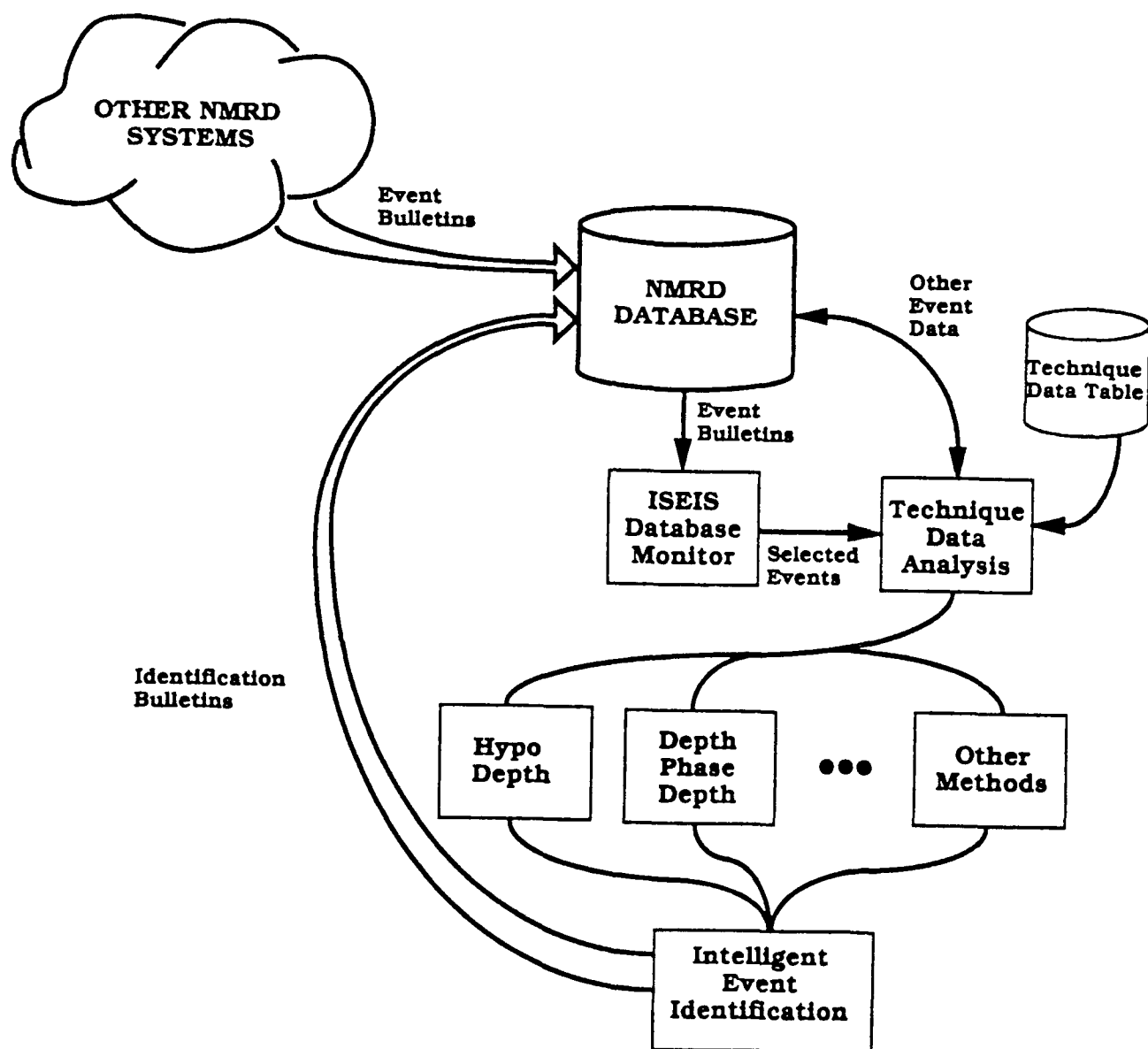
FIGURE 2:   ISEIS Automated Processing Concept

7

selected events are then passed into *Technique Data Analysis* which applies the active set of regional and/or teleseismic discriminants. These discriminants are applied once to give an initial, quick-look assessment of the identity of the event. The results are then placed into the database.

Figure 3 shows the functional flow for the interactive processing in ISEIS. In this mode, events formed by the front-end NMRD processes are examined by the analyst. Events of interest will also be plotted in the *ISEIS Geographic Display*, or map, along with other geophysical and seismological information. These events may have already been run through ISEIS in the automated mode and may have initial identifications. The analyst can then select events for subsequent processing, which are again passed to the *Technique Data Analysis* module. As shown, these processes can be applied iteratively or repeatedly to further refine the event characterization.

In the interactive mode, the events will then be presented to the analyst in the form of a status-results spreadsheet display. A highly schematic illustration of this display, as it will appear in X11 on a SUN graphics workstation, is shown in Figure 4. The data status and discrimination results are displayed to the user in the form of numbers and color-coded buttons in a scrollable spreadsheet, showing a matrix of discriminant methods across the top for events along the left-hand column. Each square in Figure 4 provides a summary display for the status and results for a particular discriminant, shown across the top, applied to a specific event, shown plotted down the left side. Within each square are three smaller buttons and a set of numbers. The left button gives discriminant status information, which refers to whether or not the data required by the discriminant is available to the system. The middle button gives MBR results, and the right button provides CBR results. The numbers under the MBR and CBR buttons refer to the event-characterization confidences determined by the techniques for the event. Each of the three buttons is "active," meaning it can be clicked with a mouse to bring up other displays with more detailed information
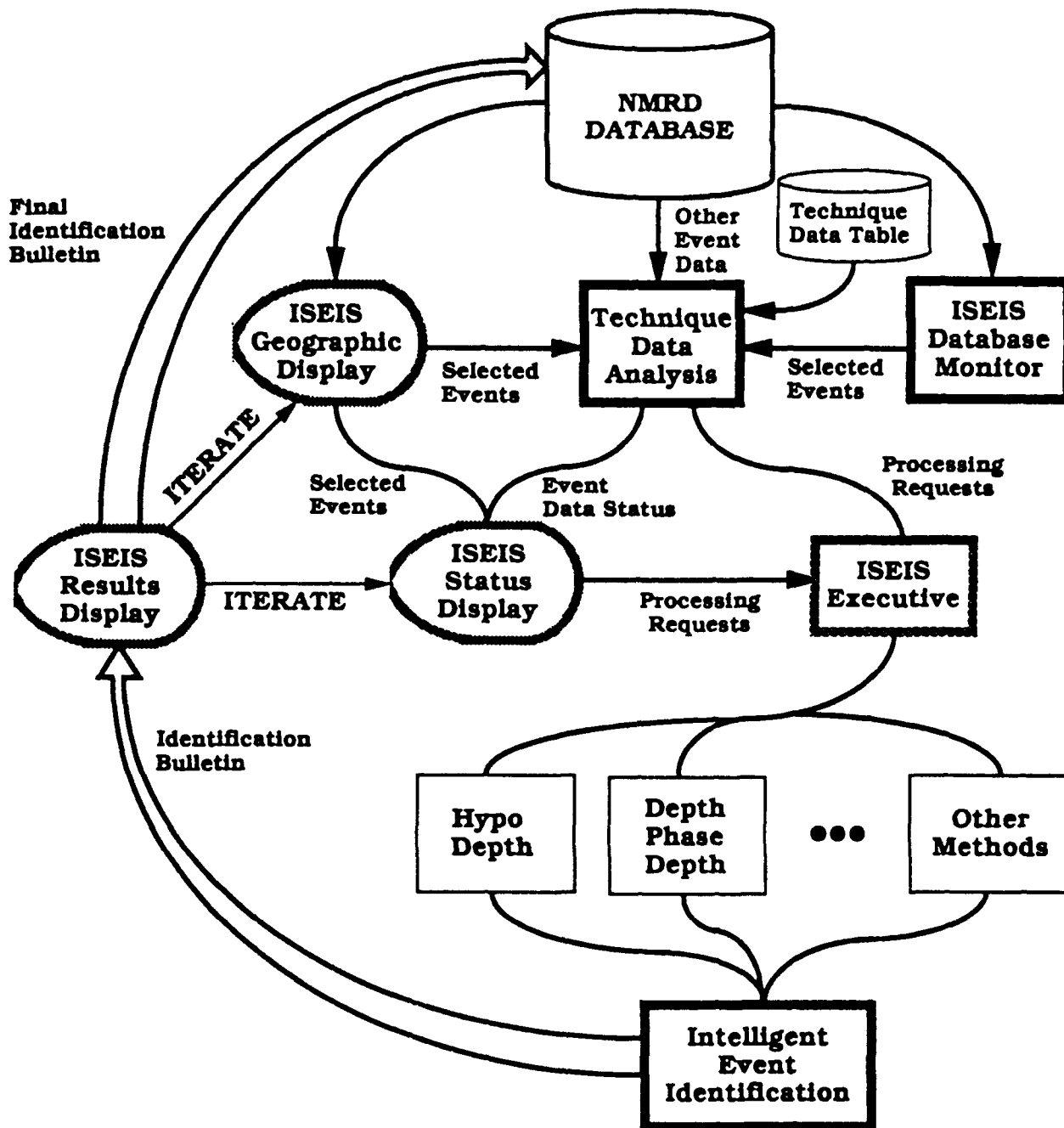
FIGURE 3: ISEIS Operational Concept

9

FIGURE 4: Schematic Illustration of the ISEIS Status-Results Spreadsheet Display

10

Each of the buttons in Figure 4 will be color coded to make the results easier for the analyst to interpret. With reference to the status buttons on the left, if the button is green, the status is "ready," meaning all data is available and the discriminant can be applied. If yellow, the status is "incomplete," meaning only part of the data required by the discriminant is available. The button can be moused to provide more information about the missing data. Finally, if the button is red, then no data is available and the discriminant cannot be applied to the event. For the center MBR button, green, red, or yellow indicates that the event is identified as either an earthquake, explosion, or unknown, respectively. For the CBR button, green, red, and yellow indicates that the event is typical, atypical, or unknown, respectively. These determinations will be based on the confidence of match of the discriminant feature to reference events in the same region as the event. As in the case of the status buttons, the MBR and CBR buttons can be moused to bring up more detailed displays of the processing results for each discriminant.

The spreadsheet will have functions, selectable from pull-down menus (not shown in Figure 4), which will allow the analyst to apply any combination of discriminants to any combination of events, or to apply all active discriminants to all events. It will be possible for the analyst to add or delete events or discriminants from the display. Moreover, the analyst can invoke from this display the various signal-analysis functions either for research purposes or for providing data needed by the discriminants.

1.5 PROCESSING REQUIREMENTS

Our design of the ISEIS system has been based on our assessment of the current state of knowledge in seismic-event identification and the current and future needs of a monitoring system for a Comprehensive Testban Treaty (CTBT). ISEIS is being developed as an integrated system to characterize seismic events using both MBR and CBR and utilizing both regional and teleseismic data.

Because seismic-event identification, particularly at regional distances, is not well understood and is a field of active research, we believe it is important that a case-based reasoning capability be provided. With this facility, we can at least determine if the event looks like previous events, even if a discriminant cannot be relied on to determine if the event is an earthquake or explosion.

Although regional discrimination will be of greatest importance for CTBT monitoring, ISEIS may still be required to process events from third countries which are not part of the CTBT and for which regional seismic data may be unavailable. Thus, there will still be the need to utilize teleseismic data for these regions. Therefore, ISEIS will have the capability of identifying events using teleseismic data for larger events. Moreover, for larger events, combined regional and teleseismic data may provide more definitive event characterizations than just relying only on regional or teleseismic data. However, in the initial prototype, the primary emphasis will be placed on the identification of small events at regional distances.

Finally, the system we are developing will provide a useful research tool for event analysis and event identification. Our modular approach to the development and the spreadsheet implementation of the discriminants will allow for easy modification of the discrimination methods as new knowledge and discriminant techniques are developed in the future.

In the remainder of this report, we discuss in detail the processing requirements for ISEIS. Section 2.0, taken from Baumgardt and Young (1990), describes the seismological basis for regional event identification in western Norway using regional-phase amplitudes and spectral ratios. The initial prototype of ISEIS will be designed to identify events in western Norway. Many of the ISEIS displays will be similar to those shown in this study. Section 3.0 describes the system which will be included to identify ripple-fired explosions. Section 4.0 describes a new scheme for waveform shape matching which will be used as part of the case-based reasoning process. Section 5.0 presents some final conclusions relevant to the design of ISEIS.

12

SECTION 2.0

REGIONAL WAVEFORM DISCRIMINATION

2.1 INTRODUCTION

Effective seismic event identification of nuclear explosions and earthquakes has long been a major goal in testban treaty monitoring, as evidenced by the many studies reviewed by Pomeroy et al (1982) which were done up to the early 1980s. Many subsequent studies have been undertaken, motivated to a large extent by the increased availability of regional seismic data, including regional array data. In spite of all the research in this area, no consistently reliable and universally applicable regional-waveform discriminant has yet been discovered.

Part of the problem has been a lack of a unifying theory of regional seismic event identification which completely explains how seismic source phenomenology affects recorded seismic signals. For example, simple source physics of earthquakes and explosions would suggest that earthquakes, being dislocation sources, should generate more shear-wave energy relative to compressional-wave energy than explosions, and many of the studies reviewed by Pomeroy et al (1982) that tested S-to-P ratio discriminants showed some separation between earthquakes and explosions. However, studies of the P/Lg ratio discriminant by Nuttli (1981), Bennett and Murphy (1986), and Taylor et al (1989) have found significant overlap in the earthquake and explosion populations for events in Eurasia and in western U.S. However, more recent studies by Pulli and Dysart (1987), for events in Scandinavia, and Bennett et al (1989), for events in the Eurasian shield, have shown P/Lg type ratios to be effective for separating earthquakes and explosions. Evidently, differences in propagation paths may have caused the poor performance of this discriminant in some of the studies, but the exact nature of the trade-off between source and propagation path effects on the P/Lg ratio discriminant is not well understood.

Mixed results have also been reported for spectral discriminants. Murphy and Bennett (1982) and Bennett and Murphy (1986) found that NTS explosions and western U.S. earthquakes

13

separated on Lg spectral ratios, with earthquake Lg waves having more high frequency content than explosions. Similar results were obtained by Taylor et al (1988) for Lg and other phases for events in the same region. However, Pulli and Dysart (1987) and Bennett et al (1989) reported that the discriminant is less effective in separating earthquakes and explosions in Scandinavia and in the eastern European shield, respectively. Again, as pointed out by Bennett et al (1989), propagation path differences for the explosion and earthquake populations may have an effect on the performance of this discriminant.

Another problem associated with small-event identification is distinguishing economic blasting from nuclear explosions and earthquakes. Baumgardt and Ziegler (1988) and Hedlin et al (1989, 1990) have shown that economic blasting can be identified by observing persistent spectral modulations produced by ripple-fire. However, this discriminant could be spoofed since nuclear explosions can also be ripple-fired, although it might be difficult. For example, Baumgardt and Ziegler (1988) found that NORSAR recordings of presumed peaceful nuclear explosions in Eurasia had the same persistent modulations observed in ripple-fired mine blasts, indicating that the nuclear explosions were ripple-fired. Moreover, Bennett et al (1989) argue that spectral modulations are unobservable for known mine blasts in the U.S., perhaps because the ripple-fire delay times were too short to be observed in the limited bandwidth of the data. The observation of spectral modulations may identify many, perhaps most, economic explosions, depending on number and delay times of the ripple-fired explosions and the bandwidth of the recording instrumentation. However, there are conceivable scenarios where the discriminant may fail.

Taken together, these studies have shown that regional discriminants cannot be applied in the same way everywhere, that they are highly dependent on the nature of the regional phase propagation path effects, and that there is a strong regional variability in the effectiveness of discriminants. Because of this, a "case-based" approach may have to be applied, where the waveform characteristics of an event are compared with those of previously observed, known events and identified on the basis of the comparison, assuming that the propagation paths are

common. Ideally, the unknown event and the known reference events must be in the same region so that propagation-path differences do not bias the discrimination results. However, it has been difficult in previous discrimination research to find populations of earthquakes and explosions which are collocated and there is no guarantee that in practice collocated reference events of known identity will be available to compare with unknown events. Thus, in an operational event identification scenario, the seismic analyst will be forced to work with what is available and try to account for any propagation effects which might bias event identification using previously observed cases.

In this paper, we will explore some of the problems associated with using the case-based approach to event identification. Baumgardt (1990) has discussed the application of an artificial intelligence technique, known as "case-based reasoning," for systematically identifying seismic events on the basis of comparison with cases. In this paper, we will focus primarily on the seismological and signal processing aspects of the problem. Our emphasis will be on the analysis of regional-array data from the NORESS array and the discrimination of earthquakes and mine explosions located in western Norway. We will discuss the question of whether propagation-path effects bias waveform discriminants and what considerations need to be made when attempting to identify actual case events.

2.2 DATA AND PROCESSING METHODS

NORESS Database

For this study, NORESS data for a group of earthquakes and economic explosions located in western Norway were analyzed. Figure 1 shows the locations of the presumed earthquakes, labeled as Q, and the blasting sites, Blasjo (BLA), a dam excavation site, and the Titania (TITA) mine. The source parameters of the earthquakes and blasts are shown in Tables 1 and 2, respectively. All the events in Table 1 were reported in the Bergen regional bulletin, except Q12 which was presumably below the detection threshold of the Bergen network. The location of Q12

15

in Table 1 was determined by NORESS. The basis for the presumption of earthquakes for these events is simply that they were not reported as explosions in the Bergen bulletin or otherwise known to be blasts at active mines. All the events in Table 2 were reported in the Bergen bulletins and confirmed to be blasts at the Titania mine and the Blasjo dam excavation site.

In order to examine the effect of event location on seismic waveform features, the events in Table 1 and in Figure 5 have been divided into five regions. The Region 1 events occurred off-shore near the Maloy-Ulstein region. Event Q1 has the highest local magnitude reported in the Bergen bulletin (4.2) and was also reported in the Preliminary Determination of Epicenters bulletin as having a body-wave magnitude of 5.0. This event was one of the largest events to occur in Norway in the past 30 years and was felt over most of southern and central Norway (Hansen et al. 1989). The events which occurred shortly afterwards (Q2-Q6) were aftershocks of Q1, whose spectral scaling properties were studied by Chael and Cromer (1988).

The Region 2 events (Q9, Q10, and Q11) all occurred on-shore in the Maloy region. The question marks indicate that we suspect they may actually be explosions rather than earthquakes, for reasons that will be discussed later. Region 3 has one event located to the northeast of the events in Region 2. This small event was detected at NORESS, but not by the Bergen network, and the source parameters in Table 1 were determined by NORESS. We also believe this event is a blast rather than an earthquake.

Region 4 contains two events (Q14 and Q15) which occurred in the vicinity of Bergen and a third event (Q13) which occurred further south in the Stavanger region. The Q14 event, with the largest magnitude of 2.9, may have been felt locally (Frode Ringdal and Svein Mykkeltveit, personal communication). These are the closest events to the TITA and BLA sites and were not reported as blasts, although, as shall be discussed later, we suspect that the Stavanger event, Q13, may actually be a blast.
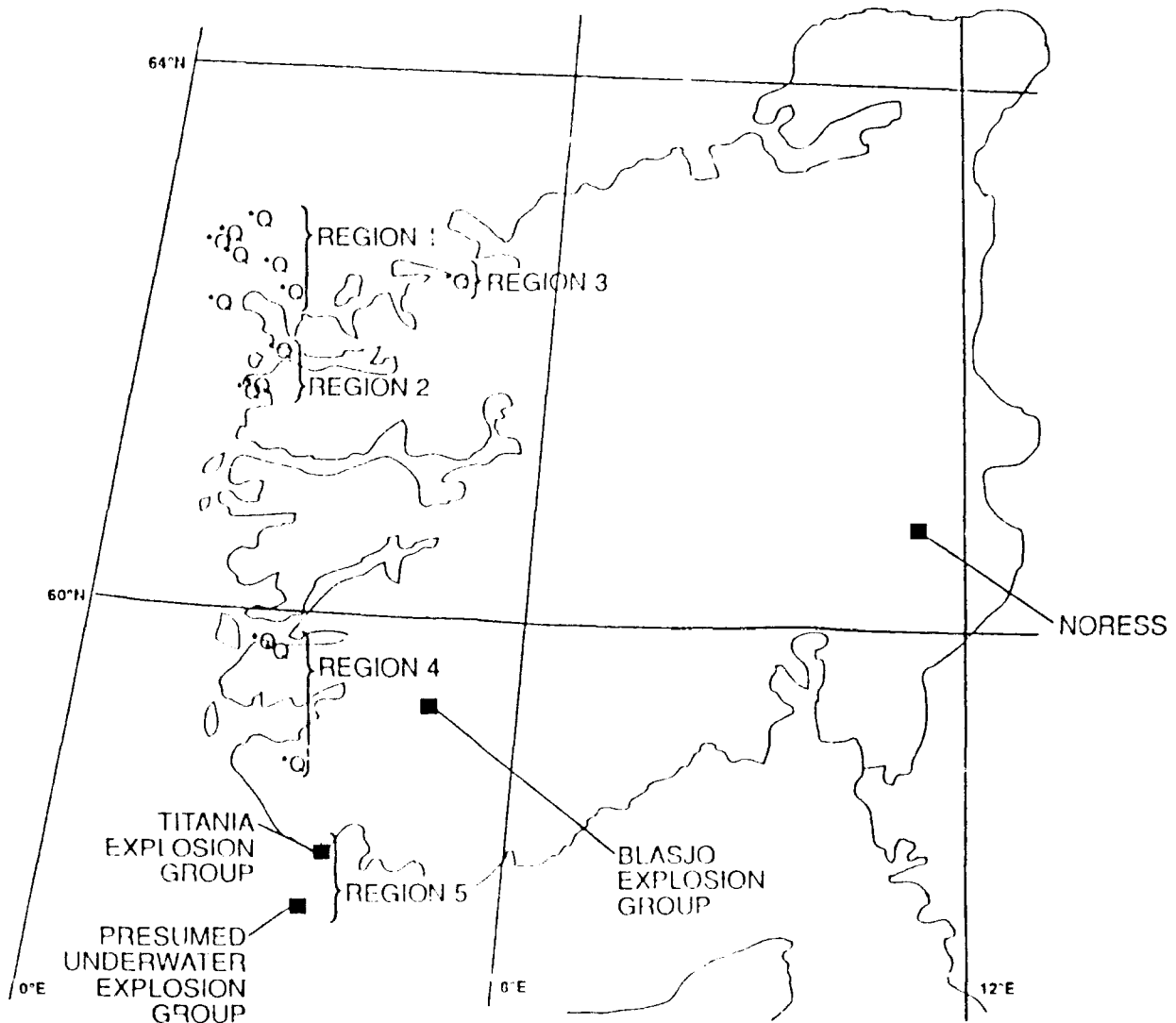
FIGURE 5: Map showing the locations of the presumed earthquakes, labelled as Q, and the locations of the Blasjo and Titania blast sites. The brackets refer to the regionalization of the events discussed in the text. All event locations, except for the event in Region 3 (Q12), were determined by the regional seismic network of the University of Bergen. The location of Q12 comes from NORESS.

17

TABLE 1

EPICENTERS OF PRESUMED WESTERN NORWAY EARTHQUAKES
AND OTHER UNKNOWN EVENTS

Event	Date (m/d/y)	Origin Time (UTC)	Latitude (deg.N)	Longitude (deg. E)	M_l	Dist. (km)
Region 1						
Q1	2/05/86	17:53:16.2	62.74	4.63	4.2	429
Q2	2/05/86	18:50:03.4	62.27	4.69	2.8	403
Q3	2/05/86	20:23:29.8	62.41	6.06	2.7	303
Q4	2/05/86	20:31:37.0	62.79	4.59	2.2	433
Q5	2/05/86	23:35:41.1	62.74	4.50	2.6	434
Q6	2/06/86	06:19:52.4	62.90	4.86	2.3	427
Q7	02/13/86	13:39:00.3	62.40	5.28	2.5	381
Q8	02/13/86	19:03:48.2	62.61	5.07	2.6	401
Region 2						
Q9(?)	2/05/86	15:57:02.4	62.05	5.37	2.0	361
Q10(?)	02/16/86	18:19:41.3	61.69	4.90	2.0	373
Q11(?)	02/14/86	16:51:05.1	61.68	4.97	1.8	369
Region 3						
Q12(?)	2/05/86	15:22:44.0	62.5	6.82	1.6	325
Region 4						
Q13(?)	12/07/85	14:39:09.0	58.90	5.98	2.0	373
Q14	11/27/85	04:53:32.8	59.73	5.71	2.9	342
Q15	02/15/86	18:31:46.4	59.86	5.73	2.1	336
Region 5						
UND1	11/20/85	22:10:44.2	57.61	5.67	2.3	483
UND2	11/20/85	22:24:38.1	57.66	5.72	2.2	478
UND3	11/20/85	22:57:10.8	57.63	6.27	2.2	459
UND4	11/20/85	23:10:47.5	57.66	5.35	2.3	493
UND5	11/20/85	23:17:28.9	57.69	5.45	2.3	486
UND6	11/20/85	23:23:10.0	57.64	5.62	2.2	483

TABLE 2

EPICENTERS FOR CONFIRMED ECONOMIC EXPLOSIONS

Event	Date	Origin Time	Size	M$_l$
(Blasjo Explosions 59.31° N 6.95° E Dist.= 301 km)				
EX1	08/05/85	17:42:58.7	62.9	2.6
EX2	08/06/85	17:50:07.9	30.8	2.4
EX3	10/17/85	10:00:00.4	32.7	2.4
(Titania Mine Explosions 58.342° N 6.425° E Dist. = 394 km)				
EX4	11/08/85	14:18:54.6	132.5	2.4
EX5	02/14/86	14:13:24.9	95.7	2.7
EX6	02/14/86	17:54:10.6	16.2	2.3
EX7	01/07/86	14:14:28.9	43.5	2.2
EX8	01/17/86	14:11:01.5	43.9	2.7
EX9	01/07/88	14:24:43.5	77.4	2.2
EX10	02/10/88	14:17:46.5	103.2	2.5
EX11	03/17/88	14:13:10.3	95.1	2.4
EX12	03/28/88	13:17:27.0	74.2	2.4

Finally, we have included a group of events in Region 5, near the TITA blast site, which we have indexed in Table 1 as UND1 through UND6. Suteau-Henson and Bache (1988) studied these events and compared Lg spectral ratios of these events with those of events at TITA. They suggested that these events were earthquakes because they occurred off-shore. However, we shall show data later which suggests that these events may have actually been underwater explosions, which is why we refer to them by the UND# index.

Incoherent Beam Analysis

Incoherent beams on bandpass prefiltered waveforms were used to measure regional-phase amplitudes. Incoherent beamforming consists of computing log-rms amplitudes in adjacent, one second time windows on each channel of the array, starting about one minute before the *Pn*-wave onset time and extending through the seismogram into the *Lg* coda. The log-rms amplitudes for each time window are then averaged across all the array elements. When plotted versus time,

incoherent beams give an envelope description of the seismic trace viewed in log-amplitude, or magnitude, space.

Figures 6 and 7 show filtered waveforms from the NRA0 element of NORESS and incoherent beams, computed using all vertical, short-period NORESS elements, plotted on the same time axes, for an earthquake and explosion. The horizontal dashed lines on the incoherent beams are the average rms noise levels over a one minute time interval ahead of the Pn onset. The 8-16 Hz incoherent beam and average noise level have been shifted up for visibility relative to the 2-4 Hz beam. The presumed onsets of the regional phases, Pn, Pg, Sn, and Lg, are indicated on both the waveform and incoherent beam plots. Comparison of the waveform plots with the incoherent beams indicates that some phases, notably Sn, are easier to see on the incoherent beam plots. A comparison of Figures 6 and 3 reveals that the Pn wave is not visible in the low frequency (2 to 4 Hz) filter band for the earthquake in Figure 6 whereas it is apparent in both the 2 to 4 Hz and 8 to 16 Hz band for the explosion in Figure 7. This observation was first pointed out by Baumgardt and Ziegler (1988) and has important implications for discriminating these events, which will be discussed in the next section.

Spectral Analysis

Our spectral analysis method is the same array stacking procedure described by that of Baumgardt and Ziegler (1988). In brief the Fourier power spectrum is computed on each channel on the windowed phases and on the noise background to Pn. The power spectra on each channel are then corrected for noise and instrument and averaged across the array. The window lengths for each phase varied depending on the duration of each phase, but in general were between 7 and 14 seconds for Pn, Pg, and Sn, and 25.6 seconds for Lg and noise.

20

Earthquake (Q4)
NRAO Filter Traces
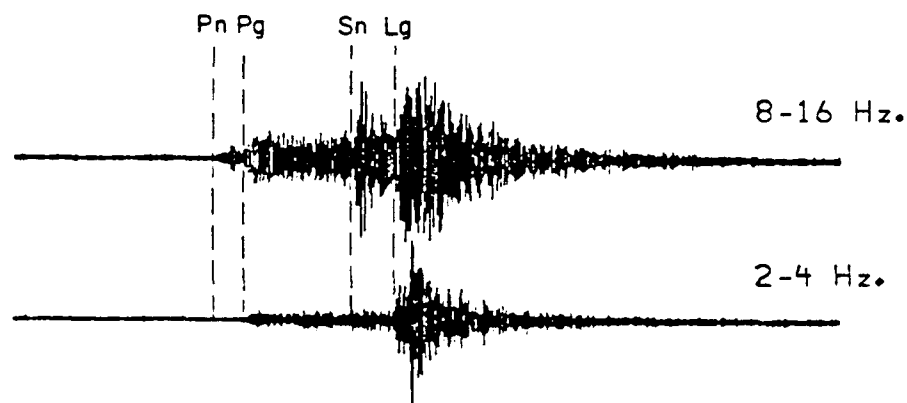
Incoherent Beams
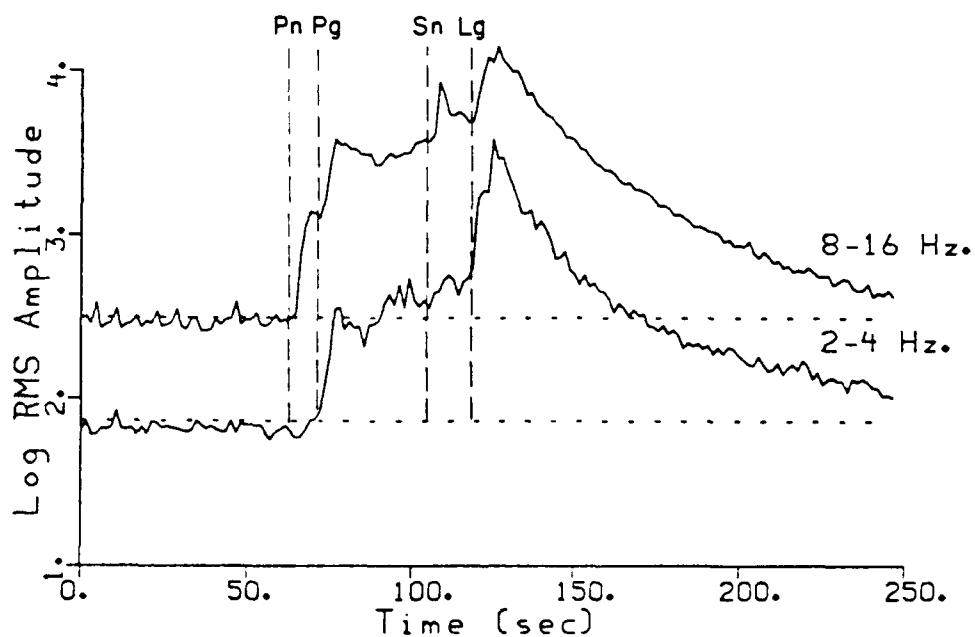
FIGURE 6: Top: Waveforms recorded at the NRAO array element of NORESS for the Q4 earthquakes after bandpass filtering in the 2-4 and 8-16 Hz bands. Bottom: Incoherent beams using one second averaging windows, computed from all 25 NORESS vertical component traces after prefiltering the traces in the 2-4 and 8-16 Hz bands.

BLA Blast (EX1)
NRAO Filter Traces

Pn Pg Sn Lg

8-16 Hz.

2-4 Hz.

Incoherent Beams

Pn Pg Sn Lg

8-16 Hz.

2-4 Hz.

Log RMS Amplitude

4.

3.

2.

1.

0.   50.   100.   150.   200.   250.

Time (sec)
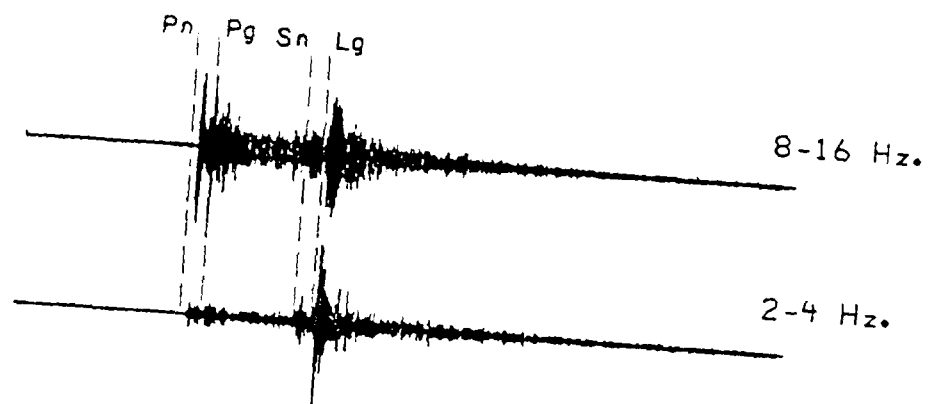
FIGURE 7: Same as Figure 6 for BLA blast EX1.

22

2.3 DISCRIMINATION ANALYSIS RESULTS

Regional Phase Spectra

Figures 8, 9, and 10 show selected array-averaged spectra for the regional phases, Pn, Pg, Sn, and Lg, for events in the five regions. In each case, the spectra for the Pg, Sn, and Lg phases were shifted upward by 0.5 log units relative to the Pn and noise spectra for purposes of visibility. The spectra of the Pn background noise are plotted as dashed lines.

Figure 8a shows the spectra for one of the Region 1 events compared with spectra for an explosion in Figure 8b. All the spectra in Region 1 resembled that in Figure 8a in that the regional phase spectra in general were very simple and, at frequencies above 2 Hz, above the frequencies where the low-frequency effects of the instrument removal are apparent, the spectra fall off linearly with frequency into the noise. In contrast, the explosion spectra in Figure 8b exhibit strong modulations or scalloping, which Baumgardt and Ziegler (1988) attributed to multiple explosions or "ripple-fire." The key feature, which is diagnostic of ripple-fire, is that the same modulation is apparent in all spectra, hence, the modulations are time independent. Hedlin et al (1989) have shown that the time-independent modulations are apparent in coda waves as well as in regional-phase spectra. Most of the events that we have studied at TITA and BLA showed obvious spectral modulations. The exception was the January 17, 1985 event (EX10), which showed no evidence of modulations. Thus, modulations may or may not be present in blasts, and when present, may vary in intensity and periodicity, depending on how the ripple-fire pattern is designed and the bandwidth of the recording seismometers.

Figure 9a shows the spectra of one of the three events in Region 2 (Q9). This event shows a strong modulation pattern apparent in all spectra which could only have been produced by a multiple event. Event Q12 in Region 3 had a very similar set of spectra, whose modulations closely resemble those observed for known blasts. Figure 9b shows a second event in Region 2
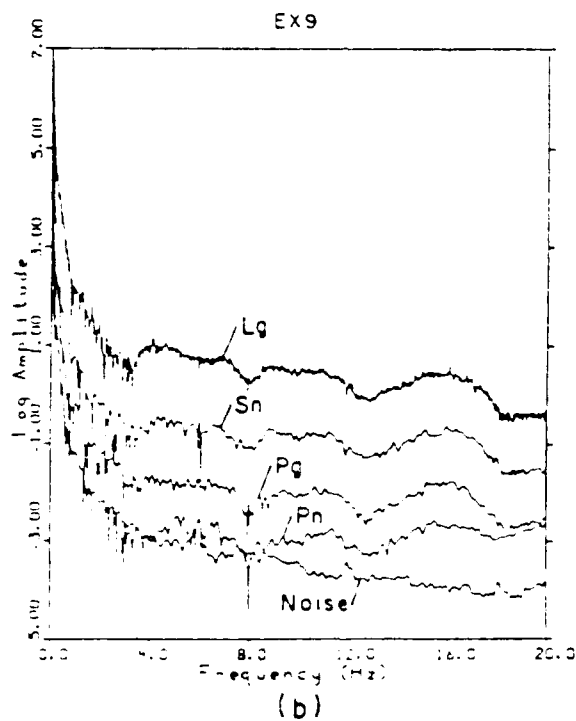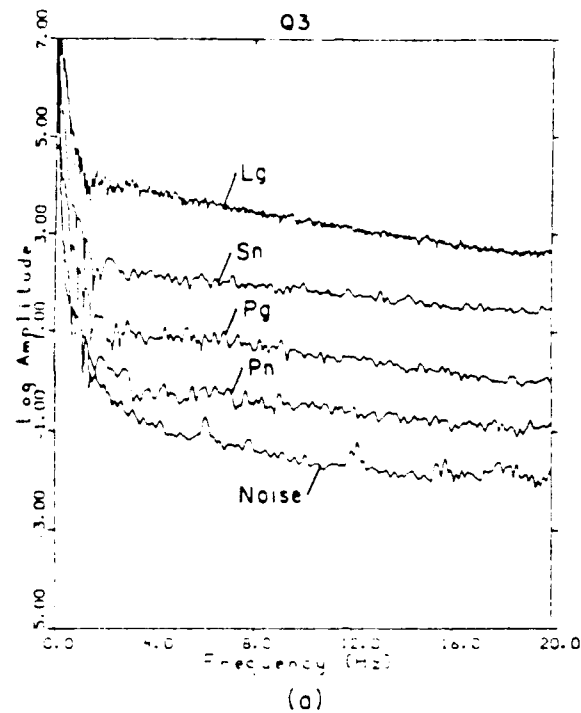
FIGURE 8: (a) Regional phase spectra for a regional event (Q3) in Region 1, strongly suspected to be an earthquake. The Pg, Sn and Lg spectra have been shifted up by 0.5 log amplitude units relative to the noise and Pn spectrum. (b) Regional phase spectra for a confirmed explosion (EX9) located at the Titania mine, which exhibits time-independent spectral modulations indicative of ripple-firing.
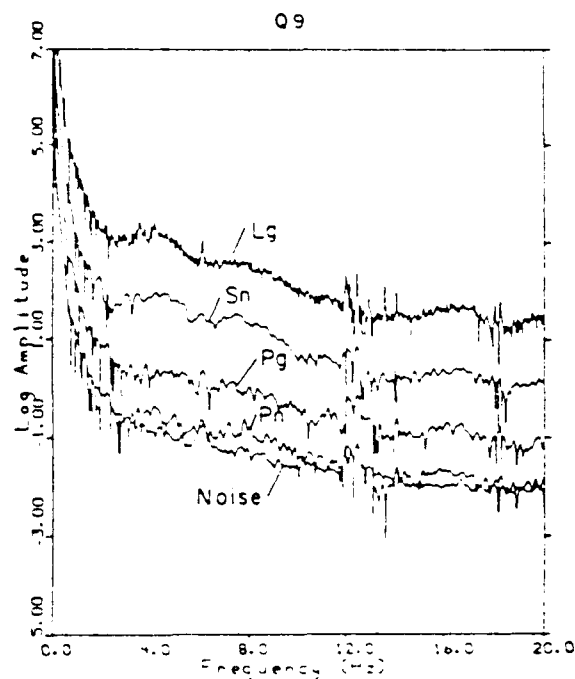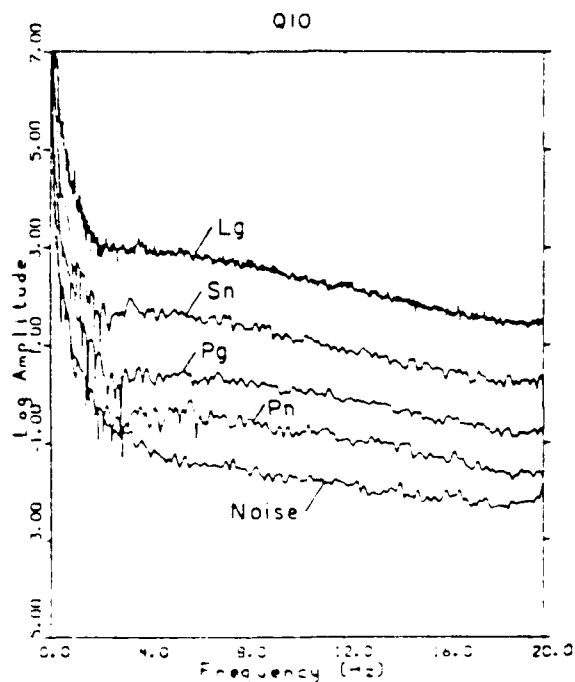
FIGURE 9: (a) Regional phase spectra for a regional event (Q9) in Region 2. Originally presumed to be an earthquake, this event has time-independent spectral modulations indicative of ripple-fire. (b) Regional phase spectra for a regional event (Q10) in Region 2, which has an indication of a single half cycle of a modulation pattern for a ripple-fire with delay time less than 0.05 seconds.

25
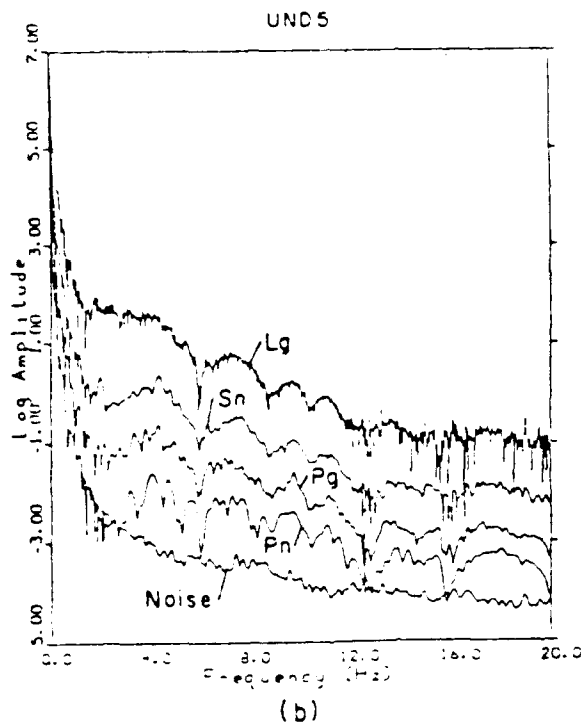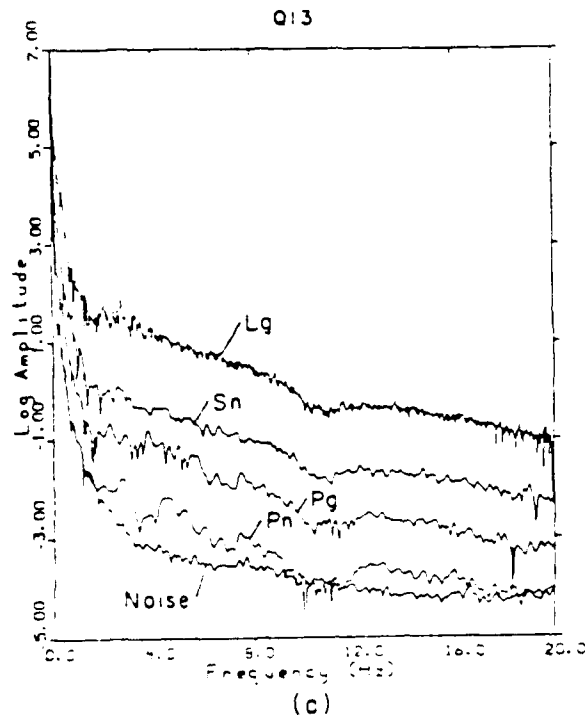
FIGURE 10: (a) Regional phase spectra for the southern-most event in Region 4 (Q13). Originally presumed to be an earthquake, the event exhibits time-independent spectral modulations indicative of ripple-fire. (b) Regional phase spectra for an event in Region 5 (UND5), which appears to be an underwater explosion. The time-independent modulations may be due to bubble-pulse interference and/or underwater reverberations.

26

(Q10) which has a broad hump from about 3 Hz to near 20 Hz. This may be a very subtle modulation produced by multiple events delayed by times near or less than 0.05 seconds, which would produce null near or beyond the Nyquist frequency of 20 Hz. Event Q11 had regional phase spectra similar to those of Q11.

Figure 10a shows the spectra of the Stavanger event Q13. These spectra have a strong null at between 10 and 11 Hz, which appears to be caused by a spectral modulation. Figure 10b shows one of the spectra of the off-shore events near TITA (UND5). This event and all the UND events had very strong spectral modulations. Interestingly, the periodicity of the modulations for all the events in this group were nearly the same.

The key question which must be addressed when considering whether time-independent spectral modulations imply ripple-fired blasts is whether or not earthquakes can produce time-independent modulations as well. In principle, there is nothing which precludes earthquakes consisting of multiple ruptures, which is commonly observed for large earthquakes. Blandford (1975), for example, has modeled complex earthquakes as consisting of the superposition of many "subearthquakes" in order to explain a number of teleseismic discriminants. It is unknown whether such a model might also apply to small earthquakes and whether such complex earthquakes can produce the kinds of coherent time independent modulations that have been observed for ripple-fired explosions. Thus, the presence of time-independent spectral modulations alone does not prove that events Q9, Q10, Q11, Q12, and Q13 are ripple fired blasts.

It is more likely that UND1 through UND6 are in fact underwater blasts. First, the origin times of the events, although uncertainly determined by the Bergen network, are very evenly spaced in time by about 14 minutes. Second, the time independent modulations in all the spectra indicate that the multiple events were delayed by nearly the same time, which is about 0.3 seconds. It is unlikely that either of these two phenomena would be observed in earthquakes. Baumgardt and Ziegler (1989) have suggested that the spectral modulations in these events, if they are

underwater explosions, may have been caused by interference of bubble pulses in the water or reverberations in the acoustic waveguide produced by the water column. The consistency of the time-independent modulations indicates that each of the underwater blasts were probably detonated at about the same depth in the water.

Comparison of Incoherent Beam Amplitude Ratios

As has been discussed above, the relative excitation of compressional and shear wave energy, represented in terms of P-to-S ratios, has been considered as a possible discriminant between explosions and earthquakes. In theory, earthquakes should generate more shear energy relative to compressional energy than explosions. However, propagation effects must also be considered when comparing these ratios for populations of earthquakes and explosions. In this section, we examine regional-phase amplitude ratios for NORESS recordings of blasts and earthquakes on a region-by-region basis in order to consider possible regional variations in these features.

Frequency-dependent amplitude ratios between the phase pairs, Pn and Pg, Pn and Sn, Pn and Lg, Pg and Sn, and Pg and Lg, were determined from the incoherent beams, discussed above. First, incoherent beams were computed for the vertical component traces after prefiltering the seismograms using a set of six-pole, Butterworth recursive filters. The prefilter bandpasses were 2.0 to 4.0, 2.5 to 4.5, 3.0 to 5.0, 4.0 to 6.0, 5.0 to 7.0, 6.0 to 8.0, 8.0 to 10.0 and 8.0 to 16.0 Hz. The beam traces were then plotted and the times of the Pn, Pg, Sn, and Lg peaks were noted, as shown in Figures 6 and 7. We have found all these phases to be most distinct on the incoherent beam in the 8 to 16 Hz filter band. Therefore, we picked the peak amplitudes in this filter band and used the same times to measure the amplitudes in the other filter bands.

For these events, we have two choices for regional P, Pn and Pg, and regional S, Sn and Lg, for computing amplitude ratios. Baumgardt (1990) considered the frequency dependence of all possible ratios, Pn/Pg, Pn/Sn, Pn/Lg, Pg/Sn, and Pg/Lg, and found that the greatest difference

between the blast and earthquake groups was apparent in the *Pn/Sn* and *Pn/Lg* ratios at high frequency (8-16 Hz). Figures 11 and 12 show the *Pn/Sn* and *Pn/Lg* ratios, respectively, on incoherent beams for the 8-16 Hz prefilter plotted separately for each of the five regions and for the two blast sites. Note that the BLA blast site is near Region 4 and the TITA blast site is close to Region 5.

Different symbols are also used to indicate the different kinds of sources. The triangles indicate the events we are reasonably sure are earthquakes and did not exhibit time-independent spectral modulations. The diamonds indicate events which were originally thought to be earthquakes, but whose spectra appear to have time-independent spectral modulations which resemble those produced by ripple-fired explosions. The circles represent all the confirmed blasts, most of which had time-independent spectral modulations.

Both Figures 11 and 12 show that the events in Region 1 and two events in Region 4, all of which we strongly suspect are earthquakes, have very low values of *Pn/Sn* and *Pn/Lg* ratios. It is interesting to note that the variance of the ratios in Region 1 is very low, in spite of the fact that the Bergen locations of these events are distributed out over a 30 to 50 km area. Also, the amplitude ratios for the two Region 4 presumed earthquakes, about 300 km south of the Region 1 events, are the same as the Region 1 earthquakes. Thus, for the events which are most likely earthquakes, the amplitude ratios are consistent and do not seem to depend on differences in propagation path from the two regions to NORESS.

The confirmed mine blasts have much higher ratios than the earthquakes. Also, the variance in these estimates for the same mine are much larger than those of the earthquake group, even though the blasts at each site supposedly occurred at the same location. The BLA blasts also appear to have greater excitation of *Pn* relative to *Sn* and *Lg* than the TITA events. However, the confirmed blasts appear to be clearly separated from the earthquake group, with the blasts having greater compressional wave energy relative to shear-wave energy than the earthquakes.

Incoherent Beam Amplitude Ratios
8-16 Hz Filter
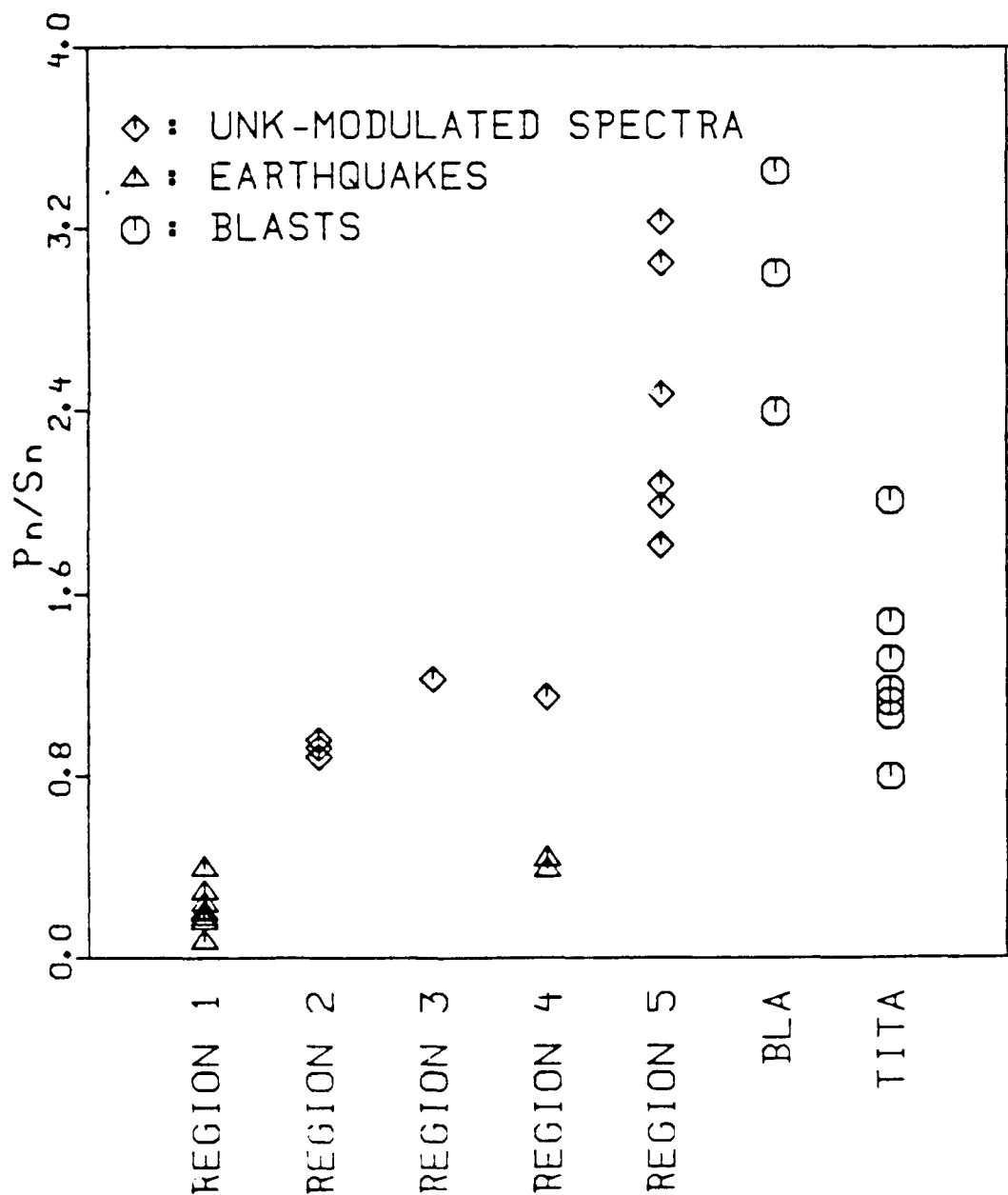
FIGURE 11: Plot of the values of the Pn/Sn ratio in the 8-16 Hz frequency band for each of the five regions and for the two confirmed economic blast regions, BLA and TITA. The values of Pn and Sn amplitudes were measured from incoherent beams of prefiltered waveforms.

Inccoherent Beam Amplitude Ratios
8-16 Hz Filter

◇ : UNK-MODULATED SPECTRA
△ : EARTHQUAKES
⊕ : BLASTS

Pn/Lg

4.0
3.2
2.4
1.6
0.8
0.0

REGION 1
REGION 2
REGION 3
REGION 4
REGION 5
BLA
TITA
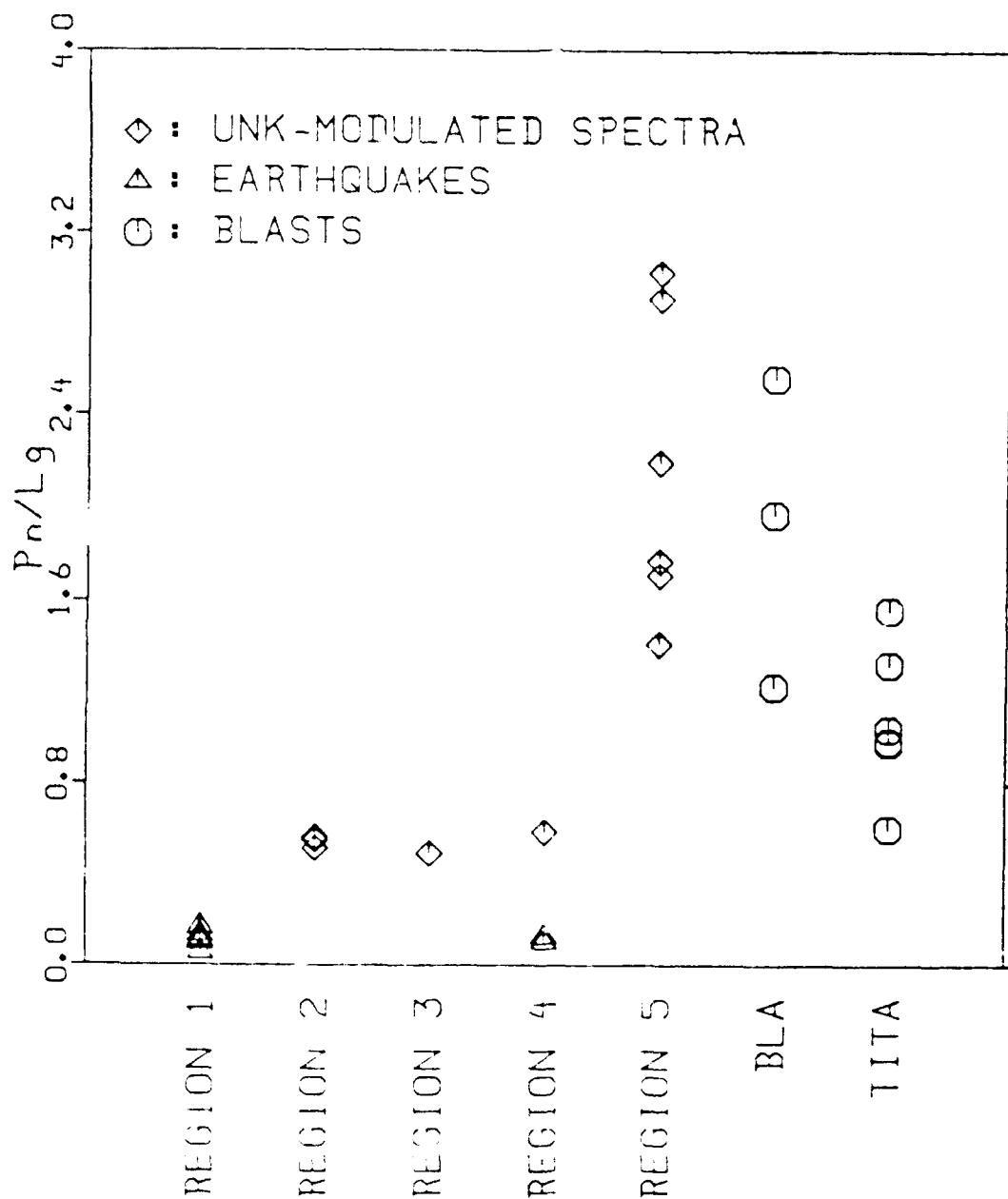
FIGURE 12: Same as Figure 11 for the Pn/Lg amplitude ratios.

41

It is also apparent in Figures 11 and 12 that the events in Regions 2, 3, and 4, which we suspected as being explosions based on their having time-independent modulations in the spectra, have higher Pn/Sn and Pn/Lg r 'os than the earthquakes, although they are not quite as high as the average of all the blast ratios. However, they do overlap the bottom part of the TITA population, as might be expected since the distances of the events in these regions are close to those of the TITA blasts.

The suspected underwater explosions in Region 5 have higher ratios than the earthquakes, and they are about the same as those of the BLA events. Also, the variance in the amplitude ratios for the Region 5 group is much smaller than those of either the TITA or BLA groups. The higher excitation of Pn relative to Sn and Lg compared with the other events is consistent with the UND events being blasts in the water, since these events should have generated no intrinsic shear-wave energy. Thus, the Sn and Lg energy comes entirely from mode conversions at the water-bottom interface with the solid earth and by scattering in the earth.

In order to determine how the amplitude ratios depend on the absolute levels of Pn, Sn, and Lg. Figure 13 shows scatter plots of the logs of the ratios versus the logs of the absolute rms amplitudes. For both the Pn/Sn and Pn/Lg ratios, we find that the variations in the ratios seem to be slightly more correlated with the Pn amplitudes than with the Sn or Lg amplitudes, particularly within the blast and modulated-spectra group. Notice also that all the events, save one, which is the large foreshock (Q1), have nearly the same Sn and Lg amplitudes and that the earthquake population cleanly separates from the explosion and modulated spectra group on the basis of the Pn/Sn and Pn/Lg ratios. This was expected since the events were selected for a limited local magnitude range, based on the Bergen coda-duration magnitude measure. Thus, we conclude that most of the variation in the ratios comes from variations in the Pn excitation, not the Lg excitation.

Our results are consistent with those of other studies that the Pn wave is stronger, relative to the other phases, for explosions than for earthquakes and that the discriminatory capability of Pn
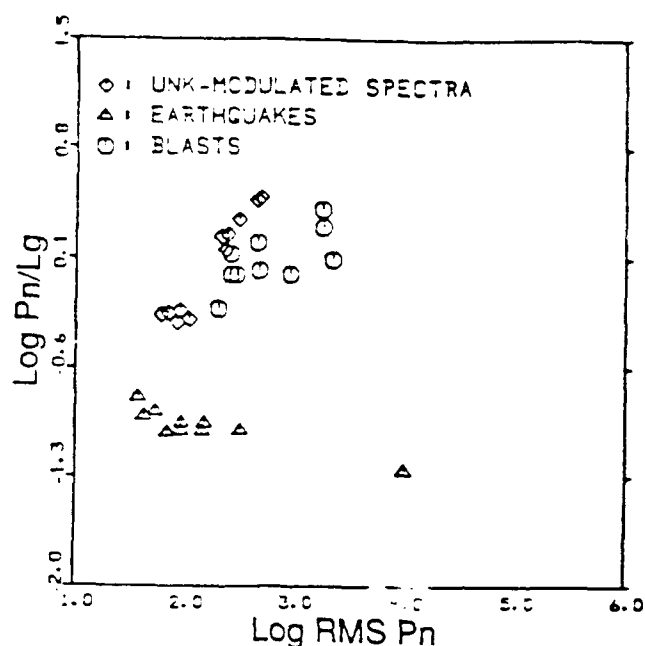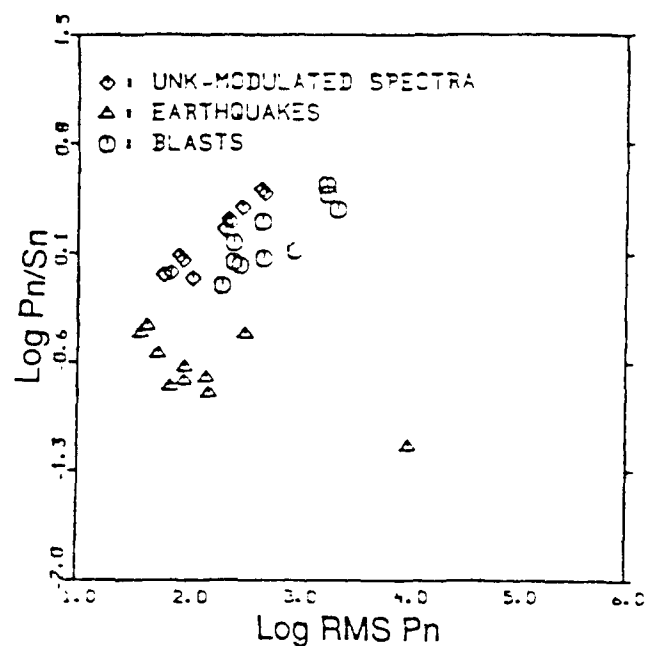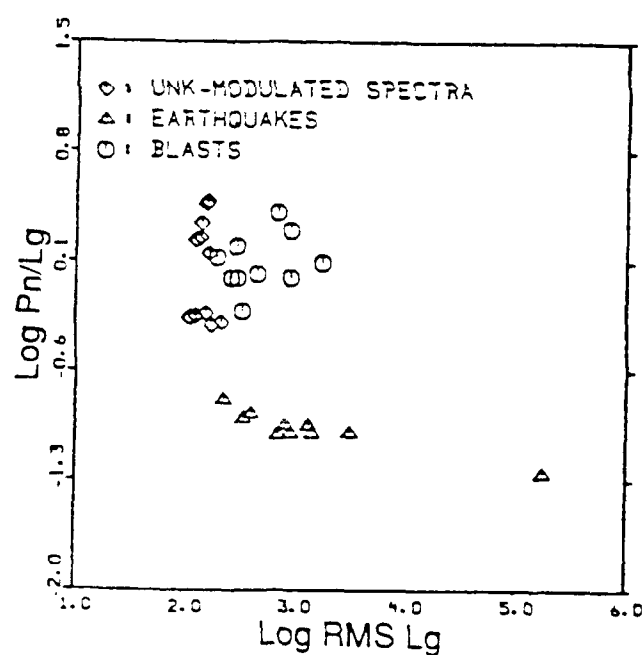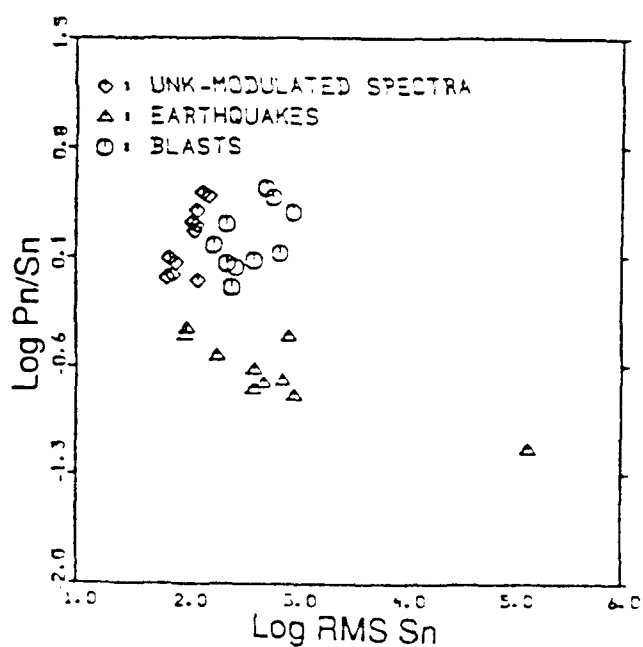
FIGURE 13: (a) Scatter plot of the log of the Pn/Sn ratios (left) and the Pn/Lg ratios (right) versus the log of the Pn amplitudes. (b) Scatter plot of the log of the Pn/Sn ratios (left) and the Pn/Lg ratios (right) versus the log of the Lg amplitudes.

33

to *Sn* and *Lg* ratios increases with frequency (e.g., Blandford, 1981; Bennett et al, 1989). However, it should be noted that for the western Norway events, this result is due to the *Pn* amplitude being much increased relative to the *Lg* amplitude.

It is surprising that the amplitude ratios for the confirmed blasts in the same blasting site have greater variance in the amplitude ratios than the suspected earthquakes in Region 1 and 4 which are distributed over a much larger area. The blast variations may be related to differences in the shooting practice from event to event, such as in the number and delay times of the ripple-fired shots. As has been shown in earlier studies (Baumgardt and Ziegler, 1988) and this study, the complexity of the spectral modulations varies significantly from shot to shot, although these variations should be the same for all phases. Sometimes, the nulls introduced by the modulations are very deep and fall below the noise level, particularly for the *Pn* phases which for some events have lower signal-to-noise ratios in the 8 to 16 Hz band than the *Sn* and *Lg* waves. Notice, for example, that the EX9 spectrum in Figure 8b has a very deep null at about 8 Hz in the *Pn* spectrum, which is the first spectrum above the noise spectrum at the bottom. This null is less deep in the case of the *Lg* spectrum at the top. Perhaps the *Pn* amplitudes are more affected by variations in the number and spacing of the deep nulls that result in more noise contamination than the *Sn* and *Lg* amplitudes, causing the observed variation in amplitude ratios. No such variation is seen for the presumed underwater explosions in Region 5 because they have more similar spectral modulations than the confirmed blasts on land, and the signal-to-noise ratios of *Pn* are high enough that the nulls do not drop into the noise.

Another possibility is that differences in the time and space distribution of the shots in the ripple-fire pattern may actually produce varying amounts of shear-wave energy compared with compressional-wave energy. However, examination of the points on the scatter plots in Figure 13 for the confirmed blasts shows that there is more correlation between the amplitude ratios with the *Pn* amplitudes than with the *Sn* or *Lg* amplitudes. This is not consistent with the amplitude-ratio

34

variations being caused by the variations in the amount of *Sn* and *Lg* wave energy produced by the different blasts.

In summary, we find that regional *Pn/Sn* and *Pn/Lg* ratios discriminate well between known blasts, suspected blasts, and known earthquakes in western Norway, and that this discriminant does not seem to be significantly related to regional propagation effects. We observe very consistent ratio values for our earthquake population, and the variations observed in the blast population seem to be caused by ripple-fire effects. We also find that the observed differences in the ratios correlate more with variations in the *Pn* amplitudes than with the *Sn* and *Lg* amplitudes, and that our populations of blasts and earthquakes in the 2.0 to 2.5 local magnitude range generate very similar amounts of shear-wave energy. However, our sample size is too small to determine if this is a result of selection. In trying to get events of comparable magnitude, determined by coda (probably *Lg* coda) duration magnitudes, we may have purposely selected events of comparable *Lg* excitation. If we had selected events on the basis of some *Pn* magnitude, we may have found more correlation of the amplitude ratios with the *Sn* and *Lg* amplitudes rather than with the *Pn* amplitude.

Comparison of Lg Spectral Ratios

We now consider regional variations in the ratio of low-to-high frequency energy in the *Lg* spectrum, a feature which has been found to effectively separate nuclear explosions and earthquakes in the western United States (Murphy and Bennett, 1982; Bennett and Murphy, 1986; Taylor et al. 1988). As mentioned above, the *Lg* spectra have all been corrected for instrument and *Pn* background noise. For each of the *Lg* spectra, the ratios of the rms levels in the 2 to 6 Hz to the 6 to 10 Hz bands were computed as follows:

$$R = log_{10} \frac{A_{rms} (2 - 6\,Hz)}{A_{rms} (6 - 10\,Hz)}$$

Figure 14 shows the *Lg* spectral ratio values by region. Previous discrimination studies in the western United States found that earthquakes had lower spectral ratios than explosions,

Lg Spectral Ratio
2-6 Hz / 6-10 Hz
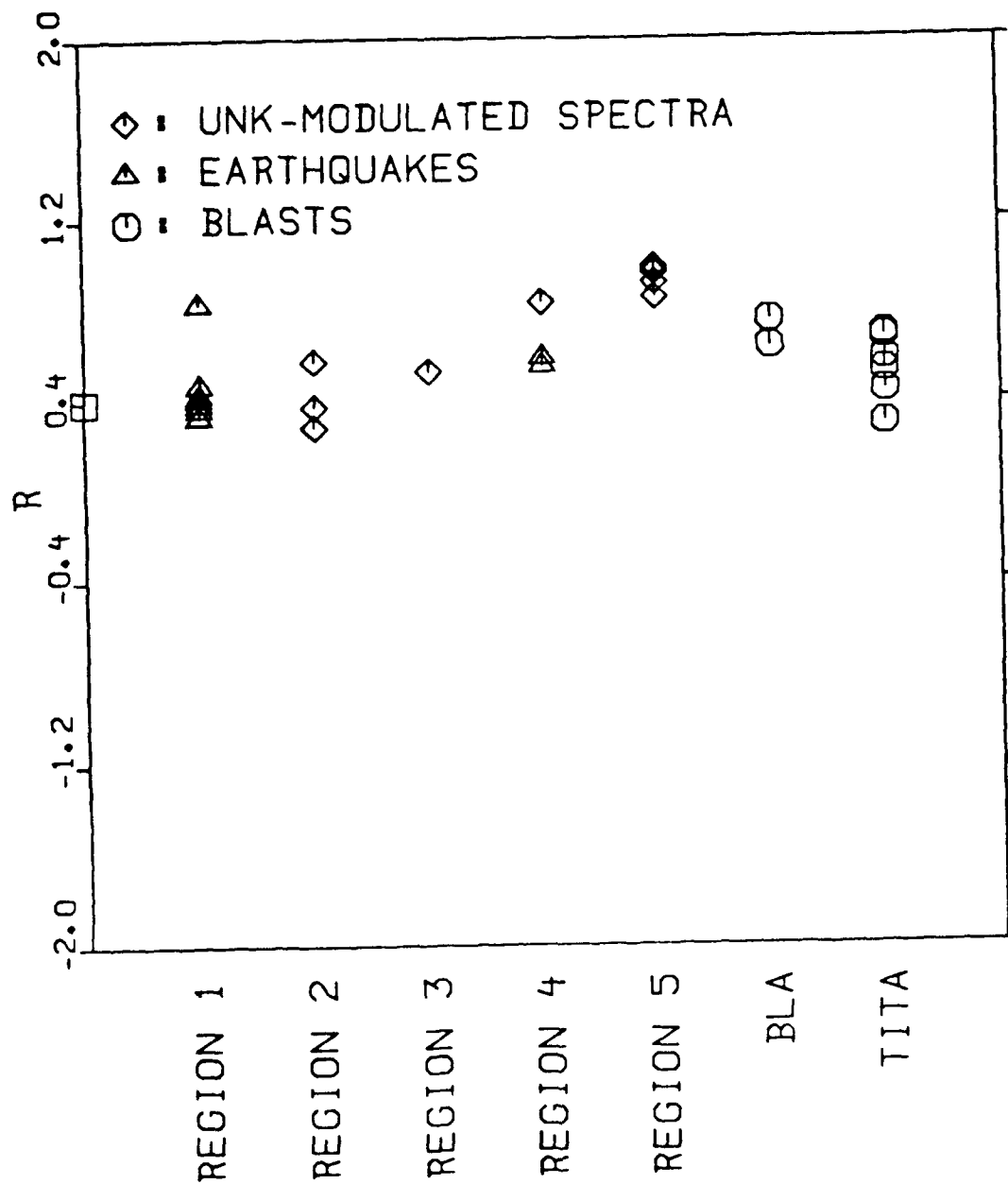
FIGURE 14: Plot of the values of Lg spectral ratio, R, for the same events as Figures 11 and 12.

indicating that earthquakes have more high frequency content than explosions. However, our populations of earthquakes and blasts almost completely overlap each other in their spectral ratios. The presumed underwater explosions in Region 5 have somewhat higher spectral ratios than the nearby TITA blasts. However, these events clearly have lower spectral ratios than the suspected earthquakes in Region 1. Since the TITA blasts are in Region 5, this difference must be an indication of source differences, with the off-shore underwater blasts having more low frequency content than the on-shore TITA blasts. Thus, these results show that spectral ratio does not discriminate between blasts and earthquakes, but may serve a means of distinguishing underwater blasts from blasts on land.

As in the case of the amplitude ratios, there seems to be no significant regional dependence of the Lg spectral ratio. The earthquakes in Region 4 have similar spectral ratios to those in Region 1. Moreover, ripple-fire effects do not seem to greatly affect spectral-ratio measurements, since the variance of the spectral ratios for the TITA and BLA blasts is comparable to that of the earthquake group.

2.4   DISCUSSION

The consideration of case-based methods has been motivated by the failure of previous seismic-discrimination research to develop a set of consistent regional seismic discriminants and a model which explains how intrinsic seismic-source differences affects seismic-waveform features. Lacking such a model, we would identify seismic events by simply comparing them with historic events of of known identity and not worry about the explanation of why the waveform features of explosions and earthquakes differ.

However, this study has pointed out some of the problems that would be encountered in an operational setting in trying to use case-based methods to identify seismic events to monitor a low-yield, nuclear testban treaty using the regional arrays. Ideally, a seismic-discrimination experiment requires there to be large populations of known earthquakes, economic blasts, and low-yield

37

nuclear explosions in the same region so that useful waveform features sensitive to source differences, not propagation-path differences, can be identified as discriminants. However, in reality, for any given region, this situation will almost never be realized. At low magnitudes, there will be many events detected by the arrays, both natural and man-made, which will usually not occur in the same region. Moreover, in any future testban treaty scenario, there will almost certainly be no small nuclear-explosion tests available for comparison.

Our study has shown how case-based methods may be useful, in spite of all the difficulties. The approach would involve first establishing a baseline of "normal" seismic activity in a region, characterized by the location of historic events and the nature of the waveform features for the events. As much as possible, demographic information would be exploited (e.g., locations of events relative to high-population centers, mines, and previous test sites, felt reports, time of occurrence of events) although not relied on exclusively. It should be possible to have a population of confirmed explosions and other events which are most likely earthquakes, although it will be hard to positively identify earthquakes in areas of low natural seismicity. We have found in our study that many of the discriminants appear to work in identifying obvious event types, and that the propagation effects in western Norway seem to be essentially homogeneous throughout the region. Earthquakes can be identified on the basis of low P-to-S ratios and lack of spectral modulations. Mine and off-shore explosions usually have time-independent spectral modulations and high P-to-S ratios. Obvious event types can be quickly identified, based on these features.

An important question about discrimination raised by this study is why the spectral ratio discriminant fails to work as well for separating earthquakes and economic explosions in western Norway as it did in separating small nuclear explosions and earthquakes in western United States (Murphy and Bennett, 1986; Bennett and Murphy, 1986), whereas the P-to-S ratio seems to work better in western Norway than it did in western United States. Bennett et al (1989) also found that P-to-S ratios worked better in separating earthquakes and explosions in the Soviet Union than Lg spectral ratio, although their earthquakes and explosions were not located in the same regions. In

our study, propagation-paths effects do not seem to have a strong effect on the Lg spectral ratios. Moreover, large variations in spectral ratios were observed for mine explosions in the same location, presumably caused by the ripple-fire effects. However, we also found that even for the closely clustered earthquakes in Region 1, whose P-to-S ratios were very similar, the Lg spectral ratios exhibited high variance.

Lilwall (1988) has offered an explanation of the spectral ratio discriminant in terms of the effects of evanescent waves or S^* on Lg-wave generation. Such waves would be be more strongly generated by shallow explosions near the surface than deeper earthquakes, and thus, the S^* waves would build up the low frequency levels in the Lg waves from explosions relative to earthquakes. Such effects do not seem to be present in our blast group. In fact, the underwater explosions in Region 5 seem to have slightly lower values of R than other events (including mine explosions), indicating that the higher frequencies in Lg are enhanced for these events.

Taylor et al (1988) suggests that the presence of a low-Q region in the upper crust of the western United States might explain why explosions, which are shallow and occur in the low Q region, have less high frequencies than earthquakes, which might occur below the highly attenuative region. ⌐ rhaps no such low-Q region exists in western Norway thus explaining why the *Lg* spectra of both earthquakes and explosions are similar. The performance of the *P*-to-*S* ratio may be more a result of intrinsic source differences, i.e., explosions have less shear energy compared to compressional energy at high frequency than earthquakes. Our *P*-to-*S* ratio data seems to correlate more with the *P*-wave levels than with the *S*-wave levels. This suggests that explosions and earthquakes generate the same amount of shear-wave energy, but that explosions produce more compressional-wave energy than earthquakes. However, this may be more a result of event sampling based on the Bergen local magnitude, as was discussed above. Differences in depth of focus may also be partly responsible. The mine explosions apparently occurred at the surface (Svein Mykkeltveit, personal communication) whereas the earthquakes were deeper.

Perhaps near-surface effects, such as PS conversions and S* generation, may build up the shear wave energy for the earthquakes.

This study has shown how seismic events can be identified, relative to case events, by means of a systematic assessment of the similarities and differences between waveform characteristics, always keeping in mind the possible effects of propagation-path differences. We have found that array-averaged spectra and incoherent beams, computed using regional-array data, provide robust estimates of waveform features important for seismic discrimination. We have shown that the explosions and earthquakes in a small region of western Norway, recorded at the NORESS, can be well separated on the basis of high-frequency amplitude-ratio discriminants, but that the Lg spectral-ratio discriminants do not separate as well. This seems to agree in general with other regional discrimination studies in Scandinavia and Eurasia.

This study has also demonstrated that the ripple-fire discriminant based on the observation of time-independent modulations, proposed by Baumgardt and Ziegler (1988) and Hedlin et al (1989), may prove to be highly useful in identifying many unknown regional events which are produced by unreported economic blasting. Apparently, at the low-magnitude monitoring level required for a low yield or comprehensive testban treaty, many such events will be detected by the regional arrays.

Because discriminants seem to be inconsistent in their performance and that we are not sure how to correct discriminants for propagation-path effects, we have advocated the use of a case-based approach to regional seismic discrimination. In this approach, events should be characterized in a step-by-step fashion, testing individual discriminants, and always trying to relate the signal characteristics of unidentified events to events of known identity in the same or similar regions. Because of the current lack of a unifying theory for regional seismic-event identification, the case-based approach may be the only way to reliably characterize and identify seismic events.

SECTION 3.0

RIPPLE-FIRE DETECTION

3.1 INTRODUCTION

In the study described in the previous section, we have found that many events recorded at NORESS, which had previously been suspected to be earthquakes because they were not reported to be mine blasts, had spectra which revealed time-independent spectral modulations or "scalloping." Several previous studies (Bell and Alexander, 1977; Baumgardt and Ziegler, 1988; Smith, 1989; Hedlin et al, 1989, 1990) have shown that this is the distinctive signature of multiple seismic events, or "ripple-firing," which is a very common practice in most commercial blasting activity. We concluded that the events were more likely to be ripple-fired blasts than earthquakes, since the spectral scalloping was so strongly pronounced and other discriminants seemed to be more consistent with the events being explosions. For this reason, we believe that most regional blasting activity can be identified if this ripple-fire pattern can be observed.

The ISEIS system design will include a subsystem which will automatically identify time-independent spectral modulations in regional seismic data and will serve as a primary discriminant for the identification of blasting activity. Two methods have been suggested in the literature for automatically detecting spectral scalloping. Baumgardt and Ziegler (1988) showed that time-independent spectral scalloping produces "quefrency-independent" peaks in power cepstra, which are Fourier transforms of the modulated spectra. As part of the development of the IAS, a system called the Multiple Event Recognition System (MERSY) was developed which automatically detected quefrency independent cepstral peaks in cepstra computed for two or more regional phases associated with an event. This work was described in an unpublished report by Baumgardt and Ziegler (1989). The second method, described by Hedlin et al (1990), also uses cepstra computed for entire regional coda derived from the Fourier transform of the time-frequency spectrograms or "sonograms" of the coda. However, their method looks for high cepstral levels,

41

relative to a threshold established from unmodulated spectra of earthquakes, as the criterion for the identification of modulated spectra due to ripple-fire. Their method is similar to using cepstral variance as the criterion, as suggested as a secondary criterion in the MERSY approach (Baumgardt and Ziegler, 1989). High cepstral values, due to spectral modulations, would also produce high cepstral variance.

In our view, it is essential that the time independence of spectral modulations be identified, since other effects can produce high cepstral value or high cepstral variance. For example, in the *Pn* coda, there may be crustal reverberations and mode conversions from high impedance-contrast interfaces in the crust beneath the source and/or receiver which could produce complex spectral modulations and high cepstral levels. Similarly, *Sn* coda may also contain shear-wave reverberations from the same crustal interfaces which could produce complex modulations in the *Sn*-coda spectra and would also produce high cepstral levels. Thus, the presence of high cepstral levels in both the *Pn* and *Sn* codas does not by itself necessarily imply that the event is ripple-fired. Only the observation of the same modulation pattern throughout the entire coda can unambiguously be used to identify ripple-fired explosions.

Bennett et al (1990) have criticized the cepstral method by pointing out that cepstral peaks can be observed in the *P* codas of earthquakes in western U.S. However, it is important to realize that it is the quefrency independence of the cepstral peaks, not the presence of the cepstral peaks themselves, which is key to identifying ripple-fired events. Stump and Reinke (1988) have pointed out that spectral modulations may be less clear if there are significant errors in the delay times of the blasting timers used in a delayed shooting sequence. Moreover, multiple shots set off in complex spatial patterns would produce complex modulations in the spectra (e.g., Smith, 1989). However, whatever modulations are produced, even if not strong, will still be time-independent in the case of ripple firing. Thus, even weak cepstral peaks produced by weak spectral modulations, which might fail the tests suggested by Hedlin et al (1989), would still be quefrency independent and could be a strong indication of ripple firing, if they can be detected reliably.

42

For the ISEIS system, we chose to adapt the MERSY approach from the IAS, since the method has proven to be effective on a large database of events used to test the IAS. The method has been discussed in detail by Baumgardt and Ziegler (1989) with numerous examples presented. However, since that report has not yet been generally published, a description of the method and some examples are presented below.

3.2 RIPPLE-FIRE DETECTION METHOD

The Multiple Event Recognition System (MERSY) was designed to be part of the post-detection, event characterization processing of the Intelligent Array System (IAS). The design requirements for this system are described in the MERSY requirements document (ENSCO, 1988). Essentially, MERSY automates the method suggested by Baumgardt and Ziegler (1988) of identifying spectral modulations by computing Fourier spectra on each phase associated with an event, then computing the cepstra by Fourier transforming the spectra, and then comparing the resulting cepstra to find two or more peaks which have the same quefrency.

Fourier Cepstral Analysis

The methodology for cepstral analysis has been described in detail by Baumgardt and Ziegler (1988). The procedure simply involves taking the Fourier transform of the base-ten logarithm of the spectral density, computed by Fourier transforming the windowed time-series of the detected phases. These spectra were computed by averaging the spectra computed for each channel of the array, following the method described by Baumgardt and Ziegler (1987). The cepstrum is closely related to the auto-correlation function, which is also the Fourier transform of the power spectrum. The main difference between the cepstrum and the auto-correlation function is that the logarithm of the spectral density is taken in computing the cepstrum, which effectively whitens the spectrum thus producing sharper cepstral peaks.

43

Before computing the second Fourier transform, any systematic trends must be removed from the spectra for if not, the trend itself will produce spurious cepstral peaks. Originally, the spectra were assumed to decay linearly with frequency. A linear trend was fit by least-squares to the spectra above 2 Hz, and then the linear trend was subtracted from the data. However, we found that most of the spectra had non-linear trends, as shown in the example in Figure 15. The bottom shows the spectrum of an *Lg* wave from a ripple-fired explosion fit by least squares with a quadratic curve. The top plot shows the same spectrum with the quadratic trend removed, which has essentially a flat slope on which the spectral modulation can be seen clearly. Thus, the linear trend removal has been replaced with a quadratic trend removal, as shown in Figure 15.

Maximum Entropy Cepstra

One of the well-known problems associated with cepstrum analysis is that the sharpness of cepstral peaks, defined by the maximum power of the peak and its bandwidth, is controlled by the bandwidth of the spectrum. Also, the shorter the time delays of delayed explosions, the less the number of cycles in the modulation within the bandwidth of the spectrum. For example, the sampling rate of high frequency NORESS data is 40 Hz which gives a 20 Hz Nyquist. Thus, the shortest delay which can resolved with this data is 25 ms, which would give a modulation of exactly 20 Hz. In order to resolve shorter delays, it would be necessary to use broader-band data.

Another problem is that even for delays greater than 50 ms, conventional Fourier cepstrum analysis involves truncating the spectrum at some high-frequency cut-off point, usually the Nyquist frequency. This could cut-off a spectral modulation in midcycle and produce a spurious peak at a different quefrency than the actual quefrency of the modulation. Moreover, aliasing and noise effects at frequencies near the Nyquist frequency can produce other spurious peaks.
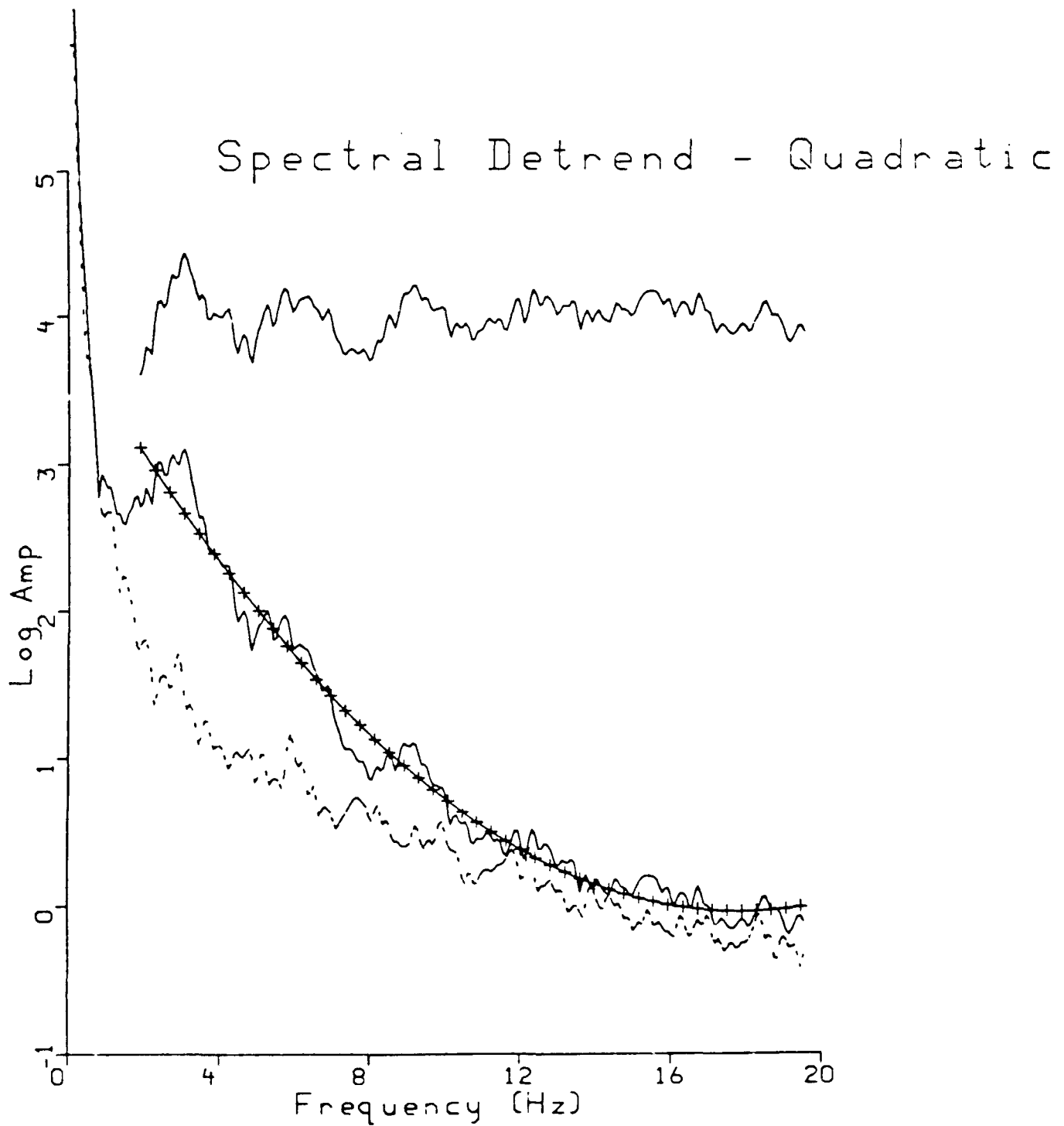
44

FIGURE 15: Example of the fit of a second-order polynomial to the spectrum recorded at NORESS. The dashed line indicates the pre-Pn noise spectrum. The top plot is the spectrum after the quadriatic trend has been removed.

We implemented and experimented with a maximum entropy method (MEM) algorithm for computing the cepstrum in MERSY in order to eliminate cepstral peaks due to noise and processing artifact. We were motivated by the fact that the MEM, in spectral estimation, produces sharper spectral peaks because it, in effect, extrapolates the auto-correlation function to time lags greater than the time-window length. In our use of MEM for cepstrum analysis, we treated the log-amplitude spectrum as if it were a time-series and computed the "MEM cepstrum" which would have the effect of extrapolating the frequency-band window. Thus, we wo ld expect that MEM cepstrum analysis would broaden the bandwidth, extrapolate spectral modulations to frequencies beyond Nyquist, thus eliminating spurious peaks due to truncation and sharpen the peaks caused by the spectral modulation.

The Burg (1967) maximum-entropy power spectrum formalization was adopted and the MEM process was implemented using the algorithm described by Anderson (1974), except that the process was applied to the spectrum instead of to the time-series. The MEM power cepstrum is estimated by

$$P(\tau) = \frac{P_m \Delta f}{\left| 1 - \sum_{m-1}^{M} a_{mn} e^{-2\pi i / n\Delta f} \right|}$$

where the *quefrency*, t, is limited to the interval, defined by $-1/(2Df) < f < 1/(2Df)$ where Df is the frequency sampling interval and a_{mn} are determined by the equation,

$$
\begin{bmatrix}
\phi_0 & \phi_1 & \cdot & \cdot & \cdot & \phi_m \\
\phi_1 & \cdot & & & & \cdot \\
\cdot & \cdot & & & & \cdot \\
\cdot & & \cdot & & \cdot & \cdot \\
\cdot & & & \cdot & \phi_1 & \\
\phi_m & \cdot & \cdot & \cdot & \phi_1 & \phi_0
\end{bmatrix}
\begin{bmatrix}
1 \\
-a_{m1} \\
\cdot \\
\cdot \\
\cdot \\
a_{mm}
\end{bmatrix}
=
\begin{bmatrix}
P_m \\
0 \\
\cdot \\
\cdot \\
\cdot \\
0
\end{bmatrix}
$$

This equation gives the elements of a predictive filter, $(1,-a_{m1},\ldots,-a_{mn})$, derived from the spectral auto-correlation function with frequency lag i, or F_i. P_m is the output power of the $m+1$ long predictive filter, given above. For $m=O$, P_o is estimated by

$$P_0 = \frac{1}{N} \sum_{l-1}^{N} x_l^2$$

The MEM algorithm iteratively solves the above matrix equation, using the algorithm of Anderson (1974), except that f should be substituted for t.

Spectral/Cepstral Statistics

MERSY also computes the following statistically based features on the spectra and cepstra.

The *variance* estimate is a measure of the spectral or cepstral "width" or "variability" around the mean value. Let x_j represent the jth spectral or cepstral value and x the mean value, then the variance is defined as

$$Var\ (x_1....x_n) = \frac{1}{N-1} \sum_{j=1}^{N} (x_i - \bar{x})^2$$

where N is the number of points in the spectrum or cepstrum. The variance is also known as the *second moment*.

The *skewness* characterizes the degree of asymmetry of a function or distribution about its mean value. It is represented as the *third moment* expressed as

$$Skew\ (x_1....x_n) = \frac{1}{N-1} \sum_{j=1}^{N} \left(\frac{x_i - \bar{x}}{\sigma}\right)^3$$

47

where $s = s(x_1 ... x_n)$ is the *standard deviation* of the spectral or cepstral distribution. An estimate of the standard deviation is

$$\sigma(x_1 ... x_N) = \sqrt{Var(x_1 ... x_N)}.$$

The *kurtosis* gives a measure of the "peakedness" or "flatness" of the spectrum or cepstrum relative to a normal distribution function. This feature, also known as the *fourth moment*, is expressed as

$$Kurt \ (x_1 ... x_n) = \left\{ \frac{1}{N} \sum_{j=1}^{N} \left(\frac{x_i - \bar{x}}{\sigma} \right)^4 \right\} - 3$$

The - 3 term makes the value of *Kurt* zero when the spectrum or cepstrum is normally distributed.

These features may serve two purposes. First, they measure the shape of the spectra and cepstra which may be useful for discrimination. For example, Pulli and Dysart (1987) showed that the variance of the cepstrum discriminated between several earthquakes and mine explosions in Scandinavia recorded by NORESS. Apparently, the mine blasts had higher variance than the earthquakes as a result the spectral modulations in the former caused by the ripple-fire effects. Baumgardt and Ziegler (1989) also found that populations of earthquakes and explosions could be separated on the basis of variance, skew, and kurtosis of the cepstra for region phases. Thus, these statistics can serve as secondary features for identification of ripple-fire in addition to the observation of cepstral peaks.

The spectral variance is also useful for determining the number *m* of coefficients a_{mn} which must be included in the maximum entropy cepstrum predictive filter for *n* frequency points. The number of coefficients depends on the complexity of the cepstrum, which is partly measured

by the logarithm of the Fourier cepstral variance, *lcvar*. The following empirically derived rules are used to set the number of coefficients:

$$lcvar \ -4.1 \le -4.4 \to m=50$$
$$lcvar \ > -4.4 \ and \ lcvar \ \le -4.1 \to m = 70$$
$$lcvar \ \ge -4.1 \to m = 80.$$

In addition to these statistics, an estimate of the spectral signal-to-noise ratio *(ssnr)* is also made. The spectral snr is defined as the bandlimited ratio of the rms signal to the rms noise, or

$$ssnr = \frac{\sqrt{\sum_{m=i1}^{M_f} S_m^{\ 2}}}{\sqrt{\sum_{m=i1}^{M_f} N_m^{\ 2}}} \quad ,$$

where $i1$ and Mf are the first and last frequency points of the band, S_i is the spectrum of the detected phase and N_m is the the background noise sample to the first of a detection group. The summation is taken over the frequency band from 1.88 to 19.7 Hz.

Single-Array Peak Analysis

Peaks are identified in the Fourier and MEM cepstra and analyzed to determine if they are caused by spectral modulations caused by ripple-fire. Using the method suggested by Baumgardt and Ziegler (1988), multiple explosions are identified based on the appearance of a consistent set of significant peaks having the same quefrency in the cepstra of all the phases associated with the event. Significant peaks are defined as cepstral peaks whose amplitudes exceed some threshold. Consistent peaks are those which appear in two or more phases, but not in the noise cepstra. The specific criteria for the peaks to be significant and consistent are described in ENSCO (1989). In brief, two of the following three conditions must hold for the event to be classified as a multiple event:

49

(1)   One or more consistent significant peaks appearing in the Fourier cepstra of two or more phases associated with an event, but observed in the noise cepstra.

(2)   Same as above for MEM cepstra.

(3)   The cepstral variance must exceed a minimum threshold.

Multi-Array Analysis

If two or more arrays detect a mine explosion with ripple-fire, there should be consistency between the spectral modulations observed at all the arrays as well as between phases detected at one array. In order to detect consistent modulations at more that one array, stack cepstra and spectra are computed for each array by averaging the cepstra of all the phases associated with the event. Thus, there is one stack spectrum and cepstrum for each array. (Note: Stack cepstra are computed by averaging together the cepstra for each phase; they are not computed from the stack spectra. Stack spectra are computed for the purpose of computing signal-to-noise ratios and other spectral features.)

The stack cepstra for each array are treated in the same manner as the individual phase cepstra in single array processing. Significant peaks are identified on each of the stack cepstra for each array which have the same quefrency at two or more arrays.

3.3   MERSY PROCESSING EXAMPLES

In this section, we show some examples of MERSY processing results for events processed in the IAS. Figure 16 shows an example of a mine explosion in Estonia processed by the MERSY system. The top left window shows three filtered beam traces with the identified phases *Pn, P, Sn,* and *Lg* marked. The right three windows show the spectra, at top, the Fourier (FFT) cepstra, in the middle, and the MEM cepstra, at the bottom. Each of the spectra were computed in six second windows, beginning at the marked phase times, and have been corrected
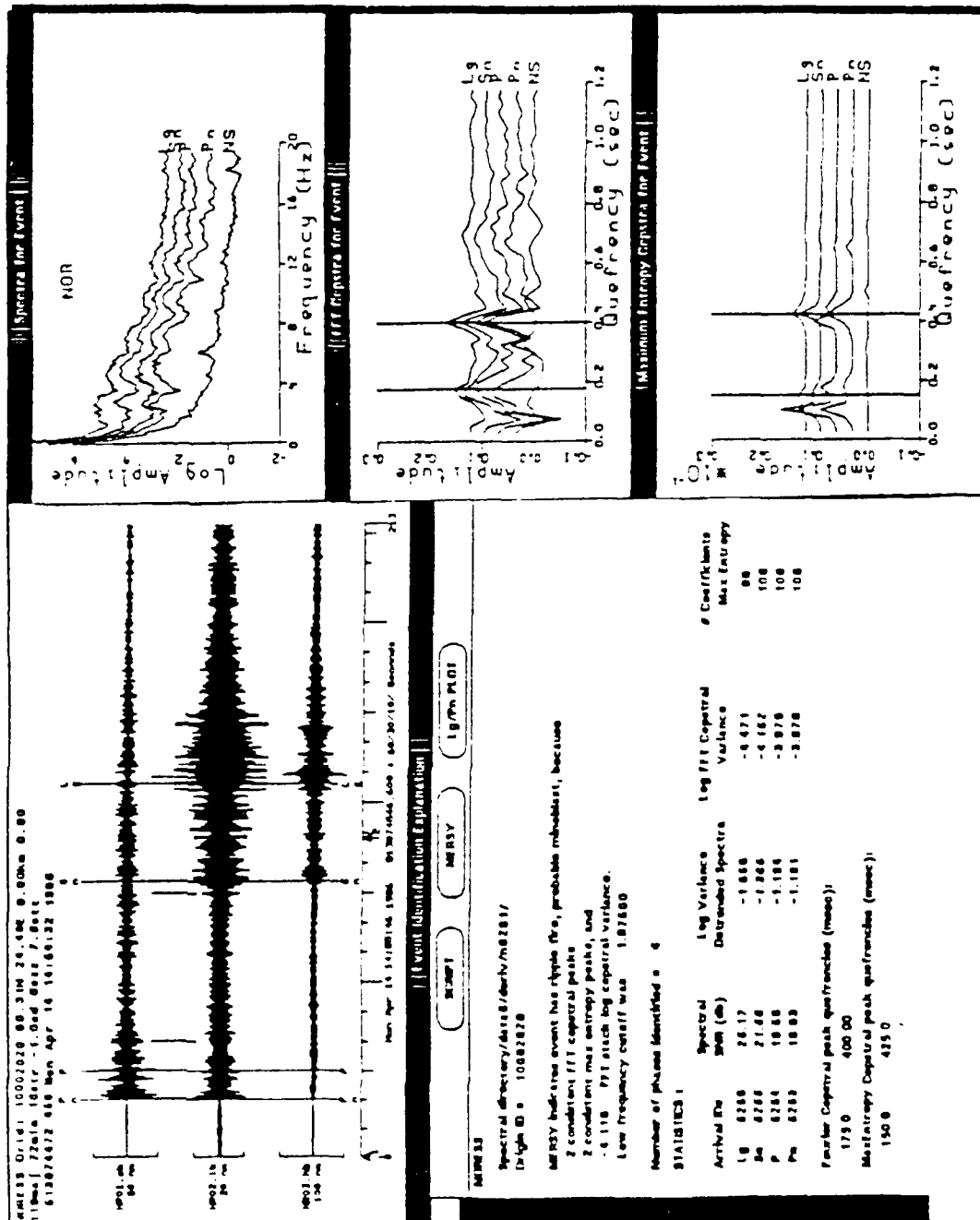
50

FIGURE 16: Example of a MERSY display for a presumed Estonia mine blast using the X window graphics, Version 10.4. The upper left plot shows three beam waveforms (vertical, horizontal, incoherent). The left three panels show the spectra, FFT cepstra, and MEM cepstra for the four phases detected and associated with the event and the pre-Pn noise. The vertical lines on the cepstra indicate the peaks picked by the MERSY algorithm. The lower right window is a textual display of the processing results.

51

for instrument. The spectra are vertical component spectra averaged across the array. The array data is sampled at 40 Hz, giving a Nyquist frequency of 20 Hz. The spectra and the cepstra are displayed for each phase associated with the event, along with the pre-Pn noise, labeled as NS. Note that the spectra and cepstra have been displaced upward, relative to the Pn spectrum and cepstrum, for display purposes. The window on the lower left gives a textual description of the results of the MERSY processing, including a statement of the number of peaks identified in the FFT and MEM cepstra, the average cepstral variance, and the low frequency cutoff of the band. The table gives the values of the spectral signal-to-noise ratios, the spectral and cepstral variances, and the number of prediction error coefficients used in computing the MEM cepstra for each phase. Finally, the actual quefrencies of the consistent peaks are written, which correspond to the dominant delay time of the multiple events.

For the case of the Estonia mine explosion in Figure 16, a clear modulation pattern can be seen in the spectra for all the phases. The nulls in the spectral scalloping are spaced apart by about 0.25 Hz, which corresponds to a delay time of about 400 ms. On the cepstral plots, vertical lines have been plotted through the peaks which were identified by MERSY as being significant and consistent. MERSY picked the primary peak on the Fourier (FFT) cepstra at 0.4 seconds, as expected, in addition to a secondary peak at about .18 seconds. Note that the spectral modulations are not observed in the noise spectra nor do either of the cepstral peaks appear in the noise cepstra.

The MEM cepstrum in the bottom right shows two consistent peaks, which were identified by MERSY and indicated by the vertical lines. These peaks are significantly sharper than those in the FFT cepstra and the variance of the rest of the cepstrum has been much reduced. However, the quefrencies of these two peaks (150 and 425 ms) are shifted relative to the quefrencies (175 and 400 ms) of the MEM cepstral peaks. Also, note that the MEM peaks are not as consistent as the FFT peaks.

Peak shifting of this kind is a well known problem in maximum entropy power spectral estimation studies (e.g., Chen and Stegen, 1974; Kaveh and Lipper, 1983). The causes of such peak shifting include (1) nonstationarity of the input time-series, (2) variations in the initial phase of the estimated time-series, and (3) noise contamination. Baumgardt and Ziegler (1989) have discussed the causes of cepstral peak shifting and have suggested some possible solutions to the problem.

One well-known MEM problem we have avoided in the design of MERSY is peak splitting. This problem arises when too many terms are used in the predictive filter (Chen and Stegen, 1974). As in spectral estimation, we have also observed cepstral peak splitting in MEM cepstra if too many predictive error coefficients are used in the frequency domain. MERSY determines the number of terms to use from the variance of the FFT cepstrum; i.e., the higher the variance, the larger the number of terms. The rule used to determine the number of coefficients from the cepstral variance was derived empirically. Many cases were run, under various signal-to-noise ratios, in order to determine the minimum number of coefficients to use to provide high peak resolution, but not too high to cause cepstral peak splitting. In all the cases we have analyzed using these rules, we have seen no cases of peak splitting.

Baumgardt and Ziegler (1988) have pointed out that there are spurious peaks observed in cepstra due to processing artifact, particularly at quefrencies near the inverse of the Nyquist frequency (0.5 sec). In Figure 16, a large negative peak (i.e., a tough) can be seen near 0.5 seconds, which we believe is caused by truncation of the spectrum at Nyquist. We have observed that the MEM cepstrum seems to eliminate these low-quefrency peaks due to processing artifact. The MERSY rules do not permit the picking of peaks or troughs at this low a quefrency.

Figure 17 shows the steps involved in multi-array processing. In this case, data were processed from a mine explosion, V12, near Leningrad, USSR, recorded at both the NORESS and FINESS regional arrays. The NORESS spectra and cepstra are plotted on the left and those for
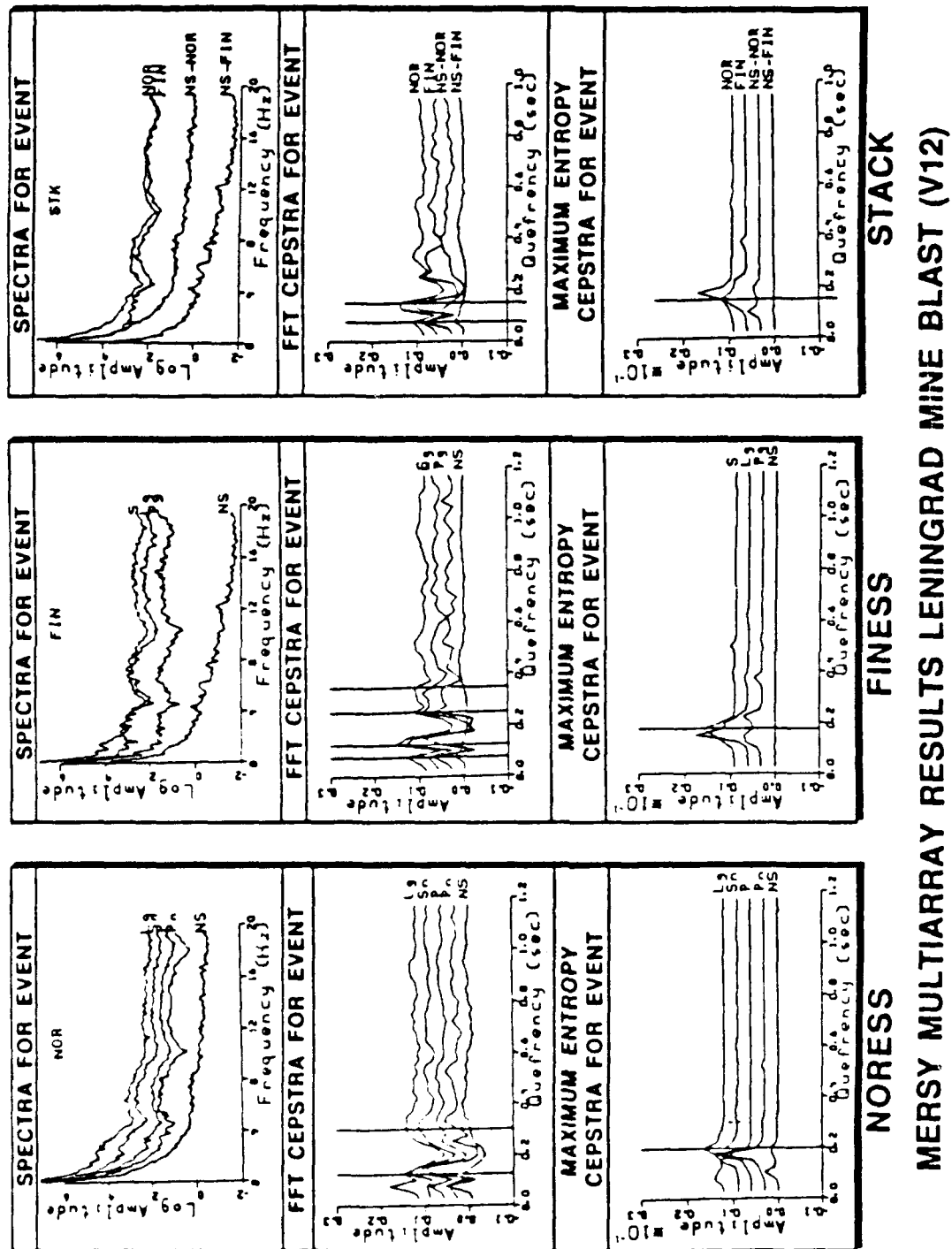
53

FIGURE 17: An example of two-array processing of a Leningrad mine blast (V12). The left and center three windows are the processing results for the detections at NORESS and FINESS. The plots on the right were obtained by averaging the spectra and cepstra of the phases detected at each array.

FINESS in the middle. On the right, the stack spectra and cepstra are shown. In addition to the stack signal spectra and cepstra, the noise spectra and cepstra at each array are plotted and labeled as NS-NOR and NS-FIN. Modulations are clearly observable in the spectra at both arrays which are identical. Cepstral peaks were also identified in all three FFT cepstra, although the number of peaks varies. In all cases, a peak at about 0.15 seconds has been picked. The MEM cepstra placed the peaks at a somewhat higher quefrency, or about 0.2 seconds. Also, there appears to be more variability in the location of the MEM peaks.

Figure 18 shows another example of a multi array processing result for a V4 mine explosion, which is also near Leningrad. This case is an example of a long-period spectral modulation which has been truncated at the Nyquist frequency. One cycle appears to start at near dc and terminate at about 13 Hz, where the first null can be observed. Then, a second modulation begins. We expect that this second modulation should have the same period as the first and extend from 13 to 26 Hz. However, the conventional FFT cepstrum would make a peak corresponding to the modulation from 13 Hz to 20 Hz, which gives a delay time of about 0.14 seconds. In the FFT stack cepstra, a number of peaks near this quefrency are apparent, in particular the FINESS stack cepstra. The MEM cepstra only have one peak at both NORESS and FINESS at about 0.1 seconds, which is close to the correct value. Evidently, the MEM cepstrum appears not to have the spurious peaks caused by truncation of the spectrum at Nyquist.

Figure 19 shows a MERSY result for NORESS and ARCESS data for an event which had no modulations which would produce cepstral peaks with quefrencies less than one second. (Note: close examination of these spectra suggests that there may be small, high-quefrency modulations, which would be consistent with multiple events with delays in excess of one second. These may be caused by aftershocks in the earthquake coda. However, these large delay times are outside the range we would expect for typical mine-blast ripple-fire delays.) This event, which was located in Norway between the NORESS and ARCESS arrays, did not occur near any known
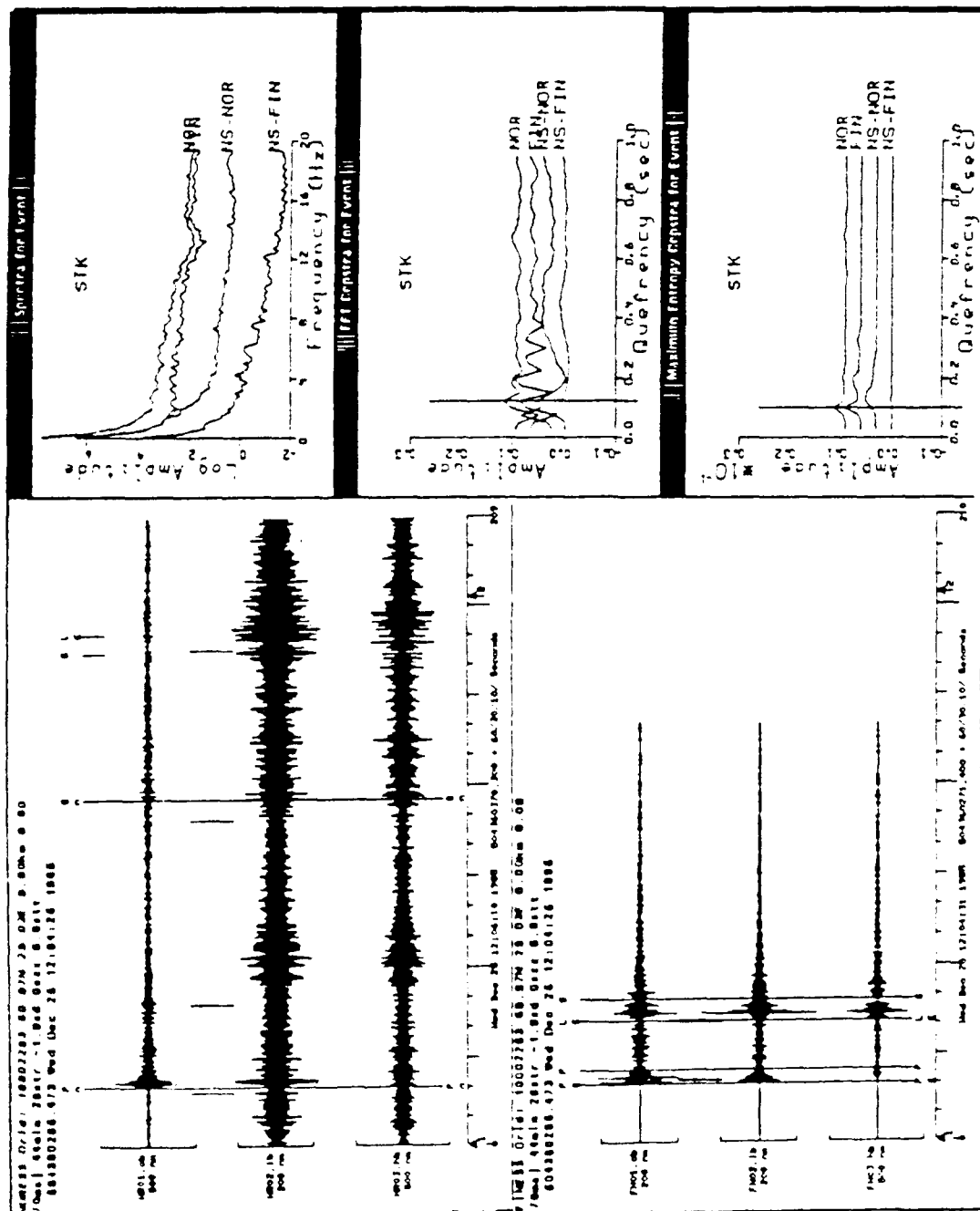
FIGURE 18: Example of NORESS/FINESS multi-array processing, MERSY display for a presumed mine explosion. Notice the spurious FFT cepstral peaks, particularly at FINESS, caused by the truncation of the spectrum at Nyquist in the middle of a spectral modulation.

56

FIGURE 19: Example of NORESS/ARCESS processing of a presumed earthquake. The spectra are essentially flat with no strong, consistent modulations apparent with quefrecies less than 1.0 second.

mine site nor was it identified as a mine blast in the regional bulletins of the University of Bergen. We conclude that this event is an earthquake.

In the previous section, we pointed out a group of events which occurred off the southern coast of Norway which had strong spectral modulations. We argued that these events may have been underwater blasts, and that the modulations were caused by source multiplicity produced by a blast-induced bubble pulse. The locations of three other examples of off-shore events, which we have processed through MERSY and may be underwater blasts, are shown on a map in Figure 20. UWB1 occurred in the Gulf of Bothnia, UWB2 in the North Sea, and UWB3 in the Baltic Sea. Figure 21 shows the spectra and cepstra for these events, computed from spectra of phases detected at NORESS. In each case a very clear spectral modulation pattern can be seen in all phases which produces very sharp cepstral peaks. As a general rule, these events appear to have delay times on the order of 300 to 600 ms. These modulations are so clear that they seem to be caused by the interference of two pulses delayed by about 0.5 seconds. Baumgardt and Ziegler (1989) showed how such modulations are consistent with explosive charges of about 2500 lbs detonated at water depths of about 300 ft.

3.4 CONCLUSIONS

Our initial assessment of the MERSY system as part of the IAS project showed that it could reliably characterize many mine explosions and underwater explosions based on the observation of spectral modulations due to ripple-fire. We have observed no known earthquakes which had spectral modulations as strong as those observed from known ripple-fired blasts, detectable by the MERSY method, which suggests that the false-alarm rate for mine-blast detection would be low. However, there have been cases where MERSY failed to pick up a weak modulation, caused by a small time delay. There have also been known blasts which did not produce observable modulations, either because they were not ripple-fired or because the longest time delay of the ripple fire never exceeded 0.05 seconds, the shortest delay time.
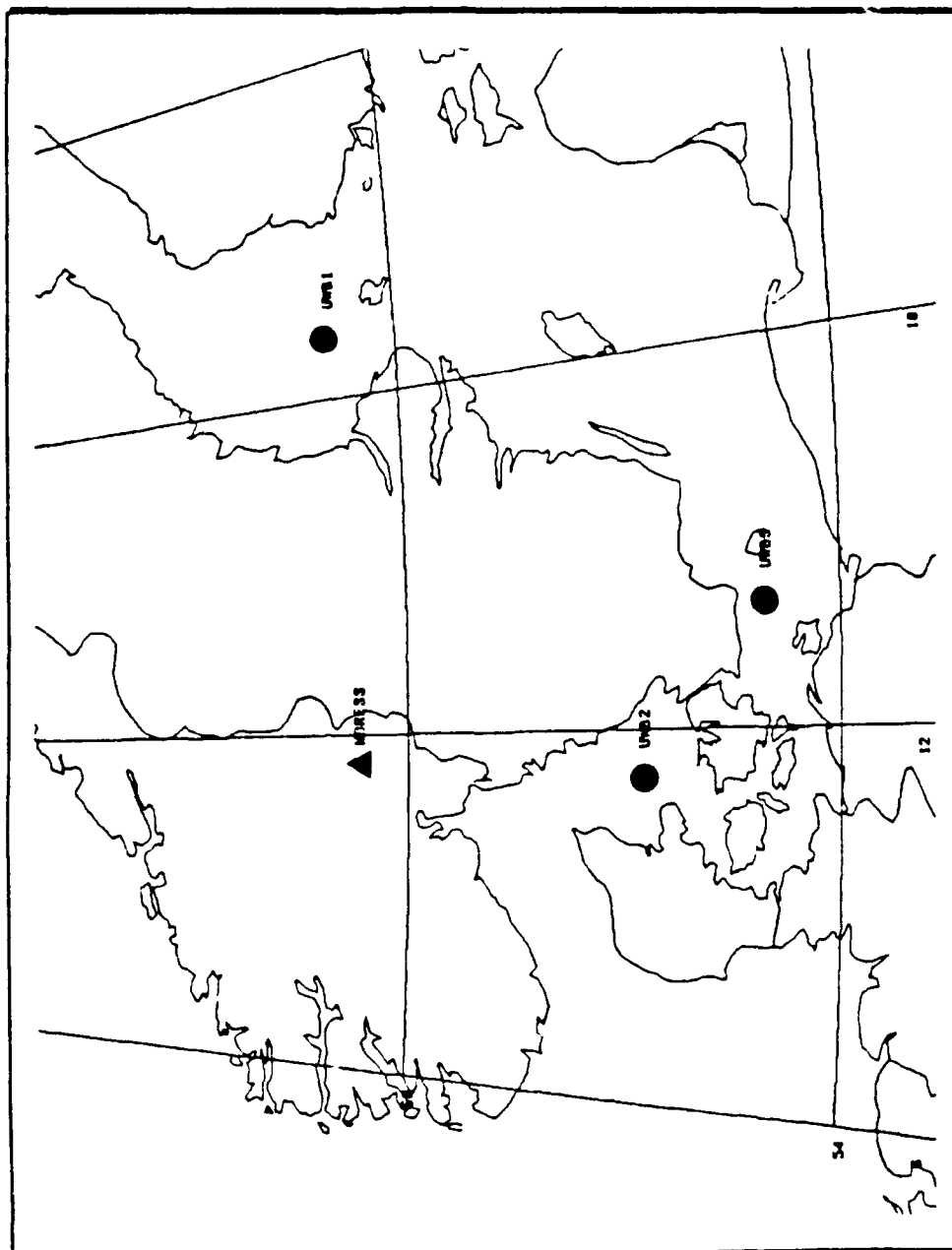
FIGURE 20: Map showing the locations of events which we presume are underwater blasts.
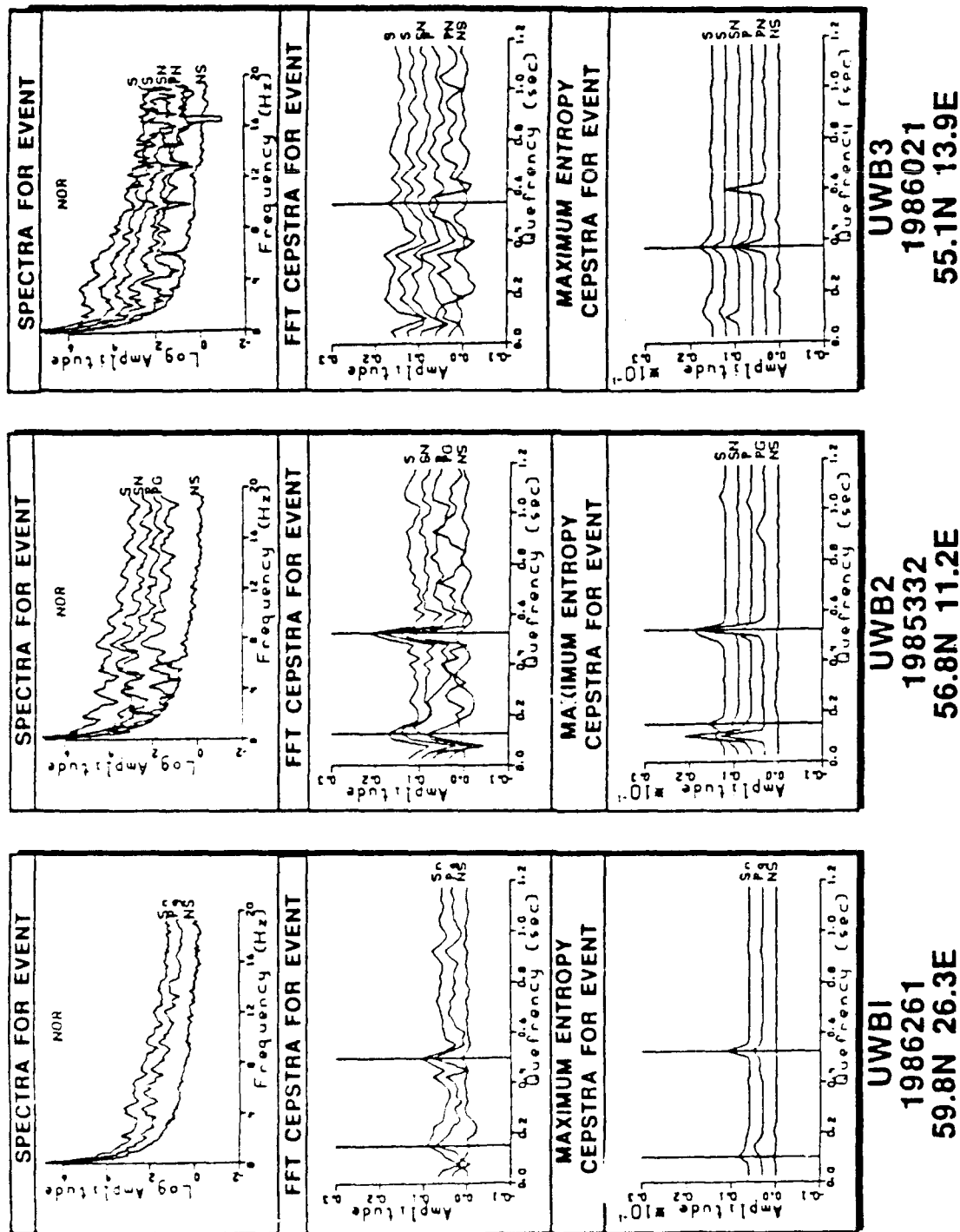
FIGURE 21: NORESS spectra and cepstra for the presumed underwater blasts shown on the map in Figure 20. Each event has a strong consistent modulation in the 0.4 to 0.6 second quefrency range.

We have decided to include the MERSY process in the ISEIS system as a model-based reasoning technique for identification of mine blasts and underwater blasts. The process will effectively identify all ripple-fired events with longest delays in excess of 0.05 seconds. The major features of the ISEIS version of MERSY is that the decision rules for determining if the cepstral peaks are significant and whether they are at the same quefrency for different phases will be coded in the expert system rather than in the actual MERSY code itself. This will enable us to change the rules in order to to make them more sensitive to weak modulations without unduly increasing the false alarm rate. We anticipate that the ISEIS version of MERSY will identify a greater number of ripple-fired blasts than the IAS version. What percentage of all events this method actually identifies will be of major interest in the evaluation of the effectiveness of MERSY and the ISEIS system overall.

SECTION 4.0

CASE-BASED REASONING: UTILITY OF DYNAMIC TIME WARPING (DTW) FOR REGIONAL EVENT CHARACTERIZATION

4.1 INTRODUCTION

In this section, we discuss one of the primary algorithms we plan to implement in ISEIS for case-based reasoning. We have observed in our analysis of regional coda shapes, in the form of incoherent beams computed for different frequency bands, that we can often identify event types from the distinctive shape of the coda. Thus, we plan to implement a matching algorithm for characterizing an event in terms of the similarity of its coda to those of nearby reference events.

Dynamic time warping (DTW) is an algorithm for matching toge   er time-series functions on dissimilar time scales. DTW has been developed in the speech processing field for word recognition. In this application, spoken words are recognized by matching a signal sequence for the unknown word against a set of template patterns for previously sampled words. Because the unknown word probably is spoken at a different speed than any of the template words, the time scale on the unknown word will also not match that of any of the templates. The time scales of either the unknown word or the template must be stretched or contracted in order to get the time scales to be aligned for matching purposes. DTW is a methodology for accomplishing this rescaling automatically.

The idea of applying DTW to seismic signal recognition was first investigated by Anderson (1981). Baumgardt (1987; 1990) suggested its use for recognizing regional seismic waveforms recorded at the regional seismic array, NORESS. As mentioned above, we have found that regional seismograms recorded at NORESS have very distinctive shapes, as revealed by incoherent-beam waveform envelopes. It has been possible, for example, to immediately tell the difference between western Norway mine blasts and earthquakes by examining the character of the

62

waveform shapes of the events. Baumgardt (1987; 1990) suggested matching incoherent beams using DTW to quantitatively estimate the similarity between two waveforms for discrimination purposes.

Given some new event of unknown identity, we wish to find all the previous case events which are most similar to it, in terms of the shape of its waveform in a set of prefiltered frequency bands. We match successively the incoherent beams or templates in different filter bands of the unknown event against the templates of various master events in the same frequency bands. The figure-of-merit for the matches, which is the distance of separation in log-rms units between the unknown event and the reference event, provides a quantitative measurement of how similar the unknown event is to the reference events. In this application, regional events that need to be matched may not occur at the same distance from the array as the reference events. Events at different distances would have different time delays between the various phases thus necessitating an algorithm which would scale the unknown event and/or the template event to a common time scale.

This section is a brief description of the algorithm and our initial results of applying the algorithm on a set of earthquakes and explosions in western Norway recorded at the NORESS array. These events were studied during a research project relating to applying case-based reasoning to seismic event identification (Baumgardt, 1990).

4.2 DYNAMIC TIME WARPING ALGORITHM

Dynamic time warping (DTW) is a dynamic programming algorithm used to find the optimal mapping of a test signal time axis and a reference signal time axis onto a common time axis. The approach we use is that suggested by Anderson (1981) based primarily on the work of Myers (1980).

We define the test signal as

$$T(n) = [t(n\ 1), t(n\ 2), t(n\ 3), ...]$$

and the reference signal is defined as

$$R(n) = [r(n\ 1), r(n\ 2), r(n\ 3), ...]$$

where t and n represent the value and time indices of the test signal and r and m are the same for the reference signal. In our application, T and R would be the incoherent beams in some filter frequency band for the new event to be identified and a reference event of known identity. For seismic incoherent-beam or envelope matching, we use log rms values computed within successive time windows in the seismogram and averaged across the array. Taking the logarithm of the rms values serves to enhance some of the envelope shape details in the envelope trace. Also, the difference values computed by DTW are in log units, which are related to log amplitude values commonly used to compute seismic magnitudes.

A warping function $c_{ij}(k)$, is defined which matches test signal index i with reference signal index i, or

$$c_{ij}(k) = [n(i), m(j)]$$

where k is the new time axis. Computing this function can be thought of as a path optimization problem, as illustrated in Figure 22. The time axes of the test and reference series represent the horizontal and vertical axes of the grid. The points in the matrix grid represent all possible match combinations (i,j) for the time points of the two time functions. If we just lined up the time-series and matched them point by point without time warping, we would be taking a diagonal linear path through the grid in Figure 22. Warping the time axes involves finding a non-linear, non-diagonal path through the grid which optimizes some match function between the two time-series.

64
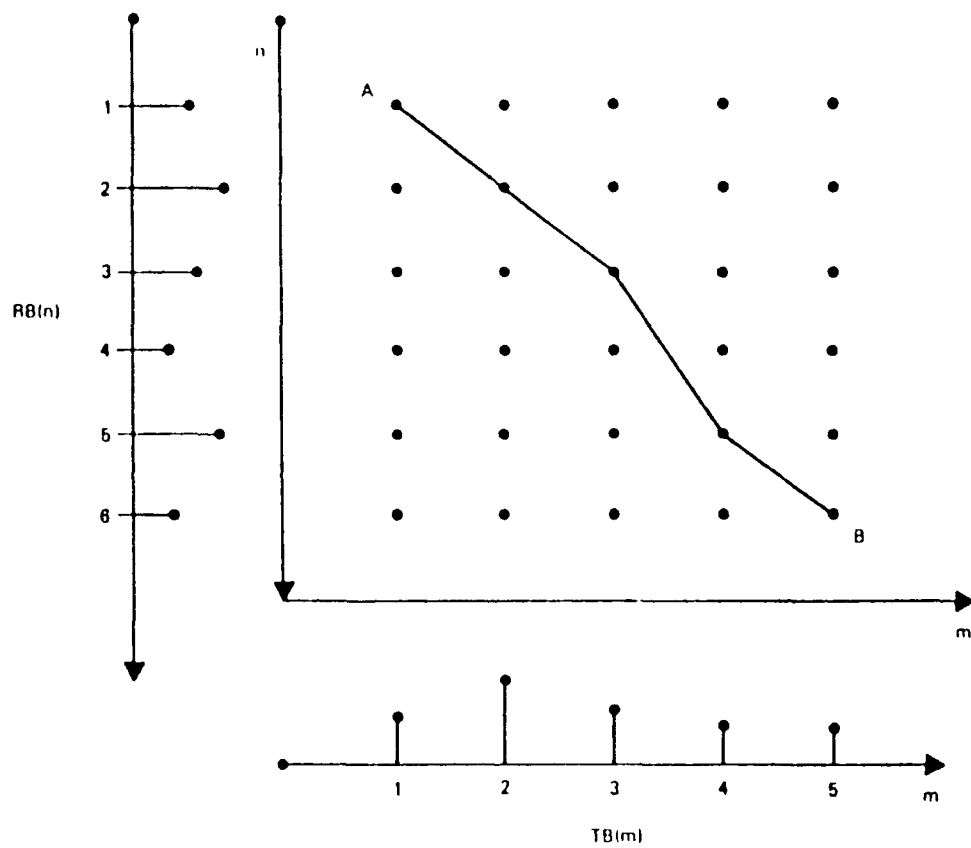
SCHEMATIC ILLUSTRATION OF DTW MATCH AS A PATH
MINIMIZA riON PROBLEM.

FIGURE 22: **Schematic illustration of DTW match as a path minimization problem.**

65

The optimal path through the grid is found by minimizing the accumulated distance function

$$D = \sum_{k=1}^{K} \frac{d\,[c\,(k)]\,W\,(k)}{N\,(k)}$$

where $c(k)$ is the warp function at grid point k (this defines the i,j values), $d\,[c(k)]$ is the local distance measure at this grid point, $W(k)$ is a local weighting function, and $N(k)$ is the corresponding normalization.

Solving the DTW problem requires specification of the following parameters (Myers, et al., 1978): (1) Local Distance measure, (2) Axis Orientation, (3) Endpoint Constraints, (4) Local Path Constraints, and (5) Global Path Constraints. In addition, $W(k)$ and N, the weighting function and corresponding normalization, must be specified. We have used the work of Anderson (1981) and Rabiner and Brown (1982) for our specifications of these constraints.

The DTW algorithm used for seismic template matching for the ISEIS project has the following specifications:

Local Distance Measure

The local distance measure for seismic template matching is given by Anderson (1981) as

$$d\,[T\,(c\,(k\,))\,R\,(c\,(k\,))] = |T\,(n\,(i\,)) - R\,(m\,(j\,))|$$

This means that the waveforms are aligned based on the area under their normalized envelopes.

Axis Orientation

Rabiner. et al (1978) report best performance with the test sequence index on the abscissa (independent variable) and the reference sequence index on the ordinate (dependent variable). as shown in Figure 22.

Endpoint Constraints

We require the path to obey the constraints $c(1) = 1$ and $c(N) = M$. This assumes the end points of the reference and test signals are accurately determined. We define the start point as the first phase onset. which is usually the Pn. Pg. or teleseismic P phase. and the end point as the place where the Lg phase drops a certain percent of its maximum. This assumption simplifies the optimum path problem.

Local Path Constraints

This constraint defines the movement from one point to another. Anderson (1981) found that the type II-d matching function given by Myers (1980) works reasonably well for seismic envelope matching. For this algorithm the valid paths are:

$$n (i). m (j) \rightarrow n (i-1). m (j - 1).$$

$$n (i). m (J) \rightarrow n (i-2). m (j-1).$$

$$n(i). m(j) \rightarrow n(i-1). m(j - 2).$$

Figure 23 shows these paths. This is a modified form of the local constraints in the symmetric DTW algorithm for a maximum slope value of two described by Itakura (1975). This type of movement through the grid allows for local continuity and ensures monotonically increasing time-series indices (Myers, 1980).
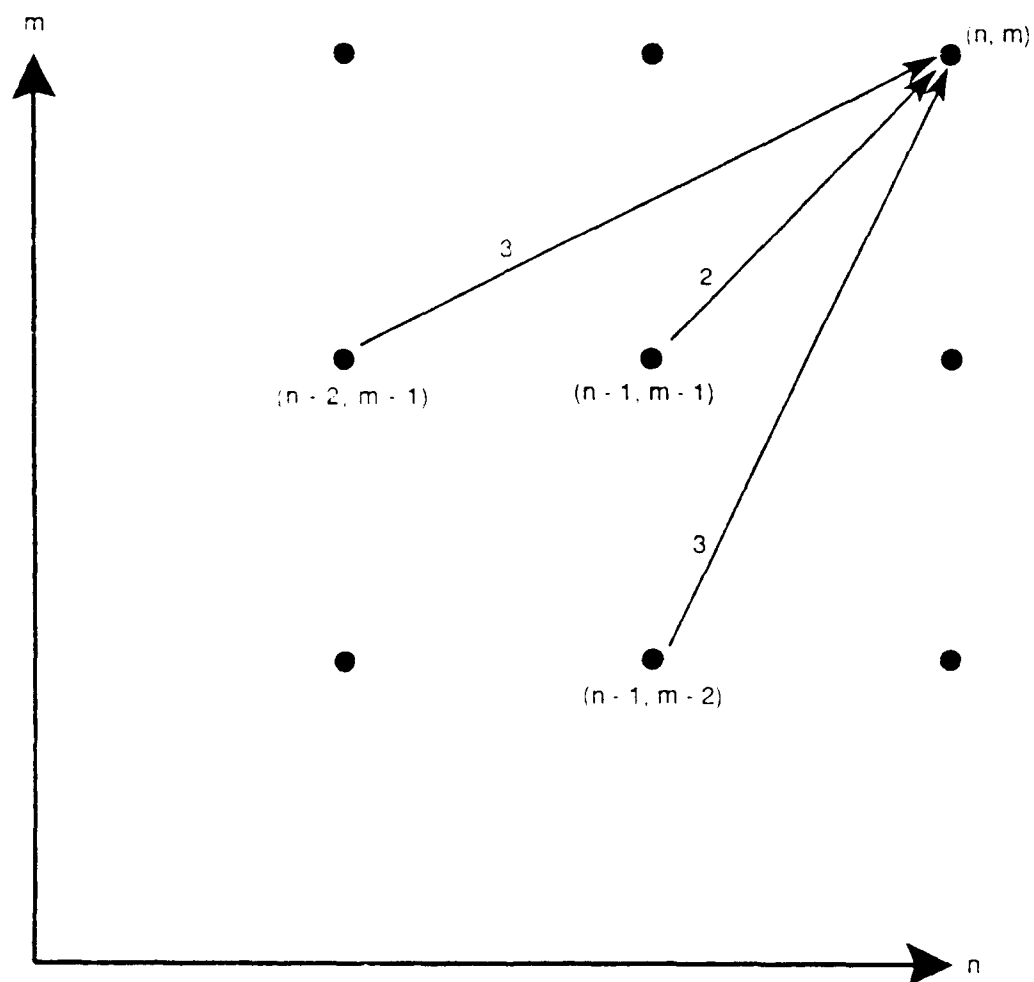
67

FIGURE 23: Allowed paths for movement through the DTW grid shown in Figure 22.

Global Path Constraints

These are limitations on where the path can wander in the grid. The slope constraint is a natural extension of the endpoint and local path constraints. An additional global constraint is added which keeps the warp factor between the two envelopes from becoming too large. It is defined by R where

$$|n(i) - m(j)| \le R$$

The combination of these global constraints describe a parallelogram on the grid which encloses all the points which could possibly occur in the path, as shown in Figure 24.

Weighting Function and Corresponding Normalization

We use the weighting function type DTW algorithm, defined by Myers (1980), which is

$$W(k) = n(i) - n(i-1) + m(j) - m(j-1)$$

Myers (1980) defines a normalization function which is independent of path in order to solve for the optimal path efficiently. This definition is

$$N = n(i) + m(j)$$

Finding the minimum for the accumulated distance function can be done by calculating the local distance at every grid point and then searching all possible paths from $(1,1)$ to (N, M). Alternatively, the accumulated distance can be computed using a dynamic programming technique (Myers, 1980). The dynamic programming principle used is that a globally optimal path is locally optimal. We can successively build the optimal path from smaller optimal paths (Bellman and Dreyfus, 1962). The dynamic programming technique and the constraints reduces significantly the number of computational operations over matching by complete search of all possible paths. Other techniques are currently being researched by the speech processing community to reduce the
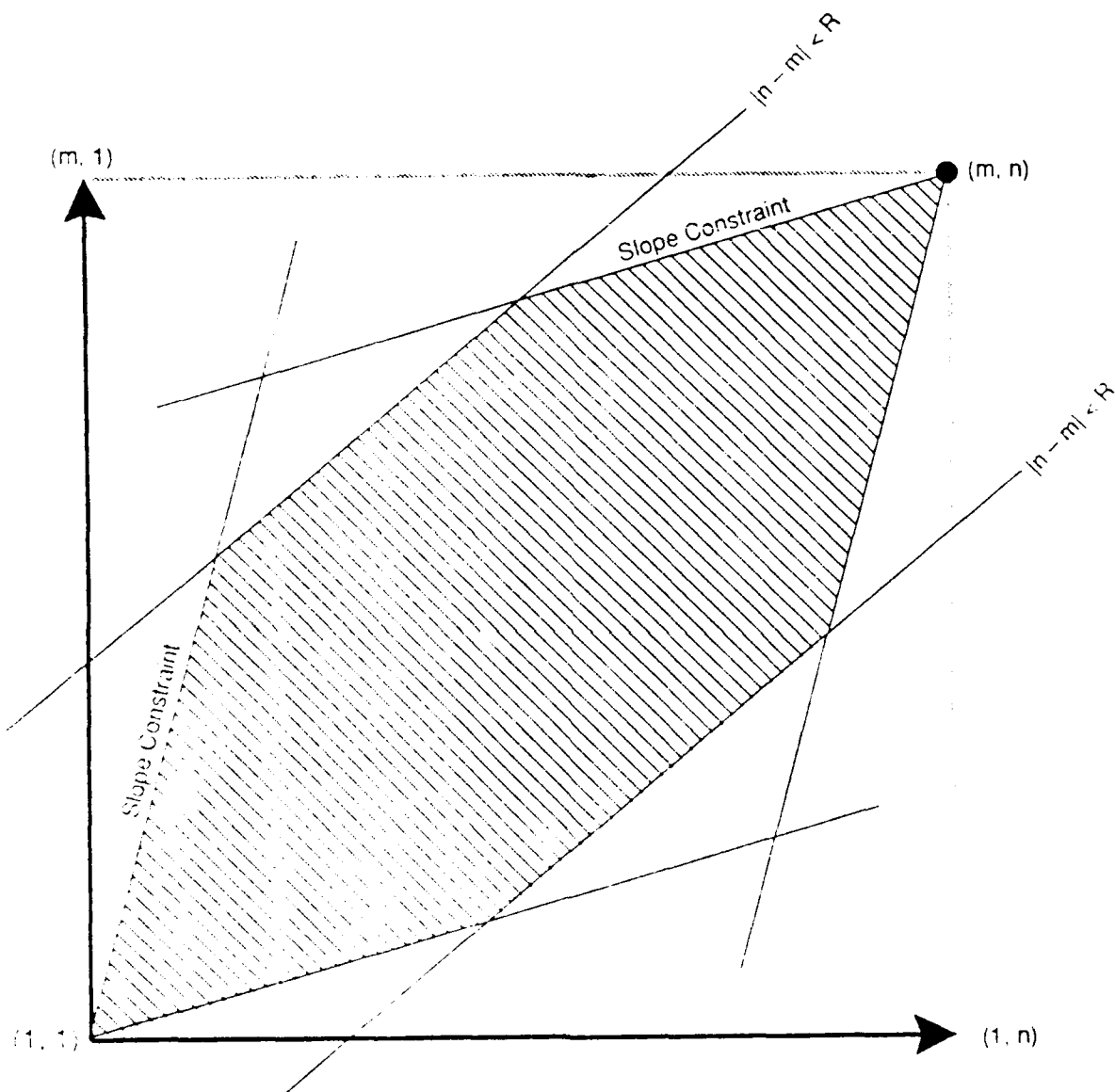
FIGURE 24: Slope constraints for the paths allowed for movement through the DTW grid shown in Figure 22.

number of operations for the grid search problem (Brown and Rabiner, 1982; Vidal et al. 1988). Other research has been directed towards implementing the DTW algorithm on array processors (e.g., Weste et al. 1983).

The DTW algorithm described by Myers (1980) computes a partial accumulated distance at each path point as it steps through the grid. The partial accumulated distance is defined recursively as

$$D_A[n(i), m(j)] = \begin{cases} D_A[n(i-1), m(j-1)] + 2d[n(i), m(j)] \\ D_A[n(i-2), m(j-1)] + 3d[n(i), m(j)] \\ D_A[n(i-1), m(j-2)] + 3d[n(i), m(j)] \end{cases}$$

where is the local distance measure, defined above. For each point in the path we store the partial accumulated distance, $D_A[n(i), m(j)]$, and the index of the previous grid point in the path. Then, at grid point, (N, M) the total accumulated distance is given by

$$D = D_A(N, M)/N$$

The normalization factor does not affect the location of the optimal path since it is defined as path independent (Myers, 1980).

The output accumulated distance value is a measure of the difference between the test waveform and the reference waveform. It takes into account the time alignment of the waveforms based on the area under their normalized envelopes. This DTW "score" can now be used in a nearest neighbor decision rule to find the best matching reference template or it can be used to cluster similar events.

4.3 APPLICATION TO WESTERN NORWAY EVENTS

In this section, we discuss the application of this algorithm to the western Norway events discussed in detail by Baumgardt (1990) and Baumgardt and Young (1990). The events are

shown on the map in Figure 25 reproduced from Baumgardt (1990). The events we originally believed to be earthquakes are labeled as "Q" on the map. However, Baumgardt and Young (1990) have argued that many of the "Q" events are actually blasts.

The event we chose as our unknown event is called eqa and occurred in the Stavanger region. This event is labeled as "U" on the map in Figure 25. (Note: This event is referred to as event U in Baumgardt (1990) and was changed to Q13 in Baumgardt and Young (1990).) Originally, we thought that this event was an earthquake because it was not reported as being a blast in the Bergen regional bulletin. However, the spectra for the regional phases all showed the same time-independent spectral modulations, which appeared to be produced by ripple-fire. Also, our studies of the S-to-P amplitude ratio discriminant revealed that the event has ratios more consistent with explosions than earthquakes. Thus, we concluded that the event was actually an unannounced blast.

DTW was run on a suite of incoherent beams, computed for eight filter-frequency bands, for the event eqa as the unknown event and all the other events as reference events. Figure 26 shows a flow diagram for the process. First, the incoherent beams are lined up in time. In this case, we lined up the templates on the first arrival Pn phase. Note that on each template, a phase identification defines a time interval, from the first break of the phase to the time when the next phase comes in. Then, the amplitudes are aligned on the Lg amplitude. The Lg phase was often, but not always, the maximum amplitude phase on the seismogram. Finally, all the points after Pn on the unknown event were matched up to reference event which is stretched in time sufficient to minimize the accumulated distances, as explained above.

Figure 27 shows a DTW solution for the match of the incoherent beam of this event, in the 8 to 16 Hz band, compared to a nearby earthquake, called eq-9. We are reasonably sure eq-9 was an earthquake because the local news media in Norway reported that it had been felt (Svein Mykkeltveit and Frode Ringdal, personal communication). The plot in Figure 27 shows the two

72
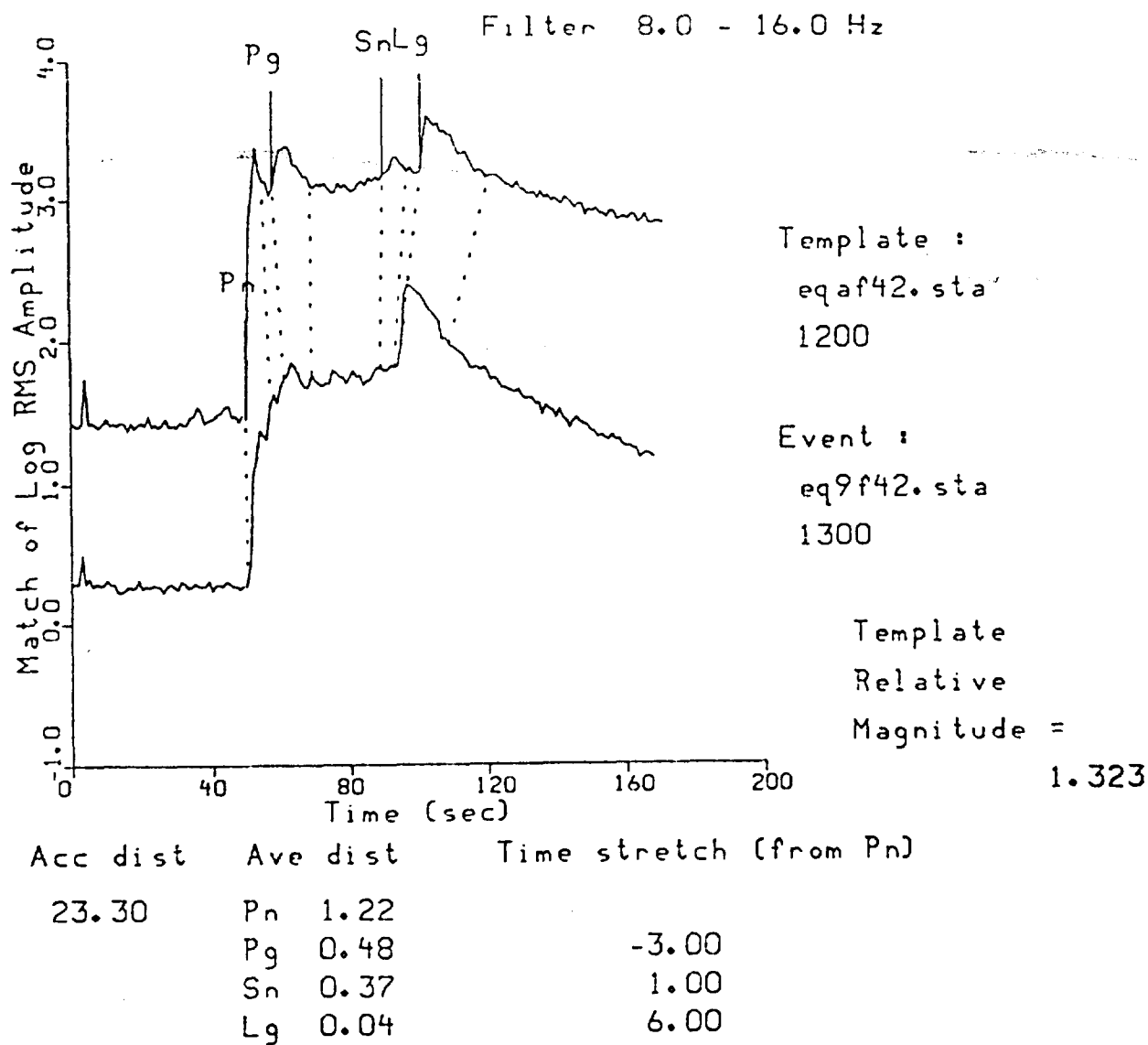
FIGURE 25: Map showing the locations of the events used in this study.

FIGURE 26: Flow diagram for the DTW algorithm.

FIGURE 27: Example of a DTW solution for the match of unknown event, eqa (top) against a known earthquake eq[9] (bottom).

incoherent beams for the events, with the phase identifications indicated. The dashed lines indicate the points, which mark the first and last point of each time interval assigned to each phase, that were connected by the DTW algorithm. At the bottom of the plot is a table showing the total accumulated distance, the average distance for the time interval assigned to each phase, and the time stretch, which is how much the time of each phase of the reference event (on the bottom) had to be warped for the envelopes to best match. To the right, the "Template Relative Magnitude" refers to the apparent difference in local magnitude based on the difference in the log-rms amplitudes of the Lg phases.

This result shows that the event eqa does not match the nearby earthquake very well. The biggest mismatch is in the Pn phase, which was 1.22 log units lower for eq-9 compared with our test event, eqa. This mismatch suggests that event eqa produced stronger Pn energy relative to Lg than the earthquake.

Figure 28 shows the DTW solution which gave the best match in the 8 to 16 Hz band, an event we called ql4. Interestingly, ql4 was not near event eqa and was in fact 316 km to the north. However, they both were almost exactly the same distance from NORESS, at 373 km. Event ql4 occurred due west of NORESS whereas event eqa was southwest. The DTW accumulated distance value was small (8.33) compared to the earthquake match in Figure 26. Also, visually, the incoherent beams look very similar. Baumgardt and Young (1990) also concluded that event ql4 was another unannounced blast, like eqa. This result shows that the presumed unannounced blasts have very similar waveforms and that their similarity, in spite of the fact that they are not in the same region, indicates that differences in propagation path do not have a great effect on the waveform characteristics of these events.

Figure 29 shows the comparison of the event with a known mine explosion, ex2, which occurred at the BLA site. This comparison is interesting because it is an example of a comparison of two events at very different distances: BLA is at 301 km whereas eqa was at 373 km. This 72
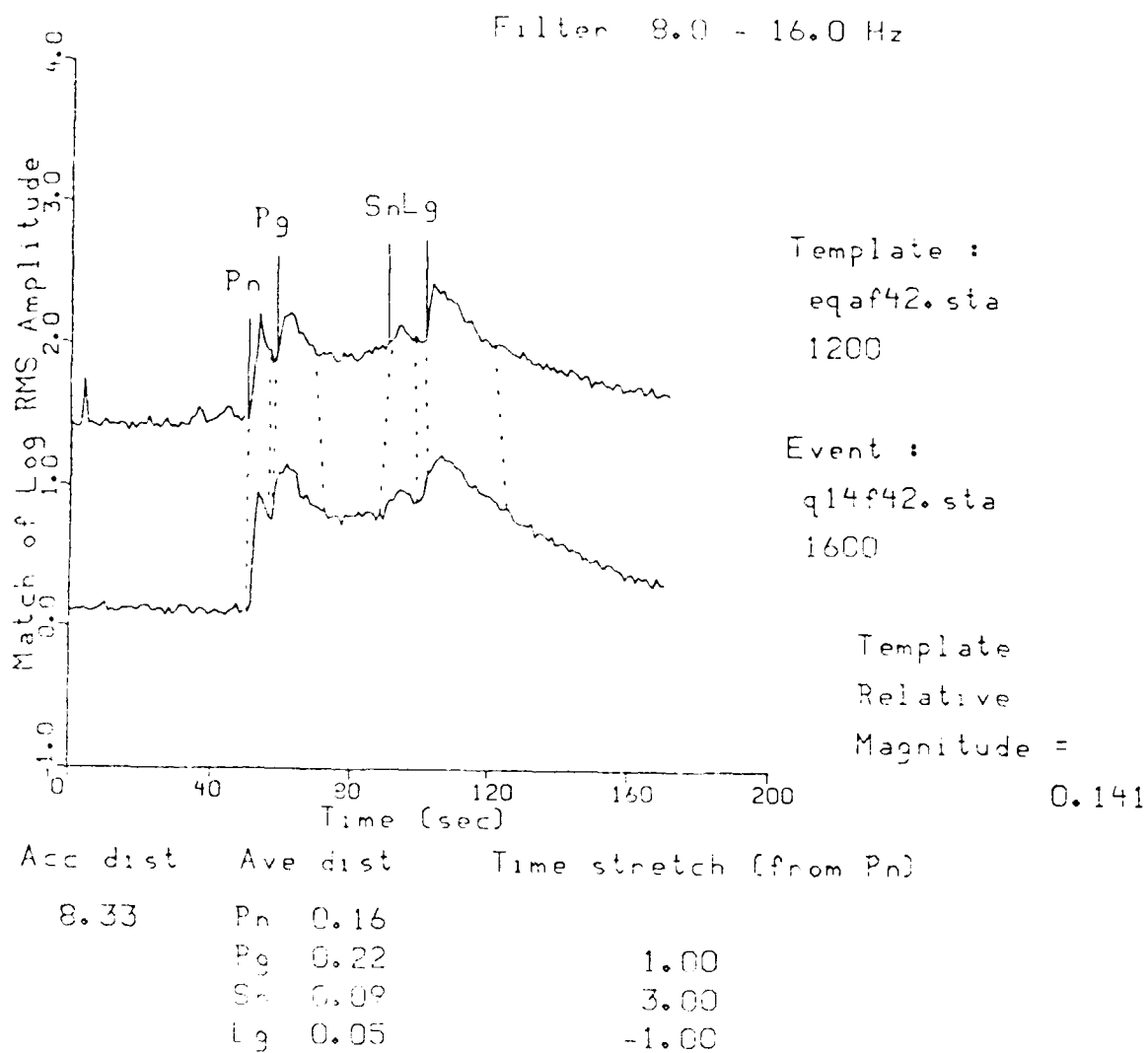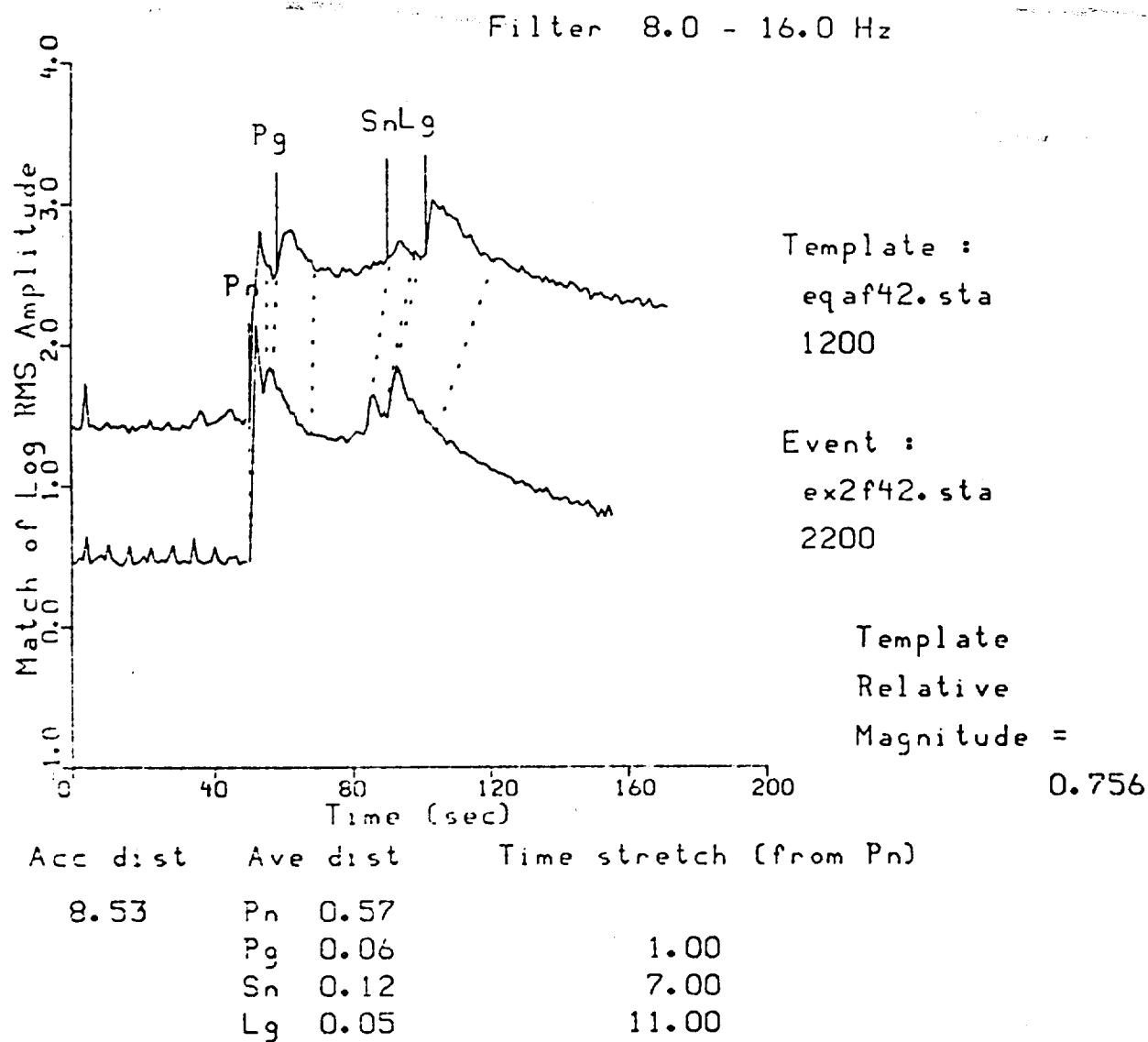
76

FIGURE 28: DTW solution for the best match to event eqa.

Filter 8.0 - 16.0 Hz

Pg

SnLg

Pn

Match of Log RMS Amplitude

4.0 3.0 2.0 1.0 0.0 1.0

0   40   80   120   160   200
Time (sec)

Template :
eqaf42.sta
1200

Event :
ex2f42.sta
2200

Template
Relative
Magnitude =
0.756

Acc dist   Ave dist   Time stretch (from Pn)

8.53   Pn 0.57
        Pg 0.06   1.00
        Sn 0.12   7.00
        Lg 0.05   11.00

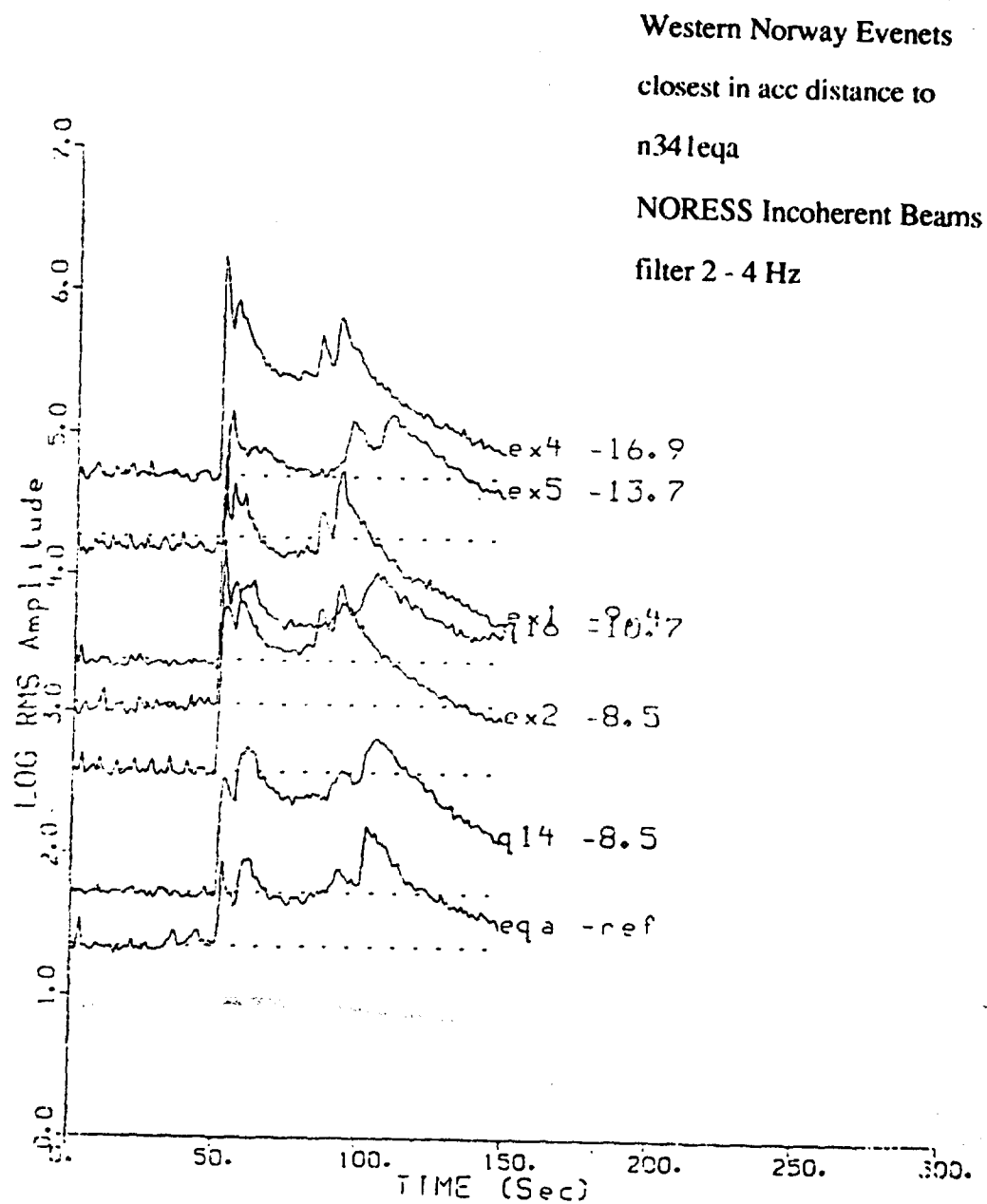**FIGURE 29:** DTW solution for the match of a known explosion, ex1, to the unknown event, eqa.

78

km difference in distance required that ex2 had to be stretched to attain the best match to eqa. As shown in Figure 29, the *Lg* of ex2 had to be warped by 11 seconds to get the best alignment. However, after doing this, the accumulated distance was 8.53 log rms units, which was the second smallest. Clearly, after time warping, eqa more closely resembles distant mine explosions than nearby earthquakes, which confirms the contention of Baumgardt (1990) and Baumgardt and Young (1990), based on other evidence, that eqa is an unannounced blast.

Figure 30 shows plots of the six best matching events to eqa in the 2 to 4 Hz band, with the incoherent beams plotted up in order of the accumulated distance of separation. Figure 31 shows the same display for the incoherent beams in the 8 to 16 Hz band. These plots show that essentially the same events match best in both frequency bands, except that the order is not always the same. We find that, for all the frequency bands, the events which match best were either known blasts or events which we strongly suspect are blasts, based on other evidence.

4.4 CONCLUSIONS

This study has demonstrated that DTW is a very useful method for quantitatively finding regional events which have similar waveforms. DTW has been implemented in ISEIS for the purpose of doing case-based reasoning to determine how similar an event is to previous events in the same region. Moreover, we also plan to use the identity of the best matching event templates to identify the new event if the cumulative distance of separation is less than a specified maximum threshold. For example, in our study, if we set the minimum separation distance at 10, we would find from Figure 31 that the best matching events were two known mine blasts (ex1 and ex2) and one strongly suspected blast (ql4). (Note: The event also matched well to ql6, with a distance of 10.7. We also believe that ql6 is an unannounced blast.) We also note that all known earthquakes matched with distances much greater than 10. Thus, we would conclude that event eqa is most likely a blast since it matches the explosion templates as a group more closely than the earthquake templates.

Western Norway Evenets

closest in acc distance to

n341eqa

NORESS Incoherent Beams

filter 2 - 4 Hz

FIGURE 30: The best matching templates in the 2 to 4 Hz band to the unknown event, eqa, shown at the bottom.
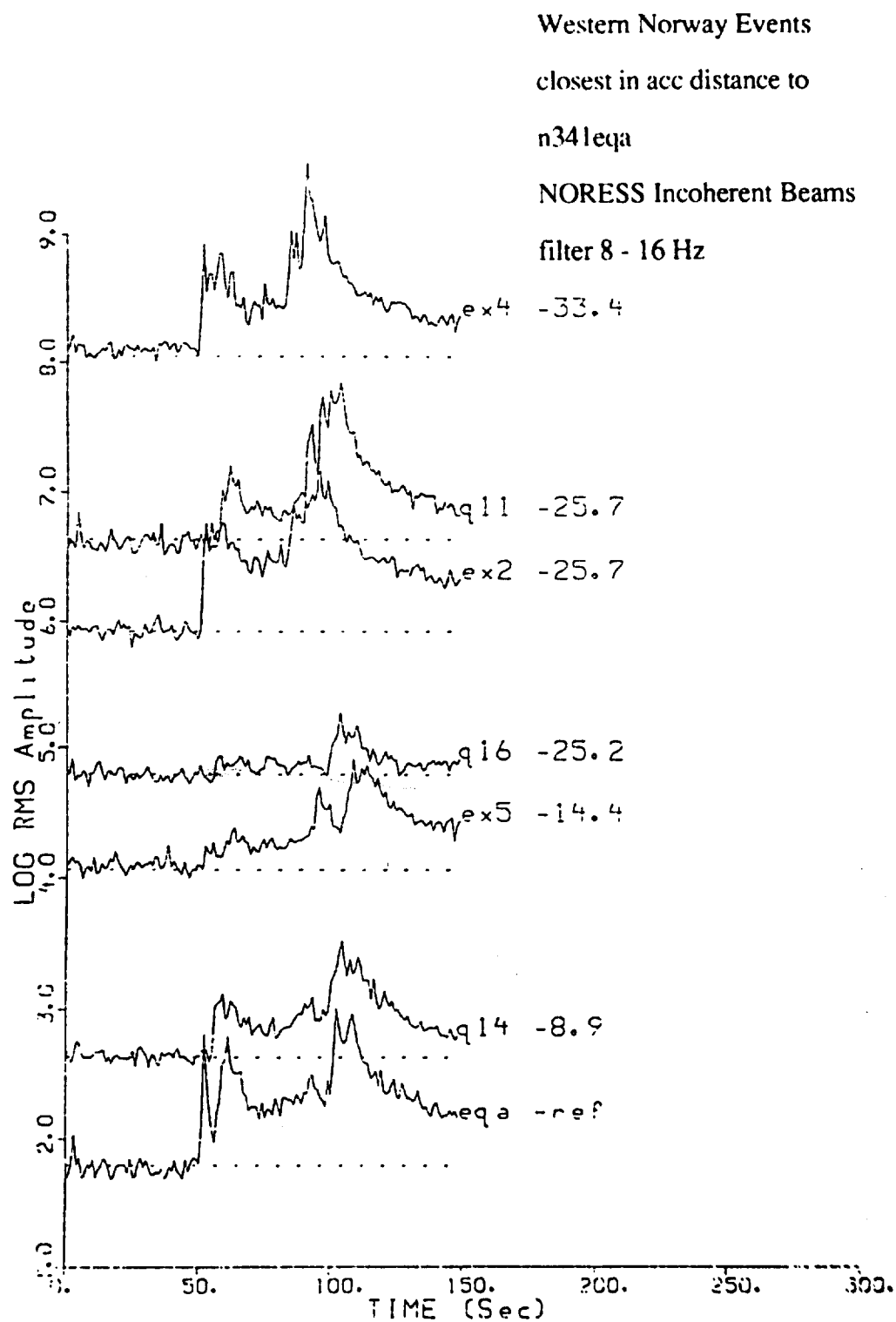
FIGURE 31: The best matching templates in the 8 to 16 Hz band to the unknown event, eqa, shown at the bottom.

SECTION 5.0

OVERALL CONCLUSIONS

This report has discussed some of the design and computational issues related to the ISEIS system. In this section, we summarize our conclusions.

System Design

(1)   The ISEIS approach to discrimination will be to test each individual event against a matrix of discriminants, rather than using the multivariate decision theory approach to discrimination. This approach will be facilitated by the spreadsheet display, discussed in Section 1.0 (Figure 4), where each column of the spreadsheet is a single discriminant and each row is an event being identified. A voting scheme will be developed where each discriminant makes an individual decision about the identity of the event at some confidence level. Then, each of the decisions is combined in a weighted average of the confidences and and overall decision about the events identity will be made.

(2)   Discriminants will be used to attempt to identify the event as a specific source type, i.e., earthquake, mine blast, underwater explosion, or other explosion. Otherwise, the event will be classed as unidentified. We refer to this type of event characterization as "model-based reasoning," or MBR. We recognize, however, that the science of seismic discrimination has not yet produced a completely reliable method for identifying seismic events. If events cannot be reliably identified, the events can still be compared to other events in the same region by comparing the waveform features of the event to be identified to those of nearby reference events. We call this kind of discrimination "case-based reasoning," or CBR. Moreover,

MBR and CBR can both be applied in a complementary manner to each event to completely characterize the event.

(3)   Certain discriminants can be used both in MBR and CBR. For example, the discriminants discussed in Section 2.0 could by applied in both ways. Amplitude ratios may be used to identify events as a specific event type. Also, they can be compared with amplitude ratios of reference events in CBR. Other discriminants, such as the ripple-fire detection method (MERSY) discussed in Section 3.0, probably only work as only as MBR methods. However, the DTW algorithm, described in Section 4.0, although primarily a waveform pattern matcher and thus a CBR method, could also be considered an MBR technique if the reference events are of known source type. Thus, if an event matched best, say, to mine-blast coda shapes in the same region, the event could be classed as a mine blast, an MBR type classification, even though a CBR matching method has been used to make the decision.

(4)   We consider effective explanation displays to be an important feature of ISEIS. Users must be able to get adequate explanations of the processing results at some level. The ISEIS system will provide different levels of explanation, where the highest level, such as the map or spreadsheet, would provide broad, summary views of the event characterization results, whereas the lowest levels would give more detailed descriptions (e.g., textual descriptions, graphs, scatter plots) of the processing results.

(5)   Because of the incomplete knowledge of seismic discrimination and the on-going research in this field, ISEIS need to be flexible enough to be easily modified to include new discriminants and to change or remove existing discriminants. To this end, ISEIS is being designed to be a modular system, with the signal analysis

processing being separated from the discriminant decision processing. This separation will be effected by coding the decision criteria as CLIPS rules in a modifiable knowledge base of an expert system. Thus, the signal analysis functions would compute many features for all detected phases which would be stored in the database, but the rules may only look at some of the features. In fact, the rules themselves will be treated as data and be read in from the database by the system along with waveform feature data. After more data has been analyzed, perhaps using some of the low-level displays of ISEIS, other features than those currently reasoned on by the rules may be found that are more effective. We may find also that certain discriminants work well in one geographic region, but less well in another, perhaps because of propagation path effects. Moreover, the threshold values for discriminant decisions may differ from one region to another. Thus, the rules can be modified or new blocks of rules can be added in the form of a new discriminant or premises added to old rules to make them region specific. Because the rules are separated from the signal processing algorithms and are treated as data, changing rules or adding new rules will not require a complete change and recompilation of existing code, making ISEIS a flexible system which can easily be changed as new discrimination knowledge is obtained.

Discriminants

(1)   As mentioned above and in Section 2.0, our knowledge of regional discrimination is at best problematic. Thus initially, ISEIS will be designed to include a set of discriminants which look promising now based on the most recent research. However, ISEIS will be designed to be flexible enough to be easily modified to take advantage of the results of new research in the field. In fact, the processing and display capabilities of ISEIS and its access to expanded databases will make a useful research tool in seismic discrimination.

(2)   The initial prototype of ISEIS will be primarily designed to process small events at regional seismic distances. Teleseismic discrimination will be less emphasized, although it has been more researched and may be important in event identification in third countries (i.e., not the Soviet Union) where there are limited in-country seismic assets. We consider it beyond the scope of ISEIS to include the signal analysis techniques needed for teleseismic discrimination, such as, for example computation of Ms or mb, location and depth estimation, since these processes will be accomplished by the front-end NMRD processes. However, ISEIS will have access to this data through the Oracle database and can include rules for teleseismic discrimination. Our current plan is to include rules in ISEIS for the teleseismic discriminants, Ms-mb and depth, if this information is available in the database.

(3)   Based on our research, described in Section 2.0 and those of other workers in the field, we have found the relative excitation of regional P and S waves to provide the greatest discriminatory power, although we have seen regional variations in these amplitudes which are undoubtedly caused by lateral variations of propagation effects. Initially, we plan to include at least two discriminants based on high-frequency amplitude ratios, Pn/Sn and Pn/Lg. The initial rules will be designed to best identify events in western Norway recorded at NORESS, since this is the region for which we currently have the most data. As ISEIS is run on more data in future, these discriminants will be made region specific.

(4) Lg spectral ratio proved to be less useful as a discriminant, for currently unknown reasons. However, ISEIS will still be designed to include this discriminant, although it may be weighted less than other discriminants in an overall decision about the identity of the event. Moreover, spectral ratio computations will be made on all other regional phases and will be available for display for research purposes.

We will also include a path-correction scheme, which can be used to correct spectral ratios for the effects of anelastic attenuation along the path. Again, a regionalization scheme is being developed which will allow region-specific path corrections to be included.

(5)   We believe the ripple-fire detector method, MERSY, to be a very useful technique for the detection of non-nuclear, chemical blasts, if they are ripple-fired. Moreover, blasting underwater may be also identified, based on spectral modulations produced by bubble-pulse interference. Of course, blasts underwater could still be nuclear, and this method alone cannot insure that any kind of blasting is not nuclear. The method has proven to be effective for identifying many ripple-fired chemical and will at least ensure that such small events are not incorrectly identified as earthquakes or just classed as unidentified.

(6)   DTW will be implemented as our primary CBR method. However, the algorithm must still be regarded as experimental, although our initial tests of the technique have been promising. The method can only be applied for events which have nearby reference events or reference events at comparable distance. Also, DTW can only be applied to events which have relative clear, uncontaminated codas. Thus, DTW could not actually be applied to events which have interfering events. For this reason, adequate displays of the DTW results will be provided to the user to judge the validity of the match based on the visual appearance of the codas themselves.

(7)   For contaminated events, other case-based methods than DTW will be developed to match feature measurement to those of reference events. Our current plan is to use the "script-matching" approach described by Baumgardt (1987) and Kandt et al (1987) as a CBR method for all waveform type discriminants (not including

MERSY), where we compute the confidence of match between a feature for the "current event" being identified and average feature values of all the reference events in the same region. A regionalization scheme is being developed in which each reference event will be tied to a specific reference geographic region. The new event feature will then be matched to the average of the reference-event features for the region that the new event is in or located closest to it. The confidence of match will then be reasoned on by CBR rules to determine if the event is similar or dissimilar to the reference events.

REFERENCES

Anderson, K.R. (1981). Dynamic waveform matching, Seismic Discrimination Report, Lincoln Laboratory, MIT, ESD-TR-339, September 1981, Cambridge, MA, ADA116884.

Anderson, J., W.E. Farrell, K. Garcia, J. Given, H. Swanger (1990). Center for Seismic Studies Version 3 database: schema reference manual, Technical Report, C90-01, Center for Seismic Studies, Arlington, VA.

Bache, T.C. (1990). Intelligent Array System, System Introduction and Functional Description, SAIC, Inc., San Diego, CA.

Baumgardt, D.R. (1987). Case-based reasoning applied to regional seismic event characterization, Proceedings of DARPA/AFGL Seismic Research Symposium, Harbor House, Nantucket, MA. 15-18 June 1987, 173-178.

Baumgardt, D.R. (1990). Knowledge-based seismic event identification using seismic event case knowledge and explanations, Technical Report, SAS-TR-90-36, ENSCO, Inc., Springfield, VA.

Baumgardt, D.R. and G.B. Young (1990). Regional seismic waveform discriminants and case-based event identification using regional arrays, Bull. Seism. Soc. Am., 80, 1874-1892.

Baumgardt, D.R. and K.A. Ziegler (1988). Spectral evidence of source multiplicity in explosions: application to regional discrimination of earthquakes and explosions, Bull. Seism. Soc. Am., 78, 1773-1795.

Baumgardt, D.R. and K.A. Ziegler (1989). Automatic recognition of economic and underwater blasts using regional array data, Unpublished report to Science Applications Incorporated, 11-880085-51, ENSCO, Inc., Springfield, VA.

Bell, A.G. and S.S. Alexander (1977). A digital technique for detection of multiple seismic events, EOS, 57, 444.

Bellman, R., and S. Dreyfus (1962). Applied Dynamic Programming, Princeton University Press, Princeton, NJ.

Bennett, T.J. and J.R. Murphy (1986). Analysis of seismic discrimination capabilities using regional data from western United States events, Bull. Seism. Soc. Am., 76, 1069-1086.

Bennett, T.J., B.W. Barker, K.L. McLaughlin, and J.R. Murphy (1989). Regional discrimination of quarry blasts, earthquakes and underground nuclear explosions, Final Report, GL-TR-89-0114, S-Cubed, La Jolla, CA, ADA223148.

Blandford (1975). A source theory for complex earthquakes, Bull. Seism. Soc. Am., 65, 1385-1405

Blandford, R.R. (1981). Seismic discrimination problems at regional distances, in Identification of Seismic Sources - Earthquake or Underground Explosion, E.S. Husebye and S. Mykkeltveit (eds.), 695-740.

Brown, J.K. and L.R. Rabiner (1982). An adaptive, ordered graph search technique for dynamic time warping for isolated word recognition, IEEE Trans. Am., ASSP-30, 535-544.

Burg, J.P. (1967). Maximum entropy spectral analysis, presented at the 37th Annual International SEG Meeting, Oklahoma City, October 31, 1967.

Chen, W.Y. and G.R. Stegen (1974). Experiments with maximum entropy power spectra of sinusoids, *J. Geophys. Res.*, **79**, 3019-3022.

Chael, E.P. and R.P. Cromer (1988). High-frequency spectral scaling of a mainshock/aftershock sequence near the Norwegian coast, *Bull. Seism. Soc. Am.*, **78**, 561-570.

ENSCO, Inc. (1988). Requirements of the IAS Multiple Event Recognition System, ENSCO, Inc., Springfield, VA.

Hansen, R.A., H. Bungum and A. Alsaker (1989). Three recent larger earthquakes off-shore Norway, *Terra Motae*, **1**, 284-295.

Hedlin, M.A., J. Bernard Minster, and J.A. Orcutt (1989). The time-frequency characteristics of quarry blasts and calibration explosions recorded in Kazakhstan, USSR. *Geophys. J. Int.*, **99**, 109-121.

Hedlin, M.A., J. Bernard Minster, and J.A. Orcutt (1990). An automatic means to discriminate between earthquakes and quarry blasts. *Bull. Seism. Soc. Am.*, **80**, Part B, 2143-2160.

Itakura, F. (1975). Minimum prediction residual principle applied to speech recognition, *IEEE Trans. ASSP*, **ASSP-23**, 67-72.

Kandt, K., P. Yuenger, and D. Baumgardt (1987). Intelligent analysis of seismic events, *Proceedings of ESIG-Third Annual Expert Systems in Government Conference*, Washington, D.C., October 19-23, 1987.

Kaveh, M. and G.A. Lippert (1983). An optimum tapered Burg algorithm for linear prediction and spectral analysis, *IEEE Trans. Accoust., Speech, Signal Processing*, **ASSP-31**, 438-444.

Lilwall, R.C. (1988). Regional m_b : M_S, Lg/Pg amplitude ratios and Lg spectral ratios as criteria for distinguishing between earthquakes and explosions: a theoretical study, *Geophys. J.*, **93**, 137-147.

Mettrey, W. (1991). A comparative evaluation of expert system tools, *Computer*, **24**, 19-31.

Murphy, J.R. and T.J. Bennett (1982). A discrimination analysis of short-period regional seismic data recorded at Tonto Forest Observatory, *Bull. Seism Soc. Am.*, **72**, 1351-1366.

Myers, C.S., L.R. Rabiner, and A.E. Rosenberg (1978). Performance tradeoffs in dynamic time warping algorithms for isolated word recognition, *IEEE Trans. ASSP*, ASSP-26, 575-582.

Myers, C.S. (1980). *A comparative study of several dynamic time warping algorithms for speech recognition*. Master Thesis, MIT, Cambridge, MA.

NASA (1989). *CLIPS Reference Manual*, Version 4.3 of CLIPS, Artificial Intelligence Section, Lyndon B. Johnson Space Center, JSC 22948.

Nuttli, O.W. (1981). On the attenuation of Lg waves in western and central Asia and their use as a discriminant between earthquakes and explosions, *Bull. Seism. Soc. Am.*, **71**, 249-261.

Pomeroy, P.W., W.J. Best and T.V. McEvilly (1982). Testban treaty verification with regional data - a review, *Bull. Seism. Soc. Am.*, **72**, S89-S129.

Pulli, J.J., and P.S. Dysart (1987). Spectral study of regional earthquakes and chemical explosions recorded at the NORESS array, Technical Report, *C87-03*, Center for Seismic Studies, Arlington, VA.

Rabiner, L.R., A.E. Rosenberg, and S.E. Levinson(1978). Considerations in dynamic time warping for discrete word recognition, *IEEE Trans. Acoust. Speech. Signal Proc.*, ASSP-26, 575-582.

Smith, A.T. (1989). High-frequency seismic observations and models of chemical explosions: Implications for the discrimination of ripple-fired mining blasts, *Bull. Seism. Soc. Am.*, **79**, 1089-1110.

Stump, B.W. and R.E. Reinke (1988). Experimental confirmation of superposition from small scale explosions, *Bull. Seism. Soc. Am.*, **78**, 1059-1073.

Suteau-Henson, A. and T.C. Bache (1988). Spectral characteristics of regional phases recorded at NORESS, *Bull. Seism. Soc. Am.*, **78**, 708-725.

Taylor, S.R., N.W. Sherman, and M.D. Denny (1988). Spectral discrimination between NTS explosions and western U.S. earthquakes at regional distances, *Bull. Seism. Soc. Am.*, **78**, 1563-1579.

Taylor, S.R., M.D. Denny, E.S. Vergino, and R.E. Glaser (1989). Regional discrimination between NTS explosions and western U.S. earthquakes, *Bull. Seism. Soc. Am.*, **79**, 1142-1176.

Vidal, E. et al (1988). On the use of a metric-space search algorithm (AESA) for fast DTW-based recognition of isolated words, *IEEE Trans. ASSP*, ASSP-36, 651-660.

Weste, N., D.J. Burr, and B.D. Ackland (1983). Dynamic time warp pattern matching using an integrated multiprocessing array, *IEEE Trans. on Comp.*, C-32, 731-744.

Prof. Thomas Ahrens
Seismological Lab, 252-21
Division of Geological & Planetary Sciences
California Institute of Technology
Pasadena, CA 91125

Prof. Keiiti Aki
Center for Earth Sciences
University of Southern California
University Park
Los Angeles, CA 90089-0741

Prof. Shelton Alexander
Geosciences Department
403 Deike Building
The Pennsylvania State University
University Park, PA 16802

Dr. Ralph Alewine, III
DARPA/NMRO
3701 North Fairfax Drive
Arlington, VA 22203-1714

Prof. Charles B. Archambeau
CIRES
University of Colorado
Boulder, CO 80309

Dr. Thomas C. Bache, Jr.
Science Applications Int'l Corp.
10260 Campus Point Drive
San Diego, CA 92121 (2 copies)

Prof. Muawia Barazangi
Institute for the Study of the Continent
Cornell University
Ithaca, NY 14853

Dr. Jeff Barker
Department of Geological Sciences
State University of New York
 at Binghamton
Vestal, NY 13901

Dr. Douglas R. Baumgardt
ENSCO, Inc
5400 Port Royal Road
Springfield, VA 22151-2388

Dr. Susan Beck
Department of Geosciences
Building #77
University of Arizona
Tuscon, AZ 85721

Dr. T.J. Bennett
S-CUBED
A Division of Maxwell Laboratories
11800 Sunrise Valley Drive, Suite 1450
Reston, VA 22091

Dr. Robert Blandford
AFTAC/TT, Center for Seismic Studies
1330 North 17th Street
Suite 1450
Arlington, VA 22209-2308

Dr. G.A. Bollinger
Department of Geological Sciences
Virginia Polytechnical Institute
21044 Derring Hall
Blacksburg, VA 24061

Dr. Stephen Bratt
Center for Seismic Studies
1300 North 17th Street
Suite 1450
Arlington, VA 22209-2308

Dr. Lawrence Burdick
Woodward-Clyde Consultants
566 El Dorado Street
Pasadena, CA 91109-3245

Dr. Robert Burridge
Schlumberger-Doll Research Center
Old Quarry Road
Ridgefield, CT 06877

Dr. Jerry Carter
Center for Seismic Studies
1300 North 17th Street
Suite 1450
Arlington, VA 22209-2308

Eric Chael
Division 9241
Sandia Laboratory
Albuquerque, NM 87185

Prof. Vernon F. Cormier
Department of Geology & Geophysics
U-45, Room 207
University of Connecticut
Storrs, CT 06268

Prof. Anton Dainty
Earth Resources Laboratory
Massachusetts Institute of Technology
42 Carleton Street
Cambridge, MA 02142

1

Prof. Steven Day
Department of Geological Sciences
San Diego State University
San Diego, CA 92182

Art Frankel
U.S. Geological Survey
922 National Center
Reston, VA 22092

Marvin Denny
U.S. Department of Energy
Office of Arms Control
Washington, DC 20585

Dr. Cliff Frolich
Institute of Geophysics
8701 North Mopac
Austin, TX 78759

Dr. Zoltan Der
ENSCO, Inc.
5400 Port Royal Road
Springfield, VA 22151-2388

Dr. Holly Given
IGPP, A-025
Scripps Institute of Oceanography
University of California, San Diego
La Jolla, CA 92093

Prof. Adam Dziewonski
Hoffman Laboratory, Harvard University
Dept. of Earth Atmos. & Planetary Sciences
20 Oxford Street
Cambridge, MA 02138

Dr. Jeffrey W. Given
SAIC
10260 Campus Point Drive
San Diego, CA 92121

Prof. John Ebel
Department of Geology & Geophysics
Boston College
Chestnut Hill, MA 02167

Dr. Dale Glover
Defense Intelligence Agency
ATTN: ODT-1B
Washington, DC 20301

Eric Fielding
SNEE Hall
INSTOC
Cornell University
Ithaca, NY 14853

Dr. Indra Gupta
Teledyne Geotech
314 Montgomery Street
Alexanderia, VA 22314

Dr. Mark D. Fisk
Mission Research Corporation
735 State Street
P.O. Drawer 719
Santa Barbara, CA 93102

Dan N. Hagedon
Pacific Northwest Laboratories
Battelle Boulevard
Richland, WA 99352

Prof Stanley Flatte
Applied Sciences Building
University of California, Santa Cruz
Santa Cruz, CA95064

Dr. James Hannon
Lawrence Livermore National Laboratory
P.O. Box 808
L-205
Livermore, CA 94550

Dr. John Foley
NER-Geo Sciences
1100 Crown Colony Drive
Quincy, MA 02169

Dr. Roger Hansen
AFTAC/TTR
Patrick AFB, FL 32925

Prof. Donald Forsyth
Department of Geological Sciences
Brown University
Providence, RI 02912

Prof. David G. Harkrider
Seismological Laboratory
Division of Geological & Planetary Sciences
California Institute of Technology
Pasadena, CA 91125

Prof. Danny Harvey
CIRES
University of Colorado
Boulder, CO 80309

Prof. Donald V. Helmberger
Seismological Laboratory
Division of Geological & Planetary Sciences
California Institute of Technology
Pasadena, CA 91125

Prof. Eugene Herrin
Institute for the Study of Earth and Man
Geophysical Laboratory
Southern Methodist University
Dallas, TX 75275

Prof. Robert B. Herrmann
Department of Earth & Atmospheric Sciences
St. Louis University
St. Louis, MO 63156

Prof. Lane R. Johnson
Seismographic Station
University of California
Berkeley, CA 94720

Prof. Thomas H. Jordan
Department of Earth, Atmospheric &
  Planetary Sciences
Massachusetts Institute of Technology
Cambridge, MA 02139

Prof. Alan Kafka
Department of Geology & Geophysics
Boston College
Chestnut Hill, MA 02167

Robert C. Kemerait
ENSCO, Inc.
445 Pineda Court
Melbourne , FL 32940

Dr. Max Koontz
U.S. Dept. of Energy/DP 5
Forrestal Building
1000 Independence Avenue
Washington, DC 20585

Dr. Richard LaCoss
MIT Lincoln Laboratory, M-200B
P.O. Box 73
Lexington, MA 02173-0073

Dr. Fred K. Lamb
University of Illinois at Urbana-Champaign
Department of Physics
1110 West Green Street
Urbana, IL 61801

Prof. Charles A. Langston
Geosciences Department
403 Deike Building
The Pennsylvania State University
University Park, PA 16802

Prof. Thorne Lay
Institute of Tectonics
Earth Science Board
University of California, Santa Cruz
Santa Cruz, CA 95064

Dr. William Leith
U.S. Geological Survey
Mail Stop 928
Reston, VA 22092

James F. Lewkowicz
Phillips Laboratory/GPEH
Hanscom AFB, MA 01731-5000

Mr. Alfred Lieberman
ACDA/VI-OA State Department Building
Room 5726
320-21st Street, NW
Washington, DC 20451

Prof. L. Timothy Long
School of Geophysical Sciences
Georgia Institute of Technology
Atlanta, GA 30332

Dr. Robert Masse
Denver Federal Building
Box 25046, Mail Stop 967
Denver, CO 80225

Dr. Randolph Martin, III
New England Research, Inc.
76 Olcott Drive
White River Junction, VT 05001

Dr. Gary McCartor
Department of Physics
Southern Methodist University
Dallas, TX 75275

Prof. Thomas V. McEvilly
Seismographic Station
University of California
Berkeley, CA 94720

Prof. John A. Orcutt
IGPP, A-025
Scripps Institute of Oceanography
University of California, San Diego
La Jolla, CA 92093

Prof. Art McGarr
U.S. Geological Survey
Mail Stop 977
U.S. Geological Survey
Menlo Park, CA 94025

Prof. Jeffrey Park
Kline Geology Laboratory
P.O. Box 6666
New Haven, CT 06511-8130

Dr. Keith L. McLaughlin
S-CUBED
A Division of Maxwell Laboratory
P.O. Box 1620
La Jolla, CA 92038-1620

Howard Patton
Lawrence Livermore National Laboratory
L-025
P.O. Box 808
Livermore, CA 94550

Stephen Miller & Dr. Alexander Florence
SRI International
333 Ravenswood Avenue
Box AF 116
Menlo Park, CA 94025-3493

Dr. Frank Pilotte
HQ AFTAC/TT
Patrick AFB, FL 32925-6001

Prof. Bernard Minster
IGPP, A-025
Scripps Institute of Oceanography
University of California, San Diego
La Jolla, CA 92093

Dr. Jay J. Pulli
Radix Systems, Inc.
2 Taft Court, Suite 203
Rockville, MD 20850

Prof. Brian J. Mitchell
Department of Earth & Atmospheric Sciences
St. Louis University
St. Louis, MO 63156

Dr. Robert Reinke
ATTN; FCTVTD
Field Command
Defense Nuclear Agency
Kirtland AFB, NM 87115

Mr. Jack Murphy
S-CUBED
A Division of Maxwell Laboratory
11800 Sunrise Valley Drive, Suite 1212
Reston, VA 22091 (2 Copies)

Prof. Paul G. Richards
Lamont-Doherty Geological Observatory
   of Columbia University
Palisades, NY 10964

Dr. Keith K. Nakanishi
Lawrence Livermore National Laboratory
L-025
P.O. Box 808
Livermore, CA 94550

Mr. Wilmer Rivers
Teledyne Geotech
314 Montgomery Street
Alexandria, VA 22314

Dr. Carl Newton
Los Alamos National Laboratory
P.O. Box 1663
Mail Stop C335, Group ESS-3
Los Alamos, NM 87545

Dr. George Rothe
HQ AFTAC/TTR
Patrick AFB, FL 32925-6001

Dr. Bao Nguyen
AFTAC/TTR
Patrick AFB, FL 32925

Dr. Alan S. Ryall, Jr.
DARPA/NMRO
3701 North Fairfax Drive
Arlington, VA 22209-1714

Dr. Richard Sailor
TASC, Inc.
55 Walkers Brook Drive
Reading, MA 01867

Prof. Charles G. Sammis
Center for Earth Sciences
University of Southern California
University Park
Los Angeles, CA 90089-0741

Prof. Christopher H. Scholz
Lamont-Doherty Geological Observatory
 of Columbia University
Palisades, CA 10964

Dr. Susan Schwartz
Institute of Tectonics
1156 High Street
Santa Cruz, CA 95064

Secretary of the Air Force
(SAFRD)
Washington, DC 20330

Office of the Secretary of Defense
DDR&E
Washington, DC 20330

Thomas J. Sereno, Jr.
Science Application Int'l Corp.
10260 Campus Point Drive
San Diego, CA 92121

Dr. Michael Shore
Defense Nuclear Agency/SPSS
6801 Telegraph Road
Alexandria, VA 22310

Dr. Matthew Sibol
Virginia Tech
Seismological Observatory
4044 Derring Hall
Blacksburg, VA 24061-0420

Prof. David G. Simpson
IRIS, Inc.
1616 North Fort Myer Drive
Suite 1400
Arlington, VA 22209

Donald L. Springer
Lawrence Livermore National Laboratory
L-025
P.O. Box 808
Livermore, CA 94550

Dr. Jeffrey Stevens
S-CUBED
A Division of Maxwell Laboratory
P.O. Box 1620
La Jolla, CA 92038-1620

Lt. Col. Jim Stobie
ATTN: AFOSR/NL
Bolling AFB
Washington, DC 20332-6448

Prof. Brian Stump
Institute for the Study of Earth & Man
Geophysical Laboratory
Southern Methodist University
Dallas, TX 75275

Prof. Jeremiah Sullivan
University of Illinois at Urbana-Champaign
Department of Physics
1110 West Green Street
Urbana, IL 61801

Prof. L. Sykes
Lamont-Doherty Geological Observatory
 of Columbia University
Palisades, NY 10964

Dr. David Taylor
ENSCO, Inc.
445 Pineda Court
Melbourne, FL 32940

Dr. Steven R. Taylor
Los Alamos National Laboratory
P.O. Box 1663
Mail Stop C335
Los Alamos, NM 87545

Prof. Clifford Thurber
University of Wisconsin-Madison
Department of Geology & Geophysics
1215 West Dayton Street
Madison, WS 53706

Prof. M. Nafi Toksoz
Earth Resources Lab
Massachusetts Institute of Technology
42 Carleton Street
Cambridge, MA 02142

Dr. Larry Turnbull
CIA-OSWR/NED
Washington, DC 20505

DARPA/RMO/SECURITY OFFICE
3701 North Fairfax Drive
Arlington, VA 2203-1714

Dr. Gregory van der Vink
IRIS, Inc.
16116 North Fort Myer Drive
Suite 1440
Arlington, VA 22209

HQ DNA
ATTN: Technical Library
Washington, DC 20305

Dr. Karl Veith
EG&G
5211 Auth Road
Suite 240
Suitland, MD 20746

Defense Intelligence Agency
Directorate for Scientific & Technical Intelligence
ATTN: DTIB
Washington, DC 20340-6158

Prof. Terry C. Wallace
Department of Geosciences
Building #77
University of Arizona
Tuscon, AZ 85721

Defense Technical Information Center
Cameron Station
Alexandria, VA 22314 (2 Copies)

Dr. Thomas Weaver
Los Alamos National Laboratory
P.O. Box 1663
Mail Stop C335
Los Alamos, NM 87545

TACTEC
Battelle Memorial Institute
505 King Avenue
Columbus, OH 43201 (Final Report)

Dr William Wortman
Mission Research Corporation
8560 Cinderbed Road
Suite 700
Newington, VA 22122

Phillips Laboratory
ATTN: XPG
Hanscom AFB, MA 01731-5000

Prof. Francis T. Wu
Department of Geological Sciences
State University of New York
 at Binghamton
Vestal, NY 13901

Phillips Laboratory
ATTN: GPE
Hanscom AFB, MA 01731-5000

AFTAC/CA
(STINFO)
Patrick AFB, FL 32925-6001

Dr. Michel Bouchon
I.R.I.G.M.-B.P. 68
38402 St. Martin D'Heres
Cedex, FRANCE

DARPA/PM
3701 North Fairfax Drive
Arlington, VA 22203-1714

Dr. Michel Campillo
Observatoire de Grenoble
I.R.I.G.M.-B.P. 53
38041 Grenoble, FRANCE

DARPA/RMO/RETRIEVAL
3701 North Fairfax Drive
Arlington, VA 22203-1714

Dr. Kin Yip Chun
Geophysics Division
Physics Department
University of Toronto
Ontario, CANADA

Prof. Hans-Peter Harjes
Institute for Geophysics
Ruhr University/Bochum
P.O. Box 102148
4630 Bochum 1, GERMANY

Prof. Eystein Husebye
NTNF/NORSAR
P.O. Box 51
N-2007 Kjeller, NORWAY

David Jepsen
Acting Head, Nuclear Monitoring Section
Bureau of Mineral Resources
Geology and Geophysics
G.P.O. Box 378, Canberra, AUSTRALIA

Ms. Eva Johannisson
Senior Research Officer
National Defense Research Inst.
P.O. Box 27322
S-102 54 Stockholm, SWEDEN

Dr. Peter Marshall
Procurement Executive
Ministry of Defense
Blacknest, Brimpton
Reading FG7-FRS, UNITED KINGDOM

Dr. Bernard Massinon, Dr. Pierre Mechler
Societe Radiomana
27 rue Claude Bernard
75005 Paris, FRANCE (2 Copies)

Dr. Svein Mykkeltveit
NTNT/NORSAR
P.O. Box 51
N-2007 Kjeller, NORWAY (3 Copies)

Prof. Keith Priestley
University of Cambridge
Bullard Labs, Dept. of Earth Sciences
Madingley Rise, Madingley Road
Cambridge CB3 OEZ, ENGLAND

Dr. Jorg Schlittenhaardt
Federal Institute for Geosciences & Nat'l Res.
Postfach 510153
D-3000 Hannover 51, GERMANY

Dr. Johannes Schweitzer
Institute of Geophysics
Ruhr University/Bochum
P.O. Box 1102148
4360 Bochum 1, GERMANY

7